Tow-Based Discontinuous Composites for Toughening Adhesively Bonded Composite Joints

Experimental investigation on the influence of UD/TBDC ply hybrid CFRP substrates on the mode I fracture toughness.

João Tomás Ferreira Diniz

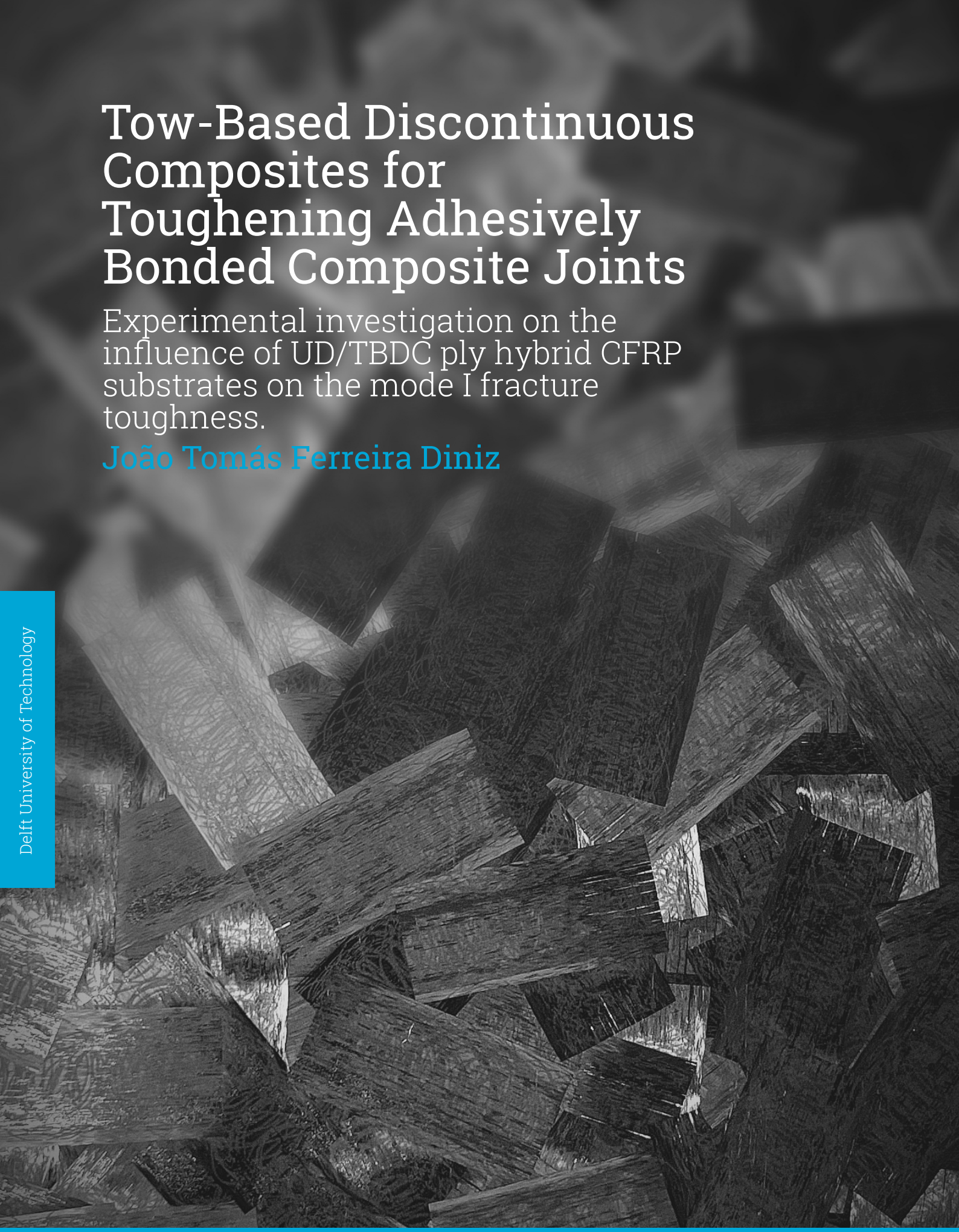

Delft University of Technology

TU Delft

Tow-Based Discontinuous Composites for Toughening Adhesively Bonded Composite Joints

by

João Tomás Ferreira Diniz

To obtain the degree of Master of Science in Aerospace Engineering
at the Delft University of Technology.

Student Name	Student Number
J. T. Ferreira Diniz	5780047

Supervisors:	Dr. S. Teixeira de Freitas
	Dr. R. A. A. Lima
	Dr. J. J. E. Teuwen
Project Duration:	March, 2024 - November, 2024
Faculty:	Faculty of Aerospace Engineering, Delft

TU Delft

Abstract

This thesis investigates the use of Tow-Based Discontinuous Composite (TBDC) interleaves to enhance the mode I fracture toughness of adhesively bonded joints with Carbon Fiber Reinforced Polymer (CFRP) substrates. Aiming to improve joint safety by slowing crack propagation and facilitating less sudden failure, this study focuses on integrating interlaminar-toughened substrates to resist crack growth and enhance the fracture behavior in the joint's substrate. Two main research questions are addressed: the influence of TBDC interleaves on mode I fracture toughness of CFRP laminates and their subsequent effect when used in CFRP-based bonded joints.

For CFRP laminates, Double-Cantilever Beam (DCB) samples were tested across three configurations: a non-toughened baseline and two TBDC-toughened variants. Based on previous research, three DCB configurations identified as the most promising for leveraging TBDC toughening in adhesive joints were tested. The $[90/45/-45/TBDC/0]_s$ and $[90/60/90/-60/TBDC/0]_s$ laminate substrates were bonded with the low-toughness adhesive Araldite 2015-1, while the $[0/TBDC/90_2/0]_s$ substrate was bonded with AF 163-2U, a high-toughness adhesive.

TBDC-toughened CFRP laminates demonstrated up to 130% higher fracture toughness compared to non-toughened counterparts. This was due to TBDC material crack propagation mechanisms such as crack branching, deflection, and fiber bridging.

In adhesively bonded joints, TBDC interleaves in CFRP substrates enhanced the decay of fracture toughness in specimens where cracks deflected from the bond line into the substrate, leading to a less abrupt reduction after reaching peak values. Joints with low-toughness adhesive exhibited more than a 100% increase in crack length from peak fracture toughness to the final value compared to non-TBDC-toughened substrate joints. Meanwhile, joints with high-toughness adhesive demonstrated toughness values 150% to 750% greater than those observed in non-toughened configurations at comparable crack lengths.

These findings highlight the potential of TBDC interleaves to enhance joint toughness, presenting new pathways to improve the safety of composite bonded structures.

Keywords: tow-based discontinuous composites, interlaminar toughening, fracture toughness, secondary bonded joints

Acknowledgments

I would like to express my gratitude to my three thesis supervisors, Dr. Sofia Teixeira de Freitas, Dr. Rosemere Lima, and Dr. Julie Teuwen, for their enlightening guidance and insights during this challenging yet rewarding final stage of my Master's studies. My special thanks to Rosemere for the time spent with me in the Aircraft Hall, which made the long lab days much more enjoyable, for passing on her lab work expertise, and for always being available and happy to help, whether with academic matters or otherwise.

To all the members of Dr. Sofia Teixeira de Freitas's research group, thank you for the valuable feedback during our weekly meetings, for your warm welcome, and for the companionship. I truly feel fortunate to have been part of such an amazing group of people.

To my friends in The Netherlands, both old and new, thank you for making me feel at home from the beginning and for making me excited to continue my life in this wonderful country. I will forever cherish the fun moments we shared, as well as the emotional and personal support you gave me during this important yet uncertain stage of my life.

To my loving girlfriend Inês, thank you for being such a wonderful person who has always supported me and my decisions. For always being with me, even when physically apart, and keeping me grounded and hopeful during most difficult moments. I am truly grateful for sharing this important and transformative transition in my life with you.

Finally, to my parents, thank you for always believing in me, supporting me unconditionally, and doing everything within your reach to provide me with the opportunities I have today. For your unwavering encouragement and faith in my abilities, which have motivated me to keep pursuing my ambitious goals.

João Tomás Ferreira Diniz
Delft, November 2024

Contents

List of Figures

List of Tables

Nomenclature

Abbreviations

Abbreviation	Definition
AE	Acoustic Emissions
CBBM	Compliance Based Beam Method
CFRP	Carbon Fiber Reinforced Polymer
CNF	Carbon Nano-Fibers
CNT	Carbon Nano-Tubes
CSR	Core-Shell Rubber
CTE	Coefficient of Thermal Expansion
DCB	Double Cantilever Beam
DIC	Digital Image Correlation
DLJ	Double-Lap Joint
DSC	Differential Scanning Calorimetry
EASA	European Union Aviation Safety Agency
ENF	End-Notched Flexure
FAA	Federal Aviation Administration
FRP	Fiber Reinforced Polymer
GNP	Graphene Nanoplates
LEFM	Linear-Elastic Fracture Mechanics
MBT	Modified Beam Theory
MMB	Mixed-Mode Bending
MWCNT	Multi-Walled Carbon Nanotubes
NDT	Non-Destructive Techniques
NWCT	Non-Woven Carbon Tissue
PA	Polyamide-12
PEI	Polyethylenimine
PES	Polyethersulfone
PI	Polyimide
PPS	Polyphenylene-Sulphide
PTFE	Polytetrafluoroethylene
RSD	Relative Standard Deviation
SEM	Scanning Electron Microscope
SHM	Structural Health Monitoring
SLJ	Single-Lap Joint
TBDC	Tow-Based Discontinuous Composite
TGA	Thermogravimetric Analysis
UD	Unidirectional

Symbols

Symbol	Definition	SI Unit
a	Crack length	[m]
a_0	Initial crack length	[m]
b	Sample width	[m]
h	Sample thickness	[m]

Symbol	Definition	SI Unit
t	Load point to DCB arm midplane vertical distance	[m]
C	Compliance	[Pa^{-1}]
E	Elastic Modulus	[Pa]
E_x^f	Flexural modulus	[Pa]
F	Large displacement effects correction	[-]
G	Mixed-mode I+II fracture toughness	[J/m^2]
G_{eff}	Effective fracture toughness	[J/m^2]
G_c	Critical fracture toughness	[J/m^2]
G_I	Mode I fracture toughness	[J/m^2]
G_{II}	Mode II fracture toughness	[J/m^2]
H	Enthalpy	[J]
ΔH	Change of enthalpy	[J]
I	Moment of inertia	[m^3]
L	Sample/Span length	[m]
L'	Load point to loading block edge horizontal distance	[m]
N	Large displacement effects correction	[-]
P	Load	[N]
δ	Load point displacement	[m]
ε	Strain	[-]
σ	Stress	[Pa]
Δ	Crack length correction	[m]

1

Introduction

With the ongoing environmental concerns, serious effort has been put into developing new more eco-efficient technology in various industries. The projected growth in the demand of commercial aviation, a considerable polluting sector, allied to the ongoing environmental concerns leads the aerospace industry to be pressured into developing more sustainable aircraft. Such concerns as climate change and air quality are being researched and solutioned through different sectors inside of the aircraft industry including engine technologies, air traffic management and operational procedures [1]. Reducing the structural weight of an aircraft significantly decreases fuel consumption and, consequently, greenhouse gas and other pollutants' emissions, such as CO_2 and NO_x, ultimately lessening the environmental impacts of aviation. In pursuit of these goals, the industry has increasingly replaced traditional metallic structural materials, like aluminum, with Fiber Reinforced Polymers (FRP), which are lighter and highly tailorable. Notable examples of this transition in the aerospace sector include the Boeing 787 and Airbus A350, both introduced in the last decade, which incorporate Carbon Fiber Reinforced Polymer (CFRP) in their fuselages [2]. The shift to fiber-reinforced polymers (FRP) in aircraft materials is projected to contribute up to 25% toward the aviation industry's CO_2 reduction goals [3]. This makes reducing structural weight through composite materials a significant factor in lowering the environmental impact of the aerospace sector.

The transition from metallic structures to their composite counterparts, however, also demands new joining techniques. The use of traditional joining methods, such as bolts and rivets, leads to cut fibers, introducing stress concentrations that compromise the structural integrity of bonded structures and joints [4]. To mitigate this loss of integrity, components are often overdesigned, resulting in thicker and heavier parts. On the other hand, the use of adhesive materials for the assembly of composite components has multiple advantages over the traditional joining techniques such as higher strength-to-weight ratio, stress distribution uniformity, design flexibility and negligible impact on the adherend's mechanical properties [4, 5]. At the time of redaction of the present report however, secondary bonding, where two fully-cured components are joined by means of adhesive bonding, is not certified for primary structures. In fact, the guidelines for EASA regulations for adhesively bonded joints in primary structures are the following [6, 7]:

"For any bonded joint, the failure of which would result in catastrophic loss of the aeroplane, the limit load capacity must be substantiated by one of the following methods:

1. The maximum disbond of each bonded joint consistent with the capability to with- stand the required loads must be determined by analysis, tests, or both. Disbonds of each bonded joint greater than this must be prevented by design features; or
2. Proof testing must be conducted on each production article that will apply the critical limit design load to each critical bonded joint; or
3. Repeatable and reliable non-destructive inspection techniques must be established that ensure the strength of each joint."

Back-up solutions to arrest crack growth such as the traditional bolts and rivets must then be used. This is the case due to the usually poor resistance to crack growth, risk of sudden failure as well as the difficulty to detect damage using Non-Destructive Techniques (NDT) and Structural Health Monitoring (SHM) in adhesively bonded joints [5].

To overcome issues with adhesively bonded joints and avoid using bolts and rivets, which compromise the properties of both the joint and adherend components, efforts have focused on enhancing joint safety and reliability. Research has aimed to increase fracture toughness, or the energy per unit area needed to cause fracture, in the joint. Several methods to increase the joints' fracture toughness through modifying and increasing the adhesive and bond line's resistance to crack growth have been researched, showing good results, mostly focusing on the increase of cohesive fracture energy [8–14]. On the other hand, multiple research projects have been conducted successfully to increase FRP laminates interlaminar fracture toughness, resulting in delayed initiation and slower propagation of delamination [15–19]. Efforts to study how the composite substrate's fracture toughness influences the fracture toughness of an adhesively bonded joint, however, have been limited. Kupski et al. [20] and Lima et al. [5] have conducted promising research on the influence of the adherends' ply thickness and layup sequence, respectively, on the fracture toughness of adhesively bonded composite joints. The promising results show that by tailoring the substrate's interlaminar fracture toughness, one can deflect and branch the crack growth and further increase the joint's toughness through energy dissipation inside the composite substrate. It is also observed, nonetheless, that after crack deflection to the substrate, delamination is bound to happen, usually with low fracture toughness compared to adhesive's cohesive failure toughness.

With the goal of enhancing adhesively bonded joint adherend's resistance to crack growth, as well as explore the full potential of composite bonded joints toughening strategies - such as crack competition and deflection - the present research project aims to use composite laminate interlaminar fracture toughening methods to do so. Using interlaminar toughened substrates in adhesively bonded joints can be the key to avoid sudden failure once unavoidable damage has been developed in the adherends. The hypothesis is that as damage progresses within the toughened substrate, higher crack resistance will be achieved, leading to more damage-tolerant joints without the need for rivets or bolts. On the other hand, and for the same reason, one can also exploit and take full advantage of crack deflection from the bond line to the substrate, as studied by Lima et al. [5], by using toughened adherends. Not only can the crack onset toughness be increased by the crack competition mechanisms triggered by tailored composite laminate layups, but also the toughness at the crack propagation stage, as the deflected crack is faced with an interlaminar toughened substrate. To accomplish this research project's goal, the influence of composite substrates interlaminar toughening in the overall adhesively bonded joints' fracture toughness will be studied.

The present report will serve to explain the steps taken in this Master's thesis project. Firstly, an overview into the literature findings regarding adhesively bonded joints and state-of-the-art toughening mechanisms will be presented in chapter 2, followed by the research gap found in the state-of-the-art. From the gap found in research, the literature study culminates in the formulation of the research objective and questions for the present research project as well as the planned methodology to address them, in chapter 3.

The design, manufacturing and post-manufacturing condition of test specimens used to address the research objective and questions are detailed in chapter 4, followed by the experimental methodology used in their testing, in chapter 5.

The results obtained will be presented in chapter 6 followed by a discussion of their underlying reasons and implications in chapter 7. Finally, chapter 8 will summarize the conclusions drawn, directly answering the research questions, reflecting on the research objective, and offering recommendations for future work to build upon the findings of this thesis project.

2

Literature Study

2.1. Adhesively bonded joints

Assemblies and joints are inevitable for full scale structures due to functional, efficiency or cost reasons [21]. There are three ways to join structures together: mechanical fastening, employing the use of bolts and rivets, for example; welding; and adhesive bonding, which will be the joining technique that this research project will be focused on [21].

Adhesive bonding works by joining together materials with the aid of an *adhesive*, a substance that can hold the joint together relying on microscopic mechanical locking and chemical bonding [21]. The adhesive bonds materials, referred to as *adherends*, by means of surface attachment and attractive forces. As a result, adhesive bonding typically causes minimal damage to the mechanical properties of the adherends. Furthermore, adhesive bonding can be used to join various material types such as metals, ceramics, glasses, polymers, composites and different combinations of these [21]. More uniform stress distributions, better load transmission between parts and higher joint stiffness, good damping properties, high fatigue strength and flexibility, making it possible to join materials with different coefficients of thermal expansion (CTE), are some of the reasons why adhesive joints are increasingly becoming an alternative to the more traditional joining techniques, such as mechanical fasteners [22].

Although adhesive bonding might offer numerous advantages over mechanical fastening, adhesive joints, more specifically secondary bonded joints as described in subsection 2.1.1, are at the time of writing of the present thesis not certified for primary load bearing structures in the civil aviation sector [5]. This is mostly due to two main problems that arise from this type of joining: the risk of sudden joint failure and difficulty to assess structural damage using NDT and SHM. These two problems coupled cause the damage and fracture behavior of adhesively bonded joints to be quite unpredictable and difficult to monitor during operation. To advance the shift from traditional joining techniques to adhesive bonding, it is essential to address these two problems first.

Over the present section, different bonding processes and adhesively bonded joint types will be introduced and explained as well as the different failure modes and ways to determine the crack onset and propagation resistance under each of these failure modes.

2.1.1. Bonding processes

When discussing adhesively bonded composite joints, the different types of bonding processes and what they imply must first be understood. There are three main different types of composite adhesive bonding: co-curing, co-bonding and secondary bonding [23]. Schematics of these can be seen in Figure 2.1.

Co-curing consists in joining uncured composite parts, curing them together [23]. This type of joining results in fully integrated components [24] and presents the best adhesion properties out of all the three types of bonding processes. It is however rarely used in large scale assemblies as the parts are usually manufactured separately [23].

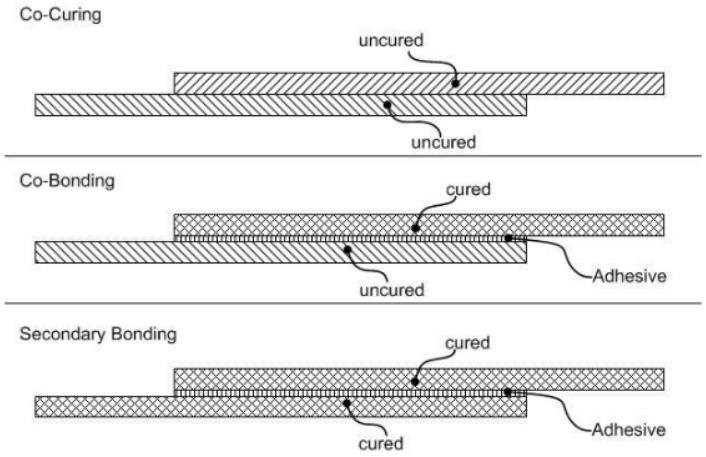

Figure 2.1: Bonding types [24].

Co-bonding is achieved by joining an uncured component with one or more fully cured components, typically using an adhesive material as the interface [24]. In addition to ensuring a fairly strong joint, it also, much like co-curing, cuts down on curing cycles and costs, making them the most used technique to perform repairs in composite parts [23].

Secondary bonding consists in joining two or more fully cured parts by means of an adhesive layer that ensures the bond between the assembly parts [23, 24]. Even though it seems logical that this type of bonding process provides the least amount of adhesion strength, research on this topic suggests that, under mode I and mixed-mode loading, secondary bonded joints present higher strength than co-bonded ones [23]. This can be explained by moisture of the uncured prepreg material being released during the co-bonding process, weakening the interface and, consequently, the joint strength [23]. Secondary bonding is usually the choice for large scale assemblies with big parts, due to the need to manufacture and cure the composite parts separately [23]. Furthermore, the extensive research present for this type of joining process can also be attributed to the recent growing interest in hybrid joints, such as composite-metal joints, for which secondary bonding is the most fitting joining process, being in this case called multi material bonding [23].

2.1.2. Joint types

Adhesively bonded joints come in different configurations, of which four are the most used ones: single-lap joint (SLJ), double-lap joint (DLJ), scarf joints and stepped-lap joints [25]. Please refer to Figure 2.2 for a schematic of the different joint configurations mentioned. The choice between different adhesively bonded joint types depends greatly on factors such as geometry and access restrictions, ease of manufacture as well as strength of the joint. A comparison in the joint strength between the different types of joints can be found in Figure 2.2.

Single-Lap joint

As can be seen in Figure 2.2, single-lap joints are the least efficient joint configuration of the ones shown, due to the fact that, as is mentioned in Figure 2.2, the load path is eccentric, leading to a high bending load in the joint. These bending loads applied in the joint result in peel stresses at the bond line's edges [2]. Furthermore, the bending moment applied to the joint generates tensile loads at the interface of the adhesive layer at the unloaded side of the adherend, while compression loads develop at the overlap edge closest to the loaded side. This difference in strain between the adherents when the joint is loaded, as can be seen in Figure 2.3, at the beginning and end of the overlap length, will form high peak shear stress in the adhesive, resulting in an uneven stress distribution. This uneven stress distribution can lead to premature failure and has been a subject of research; mechanisms for improvement will be discussed and explained in subsection 2.3.1.

Single-lap joints, however, are also found to be the most extensively researched types of joints in adhesive bonding literature. This is due to their ease of fabrication and that, out of the four mentioned,

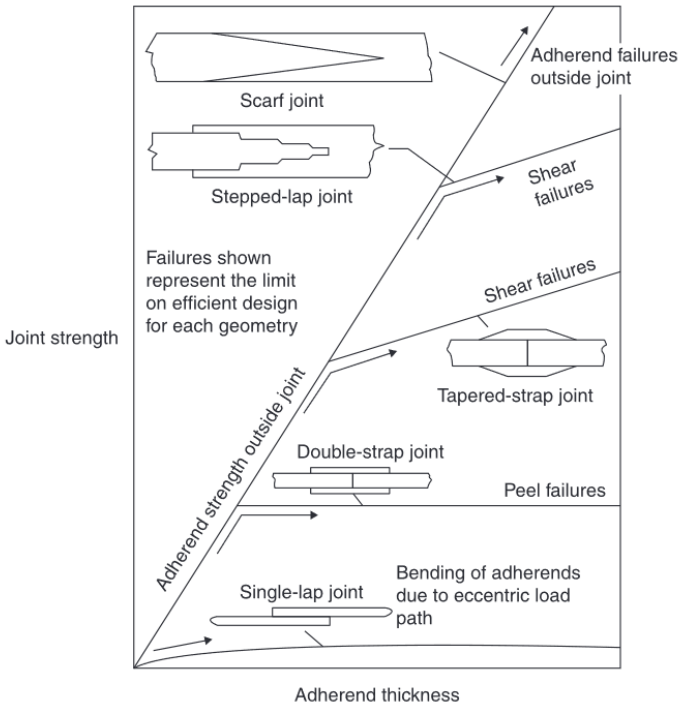

Figure 2.2: Different joint configurations' strength as a function of adhesive thickness [26].

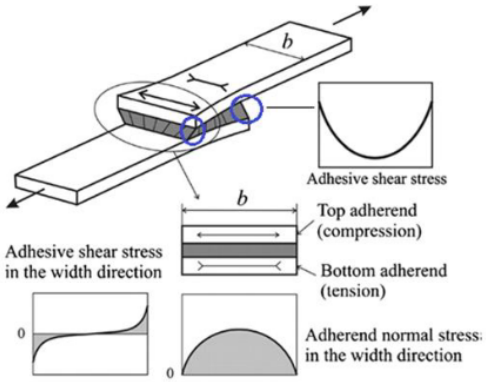

Figure 2.3: SLJ stress distribution [27].

are the only configuration that can be manufactured with access to only one side of the substrate, without requiring any modification to the adherends' geometry prior to joining them [25].

Double-Lap joint

Similar to the single-lap joint, the double-lap joint also benefits from its ease of manufacturing, however, it requires access to both sides of the adherend for proper assembly. On the other hand, it is much more efficient than a SLJ due to it having double the shear resistant area when compared to the single lap [25]. By creating a symmetric lap joint, unlike the single-lap joint, the middle adherend experiences negligible bending loads. However, the outer adherends will still suffer bending moments and a similar, uneven, stress distribution in the adhesive will arise [2].

Stepped-Lap joint

Stepped-lap joints have higher efficiency than any of the previously mentioned adhesively bonded joint configurations, as can be seen in Figure 2.2. However, they have two main geometry disadvantages:

one being that access to both sides of the adherend might be needed and the other that both adherends must be modified and perhaps machined, which makes the joining process much more complicated than the SLJ and DLJ [25]. A stepped-lap joint is essentially a SLJ where, instead of having a single, constant overlap, the adherends lose thickness in steps through overlapping area. This results in lower peel stresses in comparison with the previously mentioned configurations. The more steps used, the smoother the stress distribution becomes [2].

Moreover, the fact that the load path eccentricity found in both the SLJ and DLJ configurations can be eradicated by the geometry of the stepped-lap joint configuration, makes it also possible to avoid the bending loads. In order to do so, one must create a symmetric joint geometry, as can be seen in the stepped-lap joint presented in Figure 2.2.

Scarf joint

Scarf joints are the culmination of having multiple steps in a stepped-lap joint. So much so that, by having three or more steps, analysing the stress distribution of a stepped-lap joint as a scarf joint becomes reasonable [28]. By striving for the stepped-lap joint configuration to have infinite steps over the overlap length, not having steps but a continuous, smooth transition between the adherends, making for a single angled straight overlap, the stress distribution can be made smoother and further reduce the peel stresses. By using stepped-lap joints and scarf joints it is possible to increase the strength of SLJ and DLJ by 90 to 150% [2]. Finally, it should be said that just like in stepped-lap joints it is possible to create a symmetric joint geometry with little to no bending moments applied.

2.1.3. Joint failure types

Adhesively bonded joints can fail in diverse ways, as given by ASTM D5573 [29], such as by adhesive failure, cohesive and thin-layered cohesive failure, fiber-tear and light-fiber-tear failure and stock-break failure. The different failure types can be seen in Figure 2.4. Properly designed adhesively bonded joints should not fail in the bond itself but rather in the adherends, although, as mentioned previously a bond failure is possible. Following this philosophy, the desired failure type should be stock-break failure, as it shows that the bond is not a weak spot [30]. Importantly, bond failure refers not only to failures in the adhesive material itself but also to failures in the adherends within the bond area or length.

It should also be noted that, in this thesis, the term “failure types” is used to refer to these categories. However, in the literature, the term “failure modes” is more common. This choice aims to avoid confusion between failure types and fracture or loading modes, which are addressed in section 2.2.

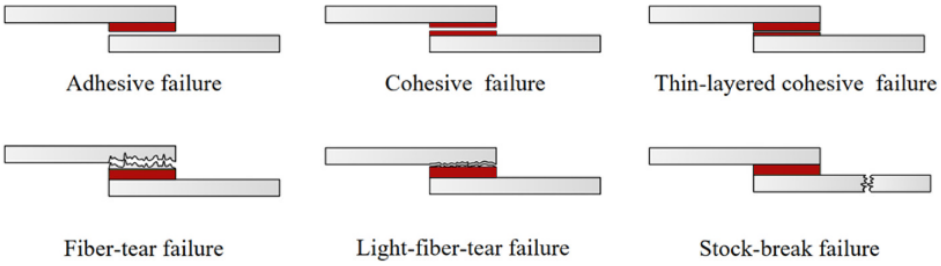

Figure 2.4: Adhesively bonded joint failure types [30].

During this subsection, the focus will be on bond failure types only, as this research project focuses on the improvement of the fracture toughness of the bond itself. Stock-break failure will, thus, be excluded. Moreover, cohesive and thin-layered cohesive failure will be reviewed and explained as one failure type, the same will be the case for fiber-tear and light-fiber-tear failure.

Adhesive failure

Adhesive failure can be characterized as a disbond between the adhesive and the adherend [30]. This type of failure typically occurs when chemical and mechanical bonds cannot form between the adherend and adhesive material at the interface. This can happen due to various factors such as poor surface treatment, adhesive curing before joining process and other operational and environmental factors [30, 31]. This failure type must be avoided, since it is unacceptable by the certification authorities [30].

Cohesive failure

Cohesive failure happens when the joint fails completely inside the adhesive layer, and as such there should be adhesive material on the fracture surface of both sides of the joint. Failure happens when the cohesive strength of the adhesive is reached and the crack propagates due to shear and peel stresses, even though the most critical are peel [30, 31]. This type of failure can also occur due to excessive porosity in the adhesive, which arises from poor conditions during the manufacturing process, resulting in voids that serve as sites for crack initiation [31].

If the failure happens close to the adhesive/adherend interface then the failure is called thin-layered cohesive failure.

Fiber-tear failure

Fiber-tear failure is caused when the adherend fails in the bond area. This failure type is governed by the adherend's transverse mechanical properties, especially the interlaminar properties, and the layup stacking sequence [30]. This type of failure can signify a good bond strength, however, it also usually shows that the adherend is not suitable for the joint [31]. Moreover, this type of failure can occur due to defects in the substrate, which can be a result of environmental effects or poor manufacturing conditions.

2.2. Fracture & Loading modes

Fracture is the separation of a solid body into two or more parts under the action of stresses. The fracture process is subdivided into three stages: damage accumulation, crack onset and crack propagation [32]. Damage accumulation depends on the ductility and strength of the solid body's material. When a sufficiently high load is applied, a crack forms, leading to the creation of two free surfaces within the material. From there on, if a high enough load is still applied to the body, the crack will propagate until the body separates itself into multiple parts: complete rupture happens [32].

The material's resistance against crack formation and propagation is called fracture toughness and is defined as the amount of energy needed to input in order to fracture that same material per unit area.

There exist 3 modes of fracture, as can be seen in Figure 2.5, depending on what type of loading the material is subject to: mode I, or opening mode; mode II, or sliding mode; and mode III, or tearing mode. Furthermore, the material can be loaded in a mix of any of the 3 modes of fracture, these modes of fracture are called mixed modes. Only mode I, mode II and mixed-mode I+II will be covered in this report since they are the most relevant in the case of adhesively bonded joints in operation [33, 34].

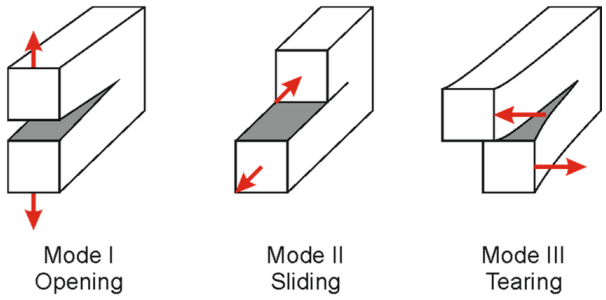

Figure 2.5: Fracture modes [35].

2.2.1. Mode I

Mode I, or opening mode, takes place when the load applied is perpendicular to the crack plane [32]. Although it is not the most representative loading mode experienced by adhesively bonded joints during operation, mode I fracture is considered the most critical fracture mode in such joints [33].

The mode I fracture toughness, G_I, of an adhesively bonded joint can be obtained with methods such as the Modified Beam Theory (MBT), based in Linear-Elastic Fracture Mechanics (LEFM), as given by the ISO 25217 [36]. Following this standard, a Double Cantilever Beam (DCB) test is performed, as seen in Figure 2.6. The specimen is loaded perpendicular to the crack plane, defined during the

manufacturing process of the specimen by introducing a starting crack using a non-adhesive insert in the specimen's end where the load blocks are attached, as shown in Figure 2.6. The fracture toughness can then be obtained from the strain energy release rate of a perfectly built-in double cantilever beam, with the MBT, from the following equation [37]:

$$G_I = \frac{3P\delta}{2ba} \tag{2.1}$$

Where P is the applied load, δ the load point displacement, b the specimen width and a the crack length.

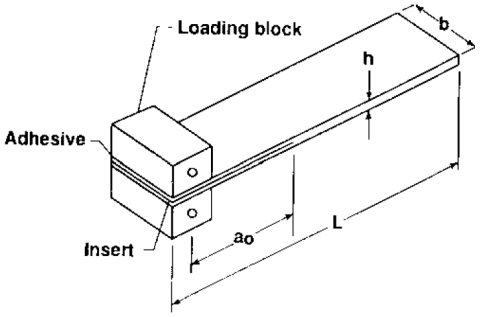

Figure 2.6: Double cantilever beam schematic [37].

2.2.2. Mode II

Mode II, or sliding mode, is caused by loads parallel to the crack plane and perpendicular to the crack length direction, as can be seen in Figure 2.5. This type of loading results in shear stresses.

The mode II fracture toughness, G_{II}, of an adhesively bonded joint can be obtained using the same process used for obtaining the mode II interlaminar fracture toughness of unidirectional (UD) FRP composites, as given by the ASTM D7905 [38]. This process is done by manufacturing a specimen similar to the one used in DCB tests, in the sense that it features a crack initiation in one end of the specimen, and performing the End-Notched Flexure (ENF) test, as seen in Figure 2.7. The similarity between the processes used to obtain the fracture toughness for UD laminates and adhesively bonded joints can be seen by comparing the standards for mode I fracture toughness measurement ISO 25217 [36], used for bonded joints, and the older ASTM D5528 [37], which was used for adhesively bonded joints before the ISO standard was established [33].

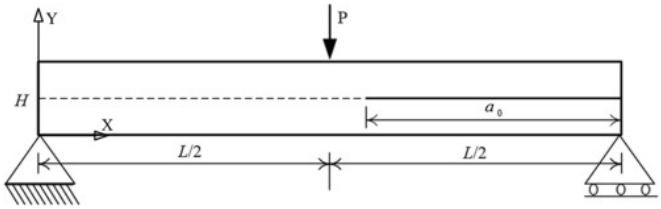

Figure 2.7: End-notched flexure test schematic [39].

2.2.3. Mixed-mode I+II

Mixed-mode I+II refers to, as the name suggests, a mixture between the fracture modes I and II: sliding and opening loads are applied to the structure, inducing both peel and shear stresses. This mixed-mode is the most representative of the loads applied during operation of adhesively bonded joints in practice [33]. Because of this, significant research has been done to obtain the appropriate fracture toughness of adhesively bonded joints under mixed-mode.

The mixed-mode fracture toughness is obtained by calculating the mixed-mode strain energy release rate: summing the mode I and II strain energy release rates. The following equation can be used [40]:

$$G = G_I + G_{II} \tag{2.2}$$

These fracture toughness values are obtained following the ASTM D6671 [40]. The described process features Mixed-Mode Bending (MMB) tests, which are performed using a combination of DCB and ENF specimens [33]. The test set-up can be seen in Figure 2.8.

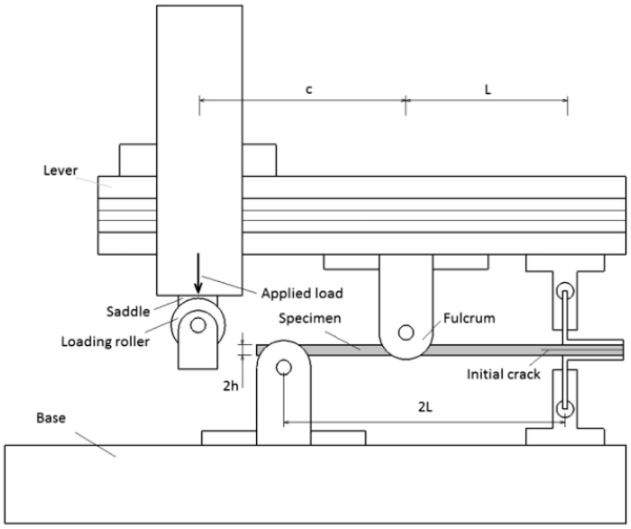

Figure 2.8: Mixed-mode bending test [33].

As different mixed-mode loading ratios G_{II}/G will result in different fracture toughness values, if a general idea of how a certain laminate behaves under mixed-mode I+II is needed, multiple loading ratios should be used. In order to change the loading ratio, the lever length c, as shown in Figure 2.8, is varied using the expressions found in the ASTM D6671 standard [40] to obtain the desired mixture. If multiple loading ratios are employed, the resulting critical fracture toughness should be presented as illustrated in Figure 2.9: a valuable toughness contour that can aid in establishing failure criteria [40]. Understanding the critical toughness at various mixed-mode loading ratios is essential for formulating these criteria.

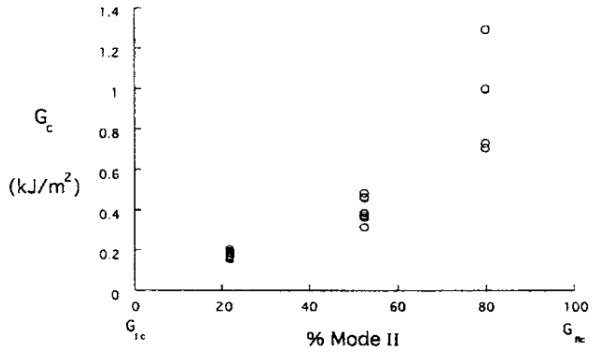

Figure 2.9: Mixed-mode summary graph [40].

2.3. Toughening mechanisms

When researching about toughening mechanisms, it is important to study their effects on the different fracture modes, since, as mentioned in section 2.2, while mode I might be considered the most critical fracture mode, mixed-mode loading is the most representative of practical bonded joints in operation.

Research on toughening mechanisms for modes I, II and mixed-mode I+II is widely available in literature for both bond line fracture toughness in adhesively bonded composite joints, focusing mostly on cohesive failure, as well as for interlaminar fracture toughness in composite materials, focusing on delaying delamination initiation and reducing delamination propagation speed. Seeing how damage can initiate and propagate in the composite substrate, leading to final failure, it is important to review not only how composite laminates can be toughened but also the effect that the substrates' mechanical and geometric properties have on the joint's fracture toughness.

In the present section, state-of-the-art bond line toughening mechanisms for adhesively bonded joints, interlaminar toughening mechanisms for composite materials and adherends' effect on bonded joints' fracture toughness will be explored. Furthermore, a research project on the damage mechanisms of adhesively bonded Tow-Based Discontinuous Composites (TBDC) will be reviewed, due to the promising fracture toughness results obtained compared to adhesively bonded composite laminates manufactured with regular unidirectional FRP prepreg plies [41].

2.3.1. Bond line toughening mechanisms

Extensive research on the toughening of adhesively bonded joints focusing on toughening strategies at the bond line itself has been done. By the use of tougher adhesive materials, however, such as by the use of the toughening mechanisms to be reviewed in the present section, damage is increasingly more likely to develop and propagate in the composite substrates.

Increasing the adhesive material's fracture toughness can be done by improving the adhesive material's mechanical properties: by tailoring the manufacturing conditions or using reinforcement particles for example. By employing surface treatment techniques, interleaves, or crack stoppers, crack bridging mechanisms can be introduced. Crack bridging occurs when ligaments form behind the crack tip, acting like springs that reduce the stress intensity at the crack tip, thereby enhancing the material's toughness [42].

Moreover, the ductility of the adhesive material over the bond line can be tailored to uniformise stress distributions and stop crack growth by introducing material transition barriers. Finally, sacrificial voids or cracks can be used to promote energy dissipation through crack competition [5, 12]. Through this subsection, four different bond line toughening mechanisms will be reviewed.

Adhesive reinforcement

Various types of reinforcement particles have been studied in literature and used to improve epoxy based adhesives, such as silica, rubber, carbon and graphene nanoparticles [16].

For instance, Quan et al. [8] have researched the effect of the addition of Core-Shell Rubber (CSR) nanoparticles to the adhesive material on the mode I fracture toughness of adhesively bonded composite joints. An epoxy adhesive was infused with CSR particles and used to manufacture DCB specimens to test the mode I fracture toughness against a control specimen with no CSR particles. It was found that the ductility added to the adhesive material by the rubber nanoparticles caused a more stable crack propagation and lead to an increase in mode I crack propagation fracture toughness. Particularly, specimens with CSR particles volume density upwards of 20-30% were able to tenfold the toughness measured in the control specimens [8].

By looking at the fracture surfaces, it was possible to identify the main damage mechanisms and crack features, which presented clear development of voids due to the particles' geometry. The crack competition between the voids and plastic deformation caused by the high ductility of the adhesive led to high energy dissipation and ultimately, an increase in crack propagation toughness [8].

On the other hand, reinforcement materials such as Multi-Walled Carbon Nanotubes (MWCNT) and Graphene Nanoplates (GNP) can be used as a reinforcement material in the adhesive not to improve the material's mechanical properties, but instead to enable crack arrest features such as pinning and crack deflection. Rao et al. [9] found that, by using MWCNT and GNP as a reinforcement material for the adhesive in composite bonded joints, depending on the weight fraction and ratio between the two types of reinforcement found in the adhesive material, the mode I fracture energy of the joint could suffer an increase of up to 286%.

By analysing the fractured specimens using a Scanning Electron Microscope (SEM) it was reported that the main toughness enhancing mechanisms enabled by MWCNT was crack pinning. As the crack tip encounters a MWCNT, to further progress it needs to break the bond between the particle and the epoxy adhesive, leading to a higher fracture energy. The GNPs, however, display a higher ability to toughen epoxy adhesives, due not only to crack pinning but also crack deflection. As the crack tip encounters a GNP, the nanoplate acts as a pin, forcing the crack to deflect around both sides of the plate to further propagate [9].

Kirigami adhesive

Many of the engineering technologies and inventions are inspired by nature and bonded joints and engineering structures in general are a very good example of that. Kirigami is a form of Japanese art which uses cuts and folds in a piece of paper to create three dimensional designs. Inspired by this form of art and the mechanisms used by some animals for vertical climbing, research has been conducted on adhesive strips with cuts and folds to make for heterogeneity and discontinuities in the adhesive, as well as change the peel angle the adhesive layer and crack tip is subject to [10]. It is possible to identify in literature two different types of kirigami inspired adhesive technologies. On the one hand, the kirigami inspired cuts can be used to form discontinuities in the adhesive layer, and on the other these cuts may be used to manipulate and alter the peel angles the crack tip it subject to.

By manipulating the local elasticity of the adhesive layer, the crack dynamics can be controlled. Hwang et al. [11] conducted research on the adhesion properties of kirigami-inspired adhesive strips. These strips feature alternating stiff and compliant material regions. It was found that the adhesion capacity was governed by two main factors: the difference in (i) bending stiffness and (ii) contact width of the different stiffness regions of the adhesive strip [11]. This increase in adhesion strength and toughness is due to the transition between stiff and compliant regions. When the crack tip reaches a discontinuity in stiffness it not only gets trapped but also needs to reinitiate at the interface, resulting in an enhancement of the toughness properties of the adhesive [11].

Moreover, cuts can be made in the adhesive layer in order to form features that alter the peel angle once the crack tip reaches a certain point, as can be seen in Figure 2.10 [10].

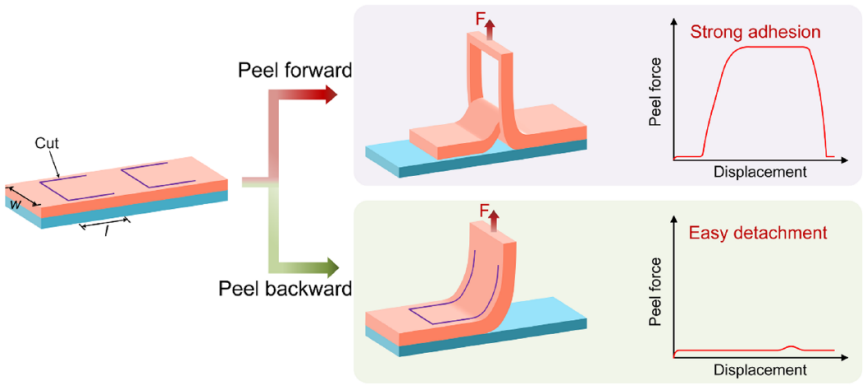

Figure 2.10: Peeling of a kirigami adhesive layer [10].

The peel angle, defined as the angle between the applied force and the crack plane of the adhesive layer, significantly influences adhesion strength, toughness, and stiffness. As illustrated in Figure 2.11, varying the peel angle from 0 to 90 degrees leads to a notable decrease in stiffness, strength, and toughness, as shown in Figures 2.11b, 2.11c, and 2.11d, respectively. Therefore, it is highly beneficial to reduce the peel angle to enhance the performance of adhesive joints.

Furthermore, the fact that upon the crack tip reaching these features, activating the toughening mechanisms in the adhesive layer, the material is stretched, as can be seen in the ”peel forward” image in Figure 2.10, results in these features acting as elastic dissipators, significantly increasing the fracture energy [10]. In sum, it is found that the energy dissipating capability coupled with the ability to lower the peel angles found in this type of kirigami-inspired adhesive strips makes for a significant increase in their adhesion fracture toughness [10].

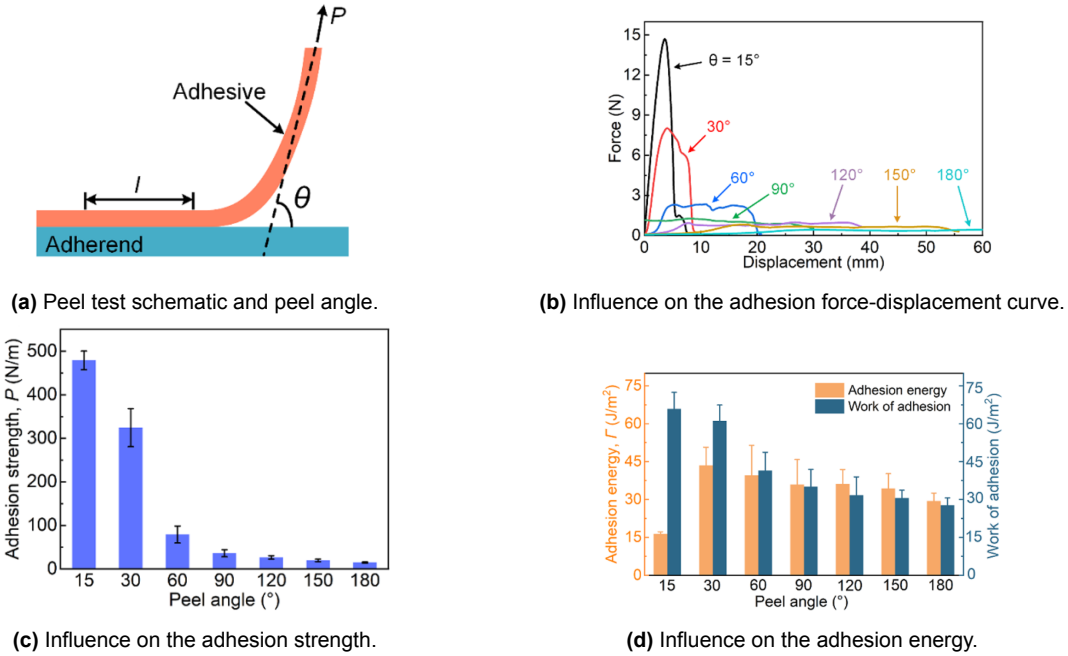

(a) Peel test schematic and peel angle.

(b) Influence on the adhesion force-displacement curve.

(c) Influence on the adhesion strength.

(d) Influence on the adhesion energy.

Figure 2.11: Peel angle influence on adhesion properties [10].

Hybrid bond line

Hybrid bond line joints, or mixed-adhesive joints are another way to increase an adhesively bonded composite joint's fracture toughness without modifying the adhesive material, much like the kirigami-inspired adhesive strips mentioned earlier. Another similarity between these two toughening mechanisms is the use of discontinuous elastic properties along the bond line in order to increase a joint's fracture toughness. It should be said that some kirigami-inspired adhesives studied in literature, such as Hwang et al.'s [11], are nothing other than a mixed-material adhesive strip. As such, the crack slowing mechanisms present are very similar. The stiffness discontinuities in the adhesive act as a disbond stopping feature that, as a crack tip encounters these physical barriers, arrest the crack growth. In order to further propagate the disbonding, a new crack must be initiated at the different material adhesive.

Löbel et al. [12] investigated the effect of hybrid bond lines on the mode I fracture toughness of adhesively bonded composite joints through DCB tests, as well as its effect on SLJs. The specimens were manufactured using high strength brittle adhesive at the edges of the bond line and a strip of a thermoplastic, a naturally more ductile family of polymers, adhesive at the middle, as illustrated in Figure 2.12. It is however mentioned that, ideally, more strips of ductile adhesive should be distributed throughout the bond line. An increase of up to 185% in mode I fracture toughness was obtained in the mixed-adhesive specimens when compared to the control specimens manufactured with an homogeneous, high strength, brittle adhesive bond line [12].

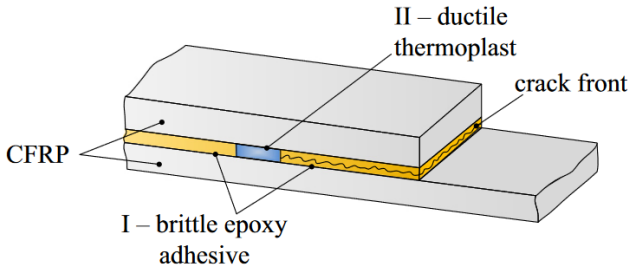

Figure 2.12: Hybrid bond line adhesively bonded joint schematic [12].

Furthermore, a mixed-adhesive bond line can be used to toughen SLJ and improve the uneven stress distribution found in this type of joint due to their load eccentricity, as explained in subsection 2.1.2. Da Silva et al. [13] studied the use of ductile adhesive material at the overlap's edges, where the strain difference between adherends is more pronounced, coupled with the use of a high strength, brittle adhesive at the center of the overlap, where the stress concentrations are lower. The use of a ductile material at the overlap's edges allows the bond line material to comply with the strains of the adherends, significantly lowering the stress concentrations at the overlap edge making for a more uniform stress distribution over the bond line and, ultimately, improving the adhesion properties of SLJ [13].

Sacrificial cracks

Another example of the use of bio-inspired mechanisms to increase the adhesion toughness in adhesively bonded composite joints is the integration of voids or sacrificial cracks in the bond line. By observing the adhesion system of *Mytilus californianus*, a mussel, voids present in their protein layers can be identified [14]. These voids are, in part, responsible for their remarkably high adhesion toughness.

Wagih et al. [14] studied the effect of introducing sacrifical cracks inside the bond line of T-joints on their pull-off strength and fracture toughness, while identifying the present damage mechanisms. It was found that, present adhesive ligaments at the edges of the voids absorbed applied energy as elastic energy, essentially acting as energy dissipators. This energy dissipation occurring at the voids' edges in turn reduced the energy going towards the crack tip, increasing the total fracture energy [14]. From the results of the study, it was concluded that by using artificial voids in the adhesive layer of T-joints, it is possible to increase the joint strength and toughness by 3.27 and 18.9 times, respectively, when compared to the traditional, reference, T-joints without any voids in the adhesive layer. Furthermore, it is also worth noting that the improvement in fracture toughness was mainly due to the resulting improvement in mode II fracture toughness of the skin-adhesive interface of the joints [14].

2.3.2. Composite laminate toughening

Past research has shown that the composite substrate's properties can greatly influence an adhesively bonded joint's toughness [5, 20]. Furthermore, and as previously mentioned, by using high toughness adhesives in a bonded joint, it becomes increasingly easier for a crack to be initiated and propagated in the composite substrates, which can easily lead to sudden failure if no crack arrest features are present. Thus, it is of great interest to study composite laminates' toughening mechanisms when researching ways to increase a bonded joint's toughness.

Due to their weak out-of-plane mechanical properties, FRP composites present poor interlaminar strength and toughness resulting in delamination being one of the main modes of failure of these materials [19]. Two main methods for achieving higher interlaminar fracture toughness in fiber-reinforced polymer (FRP) composites are the reinforcement of the matrix material with nanoparticles and the introduction of interlayers at potential crack planes [16].

The integration of reinforcement particles in the matrix material with the objective to increase a composite laminate's fracture toughness works in a similar way as reinforcing the adhesive in the bond line of an adhesively bonded joint. It is worth noting however, that the addition of nanoparticles to increase the matrix material's fracture toughness, namely rubber nanoparticles, might cause a reduction in the FRP's mechanical properties. For this reason, these particles can be used along with other type of reinforcement materials, such as silica particles for example, that compensate for the degradation caused [16], this is not a concern when reinforcing the adhesive material in a bonded joint however, as the substrate's mechanical properties, such as the elastic modulus, are those that really govern the behavior of the assembly.

As was mentioned, one way to increase FRPs' toughness, more specifically their interlaminar fracture toughness, is to introduce interlayers, also called interleaves, in possible crack planes. Different interleaving materials have been used and researched, namely Carbon Nano-Tubes (CNT), Carbon Nano-Fibers (CNF), polyamide short fibers, among other thermoplastic fibres [16]. An example schematic of a Non-Woven Carbon Tissue (NWCT) interleaved CFRP specimen, which will reviewed in the present section, can be seen in the right side of Figure 2.13.

Research on this subject shows that one of the main toughening mechanisms that take place when

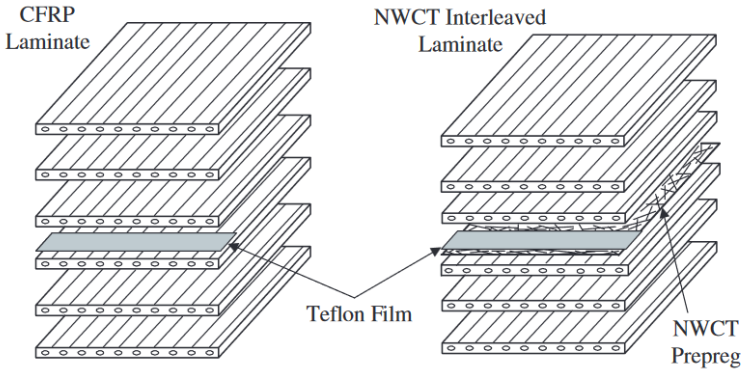

Figure 2.13: NWCT interleaved CFRP laminate schematic [19].

using interleaves in FRP composites is fiber bridging [16]. Fiber bridging takes place when fibers in adjacent plies bridge the crack plane, acting as crack arresters [43], this mechanism can be seen in action in Figure 2.14. This ultimately results in the increase of fracture toughness. Other mechanisms that might influence the interlaminar toughening of FRP laminates and can be obtained by the use of thermoplastic short fibers veils are plastic deformation, thermoplastic particle and fiber debonding and plastic void growth, depending on the different interactions the thermoplastic materials have with the FRP's epoxy matrix [17].

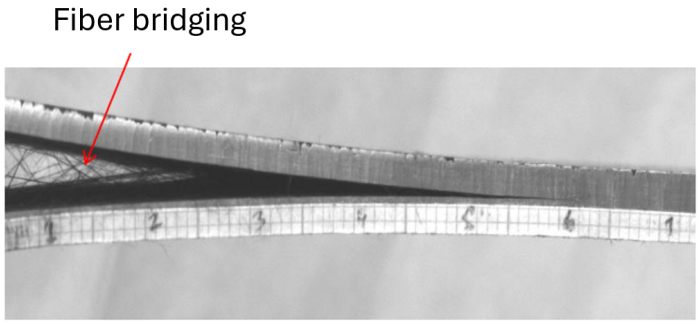

Figure 2.14: Fiber bridging in specimen under mode I loading [44].

Through this subsection, 3 different types of researched interleaving materials used to increase the fracture toughness of composite laminates will be reviewed, as well as the damage mechanisms present that cause these toughening effects.

Non-Woven Carbon Tissue

Among other researched interleaving materials, is Non-Woven Carbon Tissue (NWCT). Non-woven tissue has been used as a surface protection layer in the outside of composite structures, as well as for corrosion resistance in several applications [19]. Non-woven tissue is the denomination used for materials with short fibers discretely distributed, orientated in a random manner [19], as can be seen in Figure 2.15.

Lee et al. [18, 19] have studied the effect of interleaved NWCT on modes I and II fracture toughness of laminated composites. The toughening effect of the use of NWCT depends greatly on the number

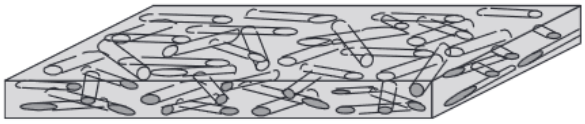

Figure 2.15: NWCT schematic [19].

of layers used, the volume fraction of short fibers in the tissue and the initial crack location [18, 19]. Increases in mode I and mode II fracture toughness of NWCT interleaved CFRP laminate of up to 28% and 260% were obtained, respectively. Moreover, it was found that while for the mode II fracture toughness, fiber bridging in the in-plane short fibers mostly governed the increase; for the mode I fracture toughness the increase was caused mostly by breakage of the out-of-plane short fibers [18, 19].

Stainless steel fibers

Quan et al. [16] have researched the mode I interlaminar fracture toughness of CFRPs interleaved with stainless steel fibres. By placing continuous fibres, transversely or longitudinally, along the crack plane, it was found that the mode I fracture toughness of the CFRP specimen increased up to 480% compared to the control pure CFRP specimen. This increase can be attributed to the effect of fibre bridging and tensile failure that took place in the interleaves [16].

The results obtained were highly dependent on the fiber density of the interleaves as well as their orientation. The results reveal that, when using transversely placed stainless steel fibres, the increase in fracture toughness is higher. On the other hand, placing fibers longitudinally has a negligible impact on the mechanical properties of the composite laminate. In contrast, arranging them transversely decreases the tensile modulus and strength by approximately 7.5% and 11.5%, respectively, when adding 320 filaments per mm — the highest fiber density studied. This configuration also results in the most significant increase in fracture toughness. The reported increase in fracture toughness was observed to be mainly due to steel fiber bridging and tensile failure [16]. Moreover, it should be noted that among all the interleaving materials reviewed in this thesis, stainless steel fibers exhibit the highest areal densities. This characteristic leads to an increase in weight of approximately 16% for specimens interleaved with the highest fiber densities [16].

It is worth mentioning that these interleaves are not of the same material of usual carbon fibers used in the aerospace industry, which might give rise to corrosion concerns and should be studied more in depth.

Thermoplastic veils

Non-woven veil, or tissue, interleaves based on thermoplastic short fibers have proven outstanding potential for toughening composite laminates, without significant tolls in either the original laminate's mechanical properties or weight [17]. Quan et al. [17] have researched the effect of various thermoplastic material veil interleaves on the mixed-mode I+II fracture toughness of CFRP laminates, through cracked lap-shear tests. For this purpose, 5 different thermoplastic material based veils were used, including Polyamide-12 (PA), Polyphenylene-sulphide (PPS), Polyimide (PI), Polyethersulfone (PES) and Polyethylenimine (PEI) [17].

The different interactions the different thermoplastic materials have with the epoxy based CFRP material used, combined with different laminate curing schedules and how these affect the resulting interlaminar toughening mechanisms and performance motivated the research conducted. During the specimens' curing process, the PA fibers melted, PPS and PI fibers remained in their original forms and PES and PEI dissolved in the CFRP's epoxy matrix [17].

PA and PI fibers exhibited the poorest performance, due to the fracture developing in the interface between the laminate and the interleaves, not allowing for activation of any toughening mechanism. On the other hand, the dissolved thermoplastic fibers, PES and PEI, presented a substantial increase in toughness with the fracture initiation and propagation energy: 92 and 171% respectively, compared to the control specimens. This increase is mostly due to debonding of the thermoplastic particles followed by plastic void growth. The best performance was recorded for the non-dissolved, non-melted PPS veils which recorded an increase in fracture initiation and propagation energy of 134 and 345%, respectively. The main toughening mechanisms observed responsible for the outstanding performance exhibited were fiber debonding and bridging [17].

2.3.3. Toughening joints through substrate tailoring

Limited effort has been made to study how the properties of the composite substrate influence the toughness of adhesively bonded composite joints. What has been researched on this matter however

shows promising results. By promoting crack deflection from the bond line to the composite substrate, mechanisms to diffuse and slow crack growth can be taken advantage of. Namely, crack competition mechanisms can increase an adhesively bonded composite joint's fracture toughness. Furthermore, in-situ effects that arise from the local geometrical properties of the composite susbtrates' plies have been shown to strengthen adhesively bonded joints.

Overall, the effect the composite substrate's properties have on adhesively bonded joints' fracture toughness, along with its underlying mechanisms is worthwhile exploring. Having a broader understanding on the mechanisms that may affect a joint's performance might help find new ways to toughen and reduce the risks associated with this joining technique, making use of researched damage mechanisms in unexplored ways.

Over the following section, two research projects on the effect of tailored CFRP layups and the thickness of the composite substrate's layers on the fracture toughness of adhesively bonded joints will be reviewed.

Thin-plies

With the continuous advances and developments in composite technology, new possibilities arise. This is the example of fiber tow spreading technology, with which it is possible to manufacture thin FRP plies, down to around 20 μm [20]. Camanho et al. [45] have researched the effect of the use of thin plies in composite laminates on their transversal mechanical properties. It was found that by the use of thinner plies, enhanced out-of-plane mechanical performance can be obtained [20]. Depending on the thickness and position of a certain ply in the laminate, in-situ properties such as the shear strength can be observed, for thin-plies these are usually higher than the strength found for the same ply in a unidirectional laminate, due to a constraining effect other orientation plies exert on each other [45]. It was demonstrated by Camanho et al. [45], as well as by related research, that the use of thin plies in FRP laminates can delay delamination growth and matrix cracking in SLJs [20].

The effect that the interlaminar enhancing abilities of thin plies have on the performance of adhesively bonded composite joints has been studied by Kupski et al. [20]. For this purpose, SLJ specimens, with three different ply thicknesses, were used to study the effect of the ply thickness on the tensile bonding strength of composite joints. The results show that, for bonded joints with thinner plies in the composite substrate, crack deflection from the bond line to the substrate occurs due to multiple matrix cracks. This results in higher energy dissipation and ultimately increases the crack initiation load and further the ultimate failure load [5, 20]. For the joints with the thinnest plies in the substrate, an increase of 16% and 47% in ultimate failure and crack initiation loads, respectively, were found [20]. It should be noted that although a significant increase in joint strength up to initiation was observed, the subsequent damage progression toward final failure was more abrupt [20].

Layup tailoring

Extensive effort has been put to study the effect of composite laminate's ply orientations on the crack paths developed on composite laminates without adhesive bond lines [5, 46]. Lima et al. [5] studied this same effect, however on adhesively bonded composite joints, with the aim to understand the damage mechanisms that can trigger toughening when tailoring the laminate's layup and how the adherend's layup and stiffness play a role in these toughening mechanisms.

Using DCB tests, load-displacement curves and mode I fracture toughness values were obtained for five different CFRP layups, utilizing two distinct toughness adhesives. It was found that when using the low toughness adhesive material Araldite 2015 (G_{Ic} = 640 J/m^2 [5]) with composite substrates, such as the unidirectional [0_8], cohesive failure takes place and the joint's fracture toughness is governed by the adhesive material's. However, by using multidirectional composite laminates with higher than 0-degrees orientated plies near the crack plane as substrates, such as [90/45/-45/0]$_s$ and [90/60/90/-60/0]$_s$, the crack is observed to be deflected from the bond line to the adherend. Crack competition takes place, increasing the crack onset toughness, and the crack is deflected until it reaches an interface with a stiff layer, i.e. 0º ply, where delamination happens and the joint's fracture energy drops [5]. This crack deflection phenomenon can very clearly be observed in the fracture surface of the tested specimens. In Figure 2.16b, the fracture surface of a specimen with [90/45/-45/0]$_s$ layup as substrate can be seen. Each crack deflection phase is marked with numbers, from where differently orientated

fibers can be identified, marking the points from which the crack is deflected from one ply to another. Using the same numbers, these phases can be observed in the R-curve of Figure 2.16a, where fluctuations in the effective fracture toughness G_{eff} occur.

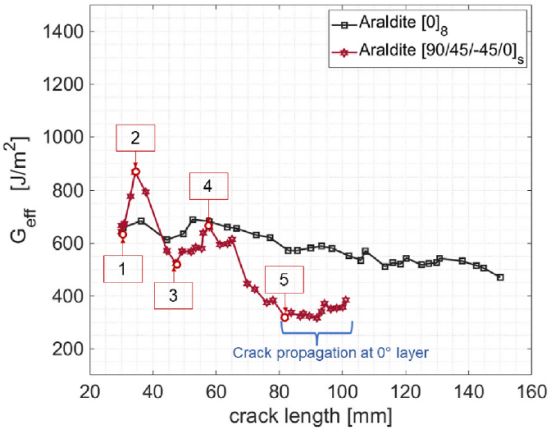

(a) R-curve.

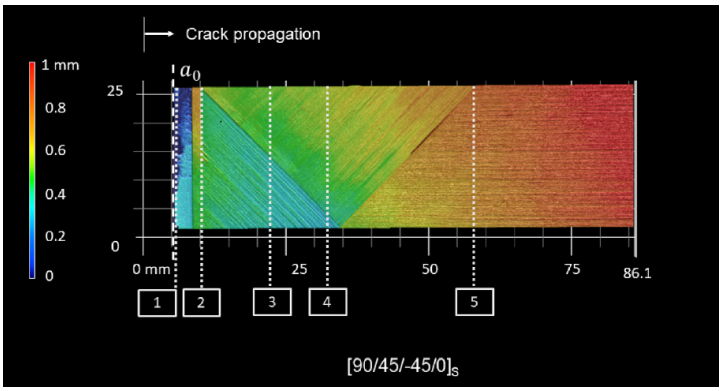

(b) Fracture surface topography.

Figure 2.16: [90/45/-45/0]$_s$ joint fracture behavior [5].

The toughness results obtained with the Araldite 2015 adhesive are illustrated in Figure 2.17a. In the two joints where the crack is deflected from the bond line into the substrate, represented by the red and green plot lines, a significant initial crack propagation toughness increase (and in the case of the green plot line, onset toughness) is observed compared to the remaining three joints, where cohesive failure of the adhesive occurred. However, after the crack reaches its final fracture location, the toughness drops below the other joints', as the substrate's delamination energy is lower than the cohesive crack propagation toughness.

The crack competition and deflection that is triggered at the crack onset and propagation, until final delamination takes place, results in a significant increase in joint toughness when compared to the cohesive failure's fracture energy.

The same crack competition and deflection mechanism was also found when the tougher adhesive material AF 163-2K (G_{Ic} = 2416 J/m^2 [5]) was used. However, due to the much higher toughness of the adhesive compared with the interlaminar fracture toughness of the composite substrates used, only in the joint with [0/90$_2$/0]$_s$ substrates did the crack competition and deflection that took place noticeably increase the joint's fracture toughness.

Using a unidirectional laminate, cohesive failure happened, leading to a high initiation and even higher propagation fracture energy due to the crack arrest features present in the adhesive material used. Using a [0/90$_2$/0]$_s$ laminate, however, the crack competition found between the composite substrate and adhesive material resulted in an increase of around 10% in mode I crack onset fracture energy

when compared to the already high cohesive fracture energy obtained with the unidirectional laminate [5].

After initiation however, the crack was deflected from the bond line to the substrate, where delamination occurred, reducting the fracture toughness to the delamination values found with the less tough, Araldite 2015 adhesive material.

The toughness results obtained with the AF 163-2K adhesive material, and more particularly the toughening effect observed in the $[0/90_2/0]_s$ substrate joint, can be seen in Figure 2.17b in the purple plot line; a peak in fracture toughness can be seen in the beginning, when it then drops to the lower plateau found for the remaining joints. The remaining laminates all failed by delamination with only slight increases in crack initiation fracture energy due to crack competition, but below the values found for the cohesive failure and $[0/90_2/0]_s$ joint's fracture initiation energies.

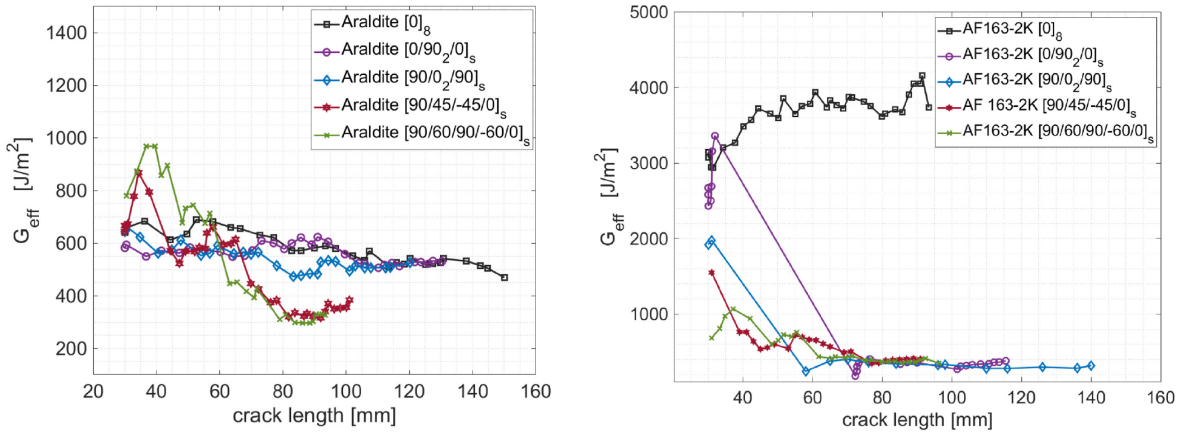

(a) Araldite 2015 (brittle) adhesive joints.

(b) AF 163-2K (tough) adhesive joints.

Figure 2.17: R-curve of CFRP joints [5].

In summary, Lima et al. [5] demonstrated that adhesive toughness, along with the substrate's ply angles and stacking sequence, significantly influences the activation of crack competition and deflection mechanisms. These mechanisms can lead to an increase in the fracture energy of adhesively bonded joints.

2.3.4. Tow-Based Discontinuous Composites

In recent years, new composites materials have been developed. One example of this are Tow-Based Discontinuous Composites (TBDC), which combine the high directional mechanical properties of FRPs with in-plane isotropy. This isotropy is achieved by placing randomly oriented thin tapes of fiber tows in a polymeric matrix [47], as can be seen in Figure 2.18. Taking into account the results obtained by Lima et al. [5] and reviewed in subsection 2.3.3, which have shown a toughening effect caused by crack competition due to stacked differently angled FRP plies, as well as the results and crack deflection observed for bonded composite joints with substrates made of thin plies obtained by Kupski et al. [20], the interest on the toughening effect of the novel Tow-Based Discontinuous Composite material arises.

Figure 2.18: Tow-based discontinuous composite representation [47].

As the name suggests, TBDCs are made from fiber tows, which are by nature thin. The combination

of these thin fiber tows in a TBDC significantly increases the local strength of the plies due to the thin-plies in-situ effect studied by Camanho et al. [45] and discussed in subsection 2.3.3. Furthermore, their tape discontinuity nature, allows for enhanced manufacturability making them suitable for large-volume industries [48, 49].

Katsivalis et al. [41] studied the damage mechanisms of adhesively bonded TBDC joints. For this, DCB tests, as well as SLJ tests were conducted with two distinct toughness adhesive materials. The results show that, for the tougher adhesive, all specimens resulted in failure in the TBDC substrate, this happens due to the high toughness of the adhesive material compared to that of the TBDC. On the other hand, in the specimens where low toughness adhesive is used, a combination of cohesive and substrate failure can be seen (Figure 2.20a) [41]. The damage mechanisms were analysed by post-mortem SEM and in-situ Acoustic Emissions (AE).

From the conducted in-situ and fracture surface analysis of the DCB specimens, it could be concluded that the most prevalent damage mechanisms found in the TBDC substrates are fibre breakage and matrix deformation. Due to the tape ends in the TBDC material, these damage mechanisms happen simultaneously at multiple locations over the bond area [41], promoting energy dissipation at several locations at the same time and, as expected, act as a toughening mechanism, increasing the joint's fracture toughness both for the crack onset and propagation phases.

The exceptionally low thickness of the tapes used to manufacture TBDC, on the other hand, makes for enhanced material strengths, compared to unidirectional FRP's, due to the same in-situ effect described in subsection 2.3.3. This effect promotes fiber pull-out, a high energy damage mechanism, delaying matrix cracking and delamination [41].

Figure 2.19 presents the measured mode I fracture toughness of the tested specimens. By comparing these values to the ones obtained by Lima et al. [5], for which the same adhesive materials were used, when damage is deflected and propagates through the composite substrates higher propagation fracture toughness can be observed for the TBDC specimens: while a fracture toughness of approximately 350 J/m^2 is evident for crack propagation in the joint substrates utilizing unidirectional CFRP plies (see Figure 2.17), a value of approximately 600 J/m^2 is observed for TBDC crack propagation (see Figure 2.19a) in Araldite 2015 joints.

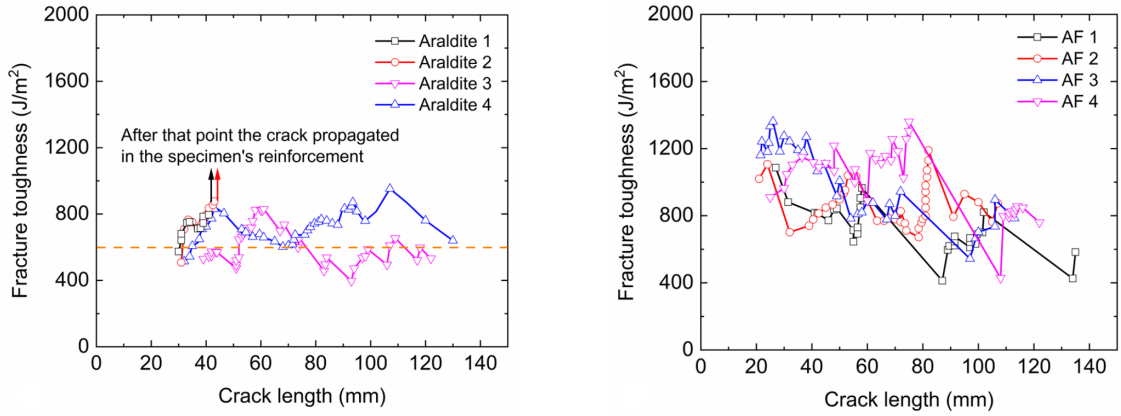

(a) Araldite 2015 (low toughness) adhesive joints.

(b) AF 163-2K (high toughness) adhesive joints.

Figure 2.19: R-curve of TBDC joints [41].

Characteristic fracture surfaces from TBDC substrates joined with Araldite 2015 and AF 163-2K can be seen in Figure 2.20. By visually analyzing the fracture surface, various simultaneous damage mechanisms can be identified, particularly when using the less tough adhesive Araldite 2015. A combination of cohesive failure and substrate failure is evident in these observations (see Figure 2.20a).

When using the tougher AF 163-2K, however, only substrate failure was obtained. From the fracture surface presented in Figure 2.20b, multiple thin tapes that constitute the TBDC material can be identified, showing how multiple damage must be developed and propagated at the same time in order to

fracture the material. The high scattering observed in the R-curves presented in Figure 2.19 can be explained by the simultaneous presence of multiple damage mechanisms.

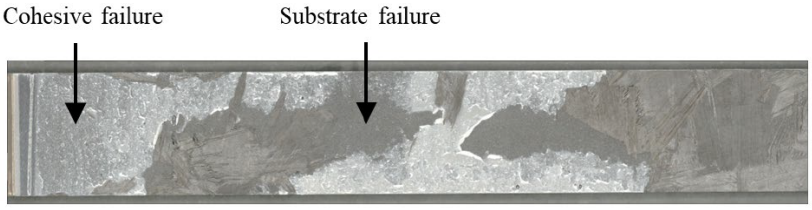

(a) Araldite 2015 (brittle) adhesive joints.

(b) AF 163-2K (tough) adhesive joints.

Figure 2.20: Characteristic TBDC joint DCB fracture surfaces [41].

Using TBDC as a replacement for unidirectional FRP plies based composite laminates however is not a solution in most applications.

By laying up UD FRP plies in different orientations it is possible to tailor the resulting composite material for specific applications. This tailorability aspect of FRP materials are what makes them so sought after and lightweight: by having a resulting anisotropic material with optimized mechanical properties in the most critical load bearing directions, the others may be minimized. This directional optimisation of material properties is lost when TBDC is used due to its in-plane isotropy. Thus, the simple replacement of unidirectional FRP plies by TBDC material would, most likely and in cases where anisotropic laminates are used, result in higher weight components.

Nonetheless, this does not mean that TBDC can't be used to make for tougher adhesively bonded composite joints. To the best of the author's knowledge and at the time of redaction of the present document, there is no research on the use of TBDC material as a toughening interleaving material (like the interleaving materials of subsection 2.3.2). The results and conclusions obtained by Katsivalis et al. [41], however, show that it might be used in such a way, avoiding some of the drawbacks associated with other studied interleaving materials such as corrosion and added weight concerns.

2.4. Research gap

Limited but promising research into the effects of the composite substrates properties on the toughness of adhesively bonded composite joints has been conducted.

The results show that by promoting energy dissipation by the means of crack competition and deflection between the bond line and the composite substrate, it is possible to increase the fracture toughness of joints, even those that feature high toughness adhesive materials [5, 20]. However, it can also be observed that this toughening effect is mostly able to increase the fracture energy at crack onset and initial propagation until delamination in the composite substrate takes place, especially using tougher adhesives.

Cohesive failure, particularly with high-toughness adhesives and those incorporating toughening features as reviewed in subsection 2.3.1, typically results in high crack propagation toughness values. However, substrate damage may still occur due to the use of very high-toughness adhesives or weak bonds within the joint. In such cases, improving the low toughness values observed during crack propagation in the substrate becomes highly desirable.

By confining the crack within high fracture propagation toughness layers, the crack deflection mechanism examined by Lima et al. can be utilized to substantially increase the crack onset fracture tough-

ness, while avoiding the low toughness values observed during substrate delamination.

As the delamination fracture energy governs the low crack propagation energy values observed when a crack is developed in an adhesively bonded composite joint's substrate, to toughen a composite joint in such circumstances, it would be beneficial to work towards increasing the substrate's delamination energy. Increasing a composite laminate's delamination energy can be done, as seen in subsection 2.3.2, by using interlaminar toughening mechanisms.

TBDC has been researched in the context of adhesively bonded joints [41]. From the results obtained, a direct comparison between the fracture propagation energy in the substrate can be made with traditional CFRP laminates tested by Lima et al. [5], from which substantially higher values are seen using TBDC. A promising potential of this novel material as an interlaminar fracture toughness mechanism for CFRP laminates can be foreseen, due to its multiple thin tapes which, through the higher in-situ strengths, matrix cracking and fiber breakage at multiple locations, promote crack competition and, subsequently, energy dissipation.

To the best of the author's knowledge, there is currently no published research addressing the toughening effect of TBDC interleaves in composite laminates. Additionally, the literature does not contain studies on enhancing the fracture toughness of adhesively bonded composite joints through interlaminar toughening mechanisms within the composite substrates. Consequently, this work seeks to investigate the impact of toughening and crack arrest features in the composite substrate — particularly focusing on TBDC as substrate toughening interleaves — on the fracture toughness of bonded joints.

3

Research Questions & Objective

In the wake of the literature study presented in chapter 2 and the existing research gap, two main research questions and a research objective pertaining to the ever increasing concern of mitigating sudden failure risk of adhesively bonded composite joints were formulated.

3.1. Research Objective

Taking into account the literature review done and the identified research gap, the following research objective was formulated.

To increase the mode I fracture toughness of adhesively bonded joints using CFRP substrates toughened with Tow-Based Discontinuous Composite interleaves.

To justify the choices made in the definition of the present MSc. thesis research objective, it is important to focus on three main points: (i) the choice of mode I fracture toughness as the main optimising parameter, (ii) the choice of CFRP as the base material for the used joint substrates and (iii) the choice of TBDC interleaves as a toughening mechanism.

As reviewed before, even though mode I loading might not be the most representative loading and fracture mode present in operational joints, it is usually regarded as the most critical. To first get a basic understanding on how the proposed mechanisms can increase adhesively bonded composite joints' fracture toughness it is important to study how the mode I fracture toughness is affected before moving on to study more complex and representative mixed-mode loadings.

Secondly, carbon fiber reinforced polymers being the most used composite materials in aircraft structures [50] due to their exceptional strength-to-weight ratio, lead to the choice of materials in the research objective and questions to be answered.

Finally, the observed high delamination energy of TBDC as substrate in the context of adhesively bonded joints and the fact that these novel, isotropic composite materials are being increasingly researched in recent years due to their high mechanical properties, isotropy and enhanced manufacturability, were taken into account. In addition, TBDC being made from the same outstandingly lightweight carbon fibers and polymers of traditional CFRPs, a close to negligible effect on the weight of the original laminates is expected, coupled with the fact that any concerns such as corrosion are eliminated, compared to some of the researched interleaving materials such as stainless steel fibers. TBDC was thus chosen as a composite laminate interleaving material with the aim to reach the presented research objective.

By taking advantage of the crack competition and deflection toughening mechanisms studied by Lima et al. [5], and enhancing the fracture toughness drop observed in substrate crack deflected joints by the use of Tow-Based Discontinuous Composite interleaves at 0-degrees ply interfaces, an overall toughening effect in adhesively bonded composite joints is expected.

3.2. Research Questions

To reach the research objective, the main problem must be divided into more specific sub-problems, which are addressed through two primary research questions, each with three associated sub-questions. Addressing each of the six sub-questions will enable a structured approach to understanding the research topic, ultimately supporting a well-founded conclusion.

To begin, due to the limited research on using TBDC as interlaminar toughening in composite laminates, it was essential to develop the first research question, targeting the initial understanding of TBDC's impact on fracture toughness.

- **How do TBDC interleaves affect the mode I fracture behavior of CFRP laminates?**

To fully understand the topic and answer the presented research question, three subquestions were formulated as the following:

1. *How do the fracture mechanisms manifest during TBDC crack propagation in TBDC interleaved CFRP laminates?*
2. *How do TBDC interleaves affect the mode I fracture toughness of CFRP laminates?*
3. *How does the amount of TBDC interleaves affect the mode I fracture toughness of CFRP laminates?*

To develop a broad understanding of how TBDC layers might affect CFRP laminates' mode I fracture behavior, it's essential to examine the specific fracture mechanisms activated by crack propagation within TBDC materials, how these mechanisms impact fracture toughness, and the influence of TBDC layer quantity.

Studies on Tow-Based Discontinuous Composites (TBDC), particularly those on mode I crack propagation in TBDC joints, suggest that observable mechanisms like crack competition between TBDC tapes, as well as fiber bridging, may occur during crack propagation. Given the fracture toughness values reported in studies such as those by Katsivalis et al. [41], the incorporation of TBDC interleaves is anticipated to yield substantial gains in fracture toughness within CFRP laminates. These studies indicate that crack propagation in TBDC often requires significantly higher fracture propagation energies compared to cracks advancing between unidirectional CFRP plies, thus highlighting TBDC's toughening potential.

Additionally, based on previous research concerning the inclusion of interleaving materials within composite laminates, such as the studies by Quan et al. [16] and Lee et al. [18, 19], increasing the number of TBDC interlayers may further amplify present toughening mechanisms. As the number of interleaves increases, so too should the activation of expected toughening mechanisms, including matrix cracking, fiber breakage, and crack competition. The presence of more tape ends within the composite laminate is expected to enhance energy dissipation, ideally reaching fracture toughness levels near those of pure TBDC laminates.

After having an idea of how TBDC interleaves can toughen CFRP laminates and increase their delamination energy, a further step can be taken and the use of TBDC interleaves in the context of adhesively bonded composite joints can be studied. The second main research question was then conceived as the following:

- ***How do TBDC interleaves in the CFRP substrates affect the mode I fracture behavior of adhesively bonded joints?***

To answer the research question, three subquestions were formulated as the following:

1. *How does the flexural modulus of TBDC interleaved CFRP substrate layups influence the mode I fracture mechanisms in adhesively bonded joints?*
2. *How do TBDC interleaved CFRP substrate layups influence the mode I fracture toughness of adhesively bonded joints?*
3. *How does the adhesive toughness influence the mode I fracture toughness of adhesively bonded CFRP joints with TBDC interleaved substrates?*

The anticipated toughening effect of TBDC interleaves in bonded joints depends largely on crack competition and deflection from the bond line into the toughened substrate. Reviewing literature reveals that composite layup configurations and adhesive toughness are the key variables expected to affect these mechanisms.

Different laminate stacking sequences and TBDC interleaves can modify a joint's substrates' flexural moduli, which may, in turn, impact crack competition at the bond line. According to the literature, high peel stresses, particularly in joints with low flexural modulus substrates, positively impact the crack competition mechanism and may influence crack deflection [5]. Increasing the flexural modulus of a joint substrate by adding TBDC material interleaves may reduce the likelihood of activating these fracture mechanisms, thereby limiting the exploring of potential TBDC toughening fracture mechanisms.

Laminates with ply orientations near 90° are anticipated to encourage crack deflection, thus engaging toughening mechanisms. However, this comes with a trade-off: low stiffness substrates from such ply orientations can lead to uncontrolled crack deflection, resulting in low-energy failure. A balance in laminate layup, therefore, is essential for effective toughness enhancement.

Adhesive choice similarly affects toughening behavior. Using less tough adhesives risks cohesive failure and may limit the ability to fully utilize the TBDC material's toughening potential. In contrast, high-toughness adhesives promote crack deflection, enabling exploration of TBDC's toughening potential, although they reduce the toughening effect from crack competition and deflection away from the bond line into the substrate. Thus, optimizing these elements — substrate layup, flexural stiffness, and adhesive toughness — is fundamental to leveraging both crack deflection and competition in achieving improved fracture toughness.

Ultimately, understanding these aspects answers crucial sub-questions, building toward the primary research objective.

3.3. Methodology

To address the conceived research questions and achieve the formulated research objective, a methodology was established based on the literature review.

Given the pressing need to enhance secondary bonding techniques for certification in civil aviation, all experimental procedures on adhesively bonded joints will be conducted on secondary bonded specimens. Since the primary focus of the research project is on mode I fracture toughness, experimental tests will be executed under mode I loading conditions, adhering to the ASTM D5528 [37] and ISO 25217 [36] standards, utilizing DCB tests. As per these standards, a minimum of four specimens will be manufactured and tested for each configuration.

To investigate the effect of TBDC interleaves on the mode I fracture toughness of composite laminates, UD/TBDC ply hybrid DCB specimens will be produced with three varying amounts of Tow-Based Discontinuous Composite interlayers positioned in the crack plane, tested based on ASTM D5528 [37].

The second research question will be approached differently, employing two separate testing methodologies. Four different CFRP layups will be bonded using two different adhesive materials and assembled as DCB specimens. One specimen series will utilize a high-toughness adhesive (AF 163–2U), while the other will use a less tough adhesive (Araldite 2015-1) to examine the adhesive toughness's effect on the expected toughening effect of the interleaves on the substrate. TBDC interleaves will be integrated at the interfaces where delamination is anticipated, particularly between compliant and stiff plies, such as 0-degrees ply interfaces. Additionally, the flexural stiffness of the DCB arm laminates will be obtained by conducting three-point bending tests on the same TBDC interleaved layups, following ASTM D7264 [51]. Given the uncertainty in analytical methods for determining the flexural modulus of discontinuous tape composite laminates, experimental procedures will be necessary to yield more accurate flexural modulus values for the manufactured composite laminates.

In all DCB tests conducted, besides obtaining the expected R and load-displacement curves for quantitative assessment of the research questions and objectives, the fracture surfaces will be visually analyzed to identify damage and toughening mechanisms present in each specimen. By executing the aforementioned series of tests, a comprehensive understanding of how TBDC interlayers in compos-

ite laminates and bonded joints influence their mechanical and joint properties should be achieved, thereby answering the research questions and ideally fulfilling the research objective.

The methodology used for the experimental investigation of the present thesis research will be covered more in depth in chapter 4 and chapter 5.

4

Test Specimen Design & Manufacturing

This chapter discusses the design, manufacturing processes, and condition of the test specimens. The rationale behind the selection of materials, design choices, and manufacturing methods is provided for the UD/TBDC ply hybrid CFRP laminates and adhesively bonded joint specimens used to address the research questions.

4.1. Specimen design

This section will outline the choice of CFRP, TBDC and adhesive materials, followed by the selection of layups and the dimensions of the manufactured test specimens.

4.1.1. Material selection

The UD carbon fiber prepregs Hexply AS4-8552 were the UD ply CFRP material selected for the manufacturing of the composite laminates. The mechanical properties of this CFRP material are summarized in Table 4.1. Each prepreg ply has a nominal cured thickness of 0.15 mm, as reported in literature [5].

Table 4.1: Hexply AS4-8552 mechanical properties [5].

Property	Symbol	Value	Units
Longitudinal modulus	E_{11T}	141	GPa
Transverse modulus	$E_{22T} = E_{33T}$	10	GPa
In-plane shear modulus	$G_{12} = G_{13}$	5.2	GPa
Transverse shear modulus	G_{23}	3.33	GPa
In-plane Poisson's ratio	$\nu_{12} = \nu_{13}$	0.27	-
Transverse Poisson's ratio	ν_{23}	0.5	-
Longitudinal tensile strength	X_T	2207	MPa
Longitudinal compressive strength	X_C	1531	MPa
Transverse tensile strength	Y_T	81	MPa
In-plane shear strength	$S_{12} = S_{13}$	114	GPa

Tow-Based Discontinuous Composite preforms, manufactured by Oxeon AB, made of 20 μm thick, 20 mm wide and 40 mm long tapes, will be used. Stacks of around 20 layers of tow-based tapes are made, making for 0.4 mm thick TBDC preforms, using HS40 carbon fibers in their fabrication. Due to the unavailability of mechanical properties for the specific TBDC material in this thesis, values derived from TBDC made with MR70 fibers are provided instead.

HS40 fibers present around 40% higher strand stiffness and 35% lower strand strength than MR70 fibers [52, 53]. Given the literature reported estimated fiber volume fraction of 60% in this type of

TBDC materials [48], comparable mechanical properties are expected.

Table 4.2: MR70 TBDC and UD tape mechanical properties [48].

Property	Symbol	Value	Units
UD tape longitudinal modulus	E_{11T_t}	172 ± 5	GPa
UD tape transverse modulus	$E_{22T_t} = E_{33T_t}$	8.11 ± 0.05	GPa
UD tape in-plane shear modulus	$G_{12_t} = G_{13_t}$	2.98	GPa
UD tape in-plane Poisson's ratio	$\nu_{12_t} = \nu_{13_t}$	0.35 ± 0.03	-
TBDC in-plane modulus	$E_{11T} = E_{22T}$	70.0	GPa
TBDC in-plane Poisson's ratio	$\nu_{12} = \nu_{13}$	0.27	-

Two different adhesive materials will be employed: the low-toughness bi-component epoxy-based Araldite 2015-1 and the high-toughness film epoxy-based AF 163-2U, their mechanical properties are summarized in Table 4.3. This selection was based on documented crack competition and deflection mechanisms in joints using these adhesive materials.

Table 4.3: Adhesive materials mechanical properties.

Property	Symbol	Value		Units
		Araldite 2015-1	AF 163-2U	
Tensile strength	X_T	22[a]	48[b]	MPa
Tensile modulus	E_T	1850[a]	1110[b]	MPa
Poisson's ratio	ν	0.33[a]	0.34[b]	-
Mode I fracture toughness	G_{Ic}	640[c]	1924[c]	J/m^2

[a] Katsivalis et al. [41].
[b] Teixeira de Freitas et al. [54].
[c] Lima et al. [5].

4.1.2. Layups design

Composite laminates will be manufactured into DCB specimens to answer the first research question. For the second research question three-point bending and DCB specimens will be produced.

This section will present and explain the layup design of test specimens for each research question.

UD/TBDC ply CFRP laminates

In order to study how TBDC interleaves can influence crack initiation and propagation behavior in a composite laminate, CFRP laminates with TBDC layers around a pre-defined crack plane were designed. A schematic that represents the selected UD/TBDC ply hybrid CFRP laminates can be seen in Figure 4.1, where *0* corresponds to 0-degrees UD AS4-8552 plies and *TBDC* to Tow-Based Discontinuous Composites material plies, for which the ply angle is inconsequential since the plies can be considered to be in-plane isotropic. The designed layups are summarized in Table 4.4.

Table 4.4: UD/TBDC ply CFRP DCB layups.

Layup	TBDC volume fraction [%]	Thickness [mm]
$[0_{24}]$	0	3.6
$[0_{12}/TBDC_2/0_{12}]$	18	4.4
$[0_{12}/TBDC_4/0_{12}]$	31	5.2

Following ASTM D5528 [37], unidirectional laminates will be used to keep the crack propagation as close to the mid-plane and the fracture as close to pure mode I fracture as possible. Furthermore, by utilizing unidirectional laminates with highly direction-dependent mechanical properties, the effect of

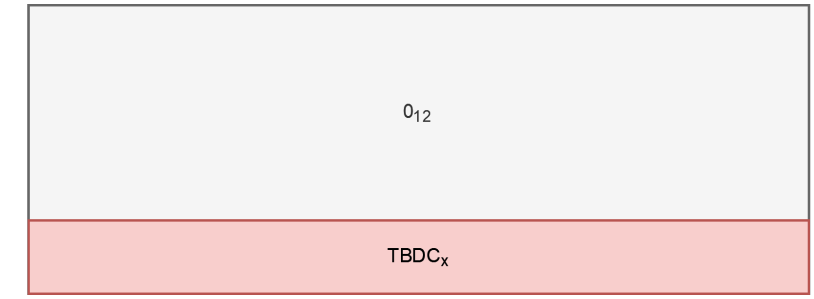

Figure 4.1: TBDC interleaved CFRP laminate schematic.

TBDC, an in-plane isotropic material, on the mode I fracture toughness of composite laminates can be more clearly understood and discussed due to the reduced number of variables involved.

The number of CFRP layers in the designed layups was chosen to be able to study different amounts of TBDC material interleaving in composite laminate's mode I fracture toughness, while generally complying with the ASTM D5528 [37] recommended specimen dimensions. The first layup is a non-toughened configuration, composed entirely of AS4-8552 CFRP prepreg, while the second and third layups contain 18% and 31% TBDC volume fractions, respectively. Although these volume fraction values may appear high, they are justifiable given the thickness of each TBDC pre-form, which is 0.4 mm, as noted in subsection 4.1.1.

To facilitate the inclusion of a starting crack in the mid-plane of the laminates, an even number of TBDC layers must be used; thus, 2 and 4 layers were selected for testing. Furthermore, since the third layup exceeds the recommended maximum thickness of 5 mm, it was not possible to add more CFRP layers without increasing the TBDC volume fraction.

TBDC-toughened adhesively bonded joints

Four different joints were designed to study the effect of TBDC interleaved composite laminates on adhesively bonded joints' mode I fracture behavior. The selected joint substrate layups are summarized in Table 4.5, with UD CFRP plies represented by their ply angles and TBDC plies labeled as *TBDC*. Each substrate layup will include two 0.4 mm thick TBDC layers, resulting in a volume fraction of approximately 35% to 40%.

Table 4.5: TBDC-toughened adhesively bonded joints DCB design.

Substrate layup	Substrate TBDC volume fraction [%]	Adhesive material used		Joint thickness [mm]
		Araldite 2015-1	AF 163-2U	
$[0_8]$	0		x	2.7
$[90/45/-45/TBDC/0]_s$	40	x		3.5
$[90/60/90/-60/TBDC/0]_s$	35	x		4.1
$[0/TBDC/90_2/0]_s$	40		x	3.5

Lima et al.'s research on the effect of substrate layup on the mode I fracture toughness of adhesively bonded joints [5] provides extensive analysis of damage behavior and crack propagation paths in tailored layups. From the layups studied, three were selected based on their crack propagation paths and reported toughening results, which allow for the introduction of TBDC material plies to potentially enhance the toughening fracture mechanisms.

High-angle oriented plies near the initiation crack in the adhesive can induce crack competition and deflection, leading the crack to propagate through the composite substrate. This behavior can result in a crack onset toughening effect. Once the crack deflects from the bond line, it typically travels through the laminate until reaching a 0-degrees ply, where delamination occurs, significantly reducing fracture energy [5].

In the current MSc. thesis project, the aim is to enhance the reduction in fracture toughness after an initial toughening phase by utilizing the damage mechanisms inherent in TBDC, as studied by Katsivalis et al. [41]. As the crack reaches a 0-degrees ply interface, it will have to traverse through TBDC instead of traditional UD CFRP delamination.

The crack path documented by Lima et al. [5] in the $[90/45/-45/TBDC/0]_s$ substrate joint using Araldite 2015-1 adhesive is illustrated in Figure 4.2, alongside the path observed in the $[0/90_2/0]_s$ substrate joint with the tougher AF 163-2K adhesive in Figure 4.3. Notably, a similar behavior to that in Figure 4.2 was evident in the $[90/60/90/-60/0]_s$ substrate joint using Araldite 2015-1, where the crack propagated through the substrate until reaching the -60/0 degrees plies interface, leading to the final fracture.

The AF 163-2K adhesive material differs from the AF 163-2U to be used in this study in that the K version includes an integrated carrier, while the U version does not. The carrier in the K version has been shown to enable crack bridging mechanisms that enhance fracture toughness as the adhesive crack propagates [5]. However, the epoxy adhesive base and mechanical properties of both versions are similar. Therefore, a comparable crack initiation and propagation behavior, particularly regarding the crack path, is expected with the AF 163-2U adhesive.

By introducing a TBDC layer at the final fracture interface, as depicted in the figures, an enhancement in the final crack propagation behavior is anticipated. This rationale supports the strategic placement of TBDC within the substrate layups presented in Table 4.5.

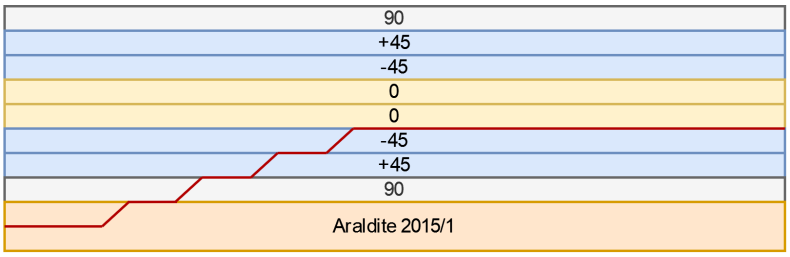

Figure 4.2: Observed crack propagation path - $[90/45/-45/0]_s$ substrate Araldite 2015-1 joint.

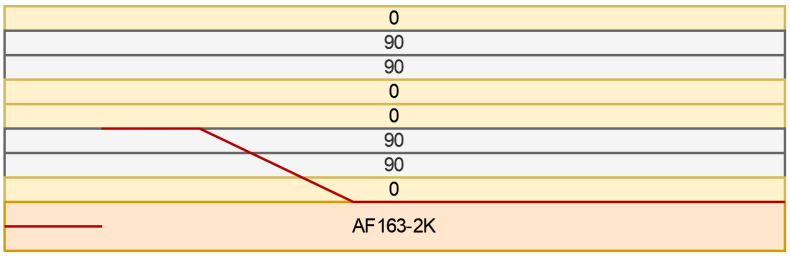

Figure 4.3: Observed crack propagation path - $[0/90_2/0]_s$ substrate AF 163-2K joint.

A UD joint specimen design will be used to measure the cohesive fracture energy of the AF 163-2U adhesive material, providing a baseline for comparison with toughened substrate joints. No baseline is necessary for the Araldite 2015 adhesive, as consistent results are documented in the literature [5, 55].

Looking at literature results [5], with the less tough Araldite 2015-1 adhesive, $[0/TBDC/90_2/0]_s$ layup substrate joints are expected to fail cohesively. As such, results akin to those obtained with the UD substrate joints should be observed, without exploiting any of the crack deflection onset toughening or expected TBDC toughening mechanisms. Thus, this layup will not be bonded using Araldite 2015-1.

In contrast, starting cracks in the other two joint layups are expected to deflect from the adhesive layer to the substrate, benefiting from crack deflection toughening, as depicted in Figure 2.17a. Their TBDC-toughened counterparts will be bonded with Araldite 2015-1.

Using the tougher AF 163-2U adhesive, all designed joints except for the UD substrate joint are anticipated to experience crack competition and deflection from the adhesive bond line to the composite substrate. However, due to the adhesive's high fracture toughness, significant toughness increases from the crack competition and deflection mechanisms are not expected in the $[90/45/-45/TBDC/0]_s$ and $[90/60/90/-60/TBDC/0]_s$ substrate joints, as illustrated in Figure 2.17b. The final fracture energy for all crack-deflected joints is projected to be similar.

Consequently, only the $[0/TBDC/90_2/0]_s$ layup will be joined with AF 163-2U. The slight crack onset toughening reported in research [5] through crack deflection justifies the study of TBDC interleaving effects in this specific joint. Furthermore, from observing Figure 2.17b, the anticipated final failure toughening effect from the TBDC layers is expected to be similar across all layups using the AF 163-2U adhesive, making further testing of the other two substrates redundant.

Finally, three-point bending tests will be performed on the adhesively bonded joints substrate laminates in order to obtain the DCB arms' flexural modulus. The laminate layups and respective thicknesses are provided in Table 4.6.

Table 4.6: Three-point bending specimen layups.

Layup	Thickness [mm]
$[0_8]$	1.20
$[90/45/-45/0]_s$ (2022)	1.20
$[0/90_2/0]_s$ (2022)	1.20
$[90/45/-45/TBDC/0]_s$	1.60
$[90/60/90/-60/TBDC/0]_s$	1.90
$[0/TBDC/90_2/0]_s$	1.60

The laminates marked with *(2022)* after the stacking sequence were manufactured for Lima et al.'s study [5] using the same AS4-8552 CFRP material. By comparing the flexural modulus of TBDC-toughened CFRP laminates with those lacking TBDC toughening, it is be possible to assess how the inclusion of TBDC layers in UD ply CFRP laminates impacts their flexural modulus. This comparison will also provide insights into how these changes might influence the mode I fracture behavior of adhesively bonded joints. It should be noted that the $[90/60/90/-60/0]_s$ laminate did not not undergo three-point bending tests due to its unavailability.

4.1.3. Specimen geometry

DCB and three-point bending specimens will be manufactured for the two types mechanical tests to be performed. As such, their geometries will be presented separately.

DCB specimens

DCB specimens will be used to study the mode I fracture toughness of both UD/TBDC ply CFRP laminates as well as adhesively bonded joints. The DCB specimen geometries can be seen in Figure 4.4. According to ISO 25217 [36], the adhesive layer must be between 0.1 mm and 1 mm thick; the chosen adhesive material layer thickness for adhesively bonded joint specimens was of 0.3 mm.

Given the similarity between the ASTM D5528 [37] and ISO 25217 [36] standards for measuring mode I fracture toughness in unidirectional laminates and adhesive joints, respectively, ASTM D5528 will be used as the reference standard for both sample types moving forward.

To mitigate large opening displacements at crack onset in specimens with high mode I fracture toughness to arm flexural modulus ratios, such as the $[0/TBDC/90_2/0]_s$ substrate AF 163 joints, a shorter initial crack length a_0 than the standard 50 mm was selected, as recommended by ASTM D5528 [37]. Additionally, the chosen geometry ensures direct comparability with results for non-toughened samples reported in the literature. To maintain consistency across all tests, the same DCB specimen geometry will be applied to all samples.

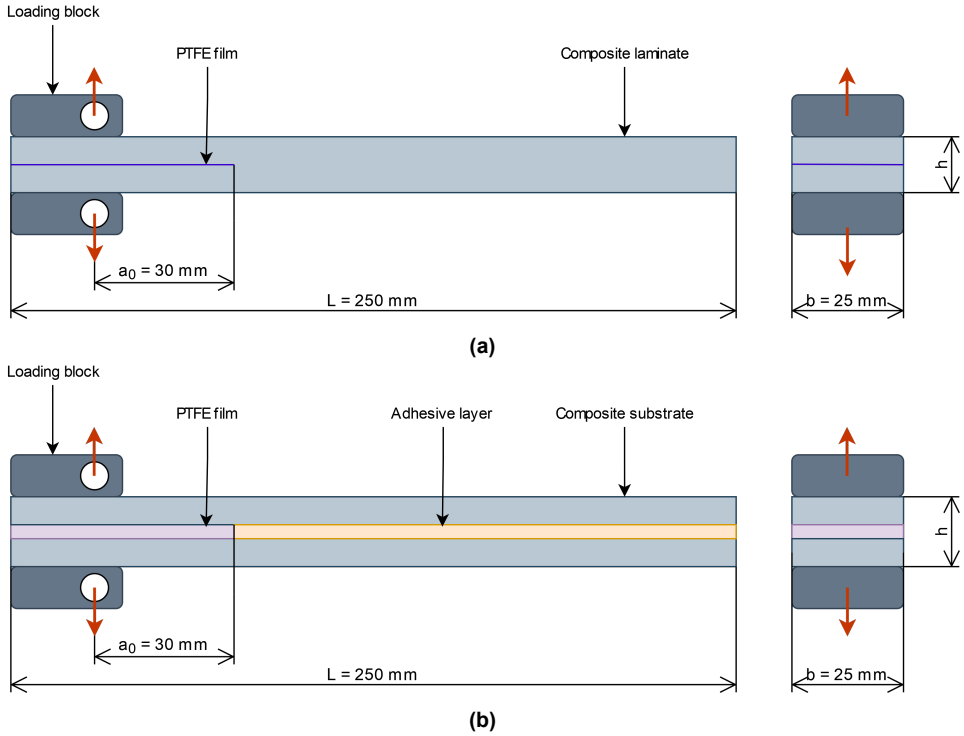

Figure 4.4: UD/TBDC ply laminate (a) and TBDC-toughened adhesive joint (b) specimen geometries.

Three-point bending specimens

The three-point bending specimen geometry can be seen in Figure 4.5. The thickness h of each test sample is correspondent to the joints substrate laminate thickness as seen in Table 4.6.

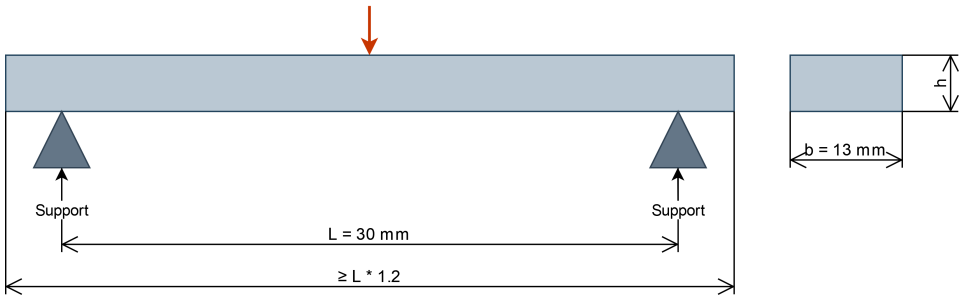

Figure 4.5: Three-point bending specimen geometries.

The recommended width of 13 mm from ASTM D7264 [51] is used, while the support span L is determined based on a 16:1 ratio of span-to-thickness, as suggested by the standard. A span of 30 mm was selected as a suitable compromise, balancing compliance with the standard's test span recommendations, the limitations of the test setup, and the desire to maintain uniformity across the test setup for all samples.

4.2. Laminate curing cycle

The UD and UD/TBDC hybrid ply CFRP laminates will be cured in an autoclave at 7 bar of pressure and 110 ºC for 60 minutes, followed by 120 minutes at 180 ºC, as seen in Figure 4.6.

The main focus is to ensure comparable results to those of AS4-8552 CFRP joints that exhibited crack deflection in published literature, while maintaining consistent manufacturing processes across all samples. Thus, although the literature reports press molding curing for TBDC preforms, the recommended autoclave curing cycle [5] for AS4-8552 CFRP laminates will be used. In order to confirm the cure

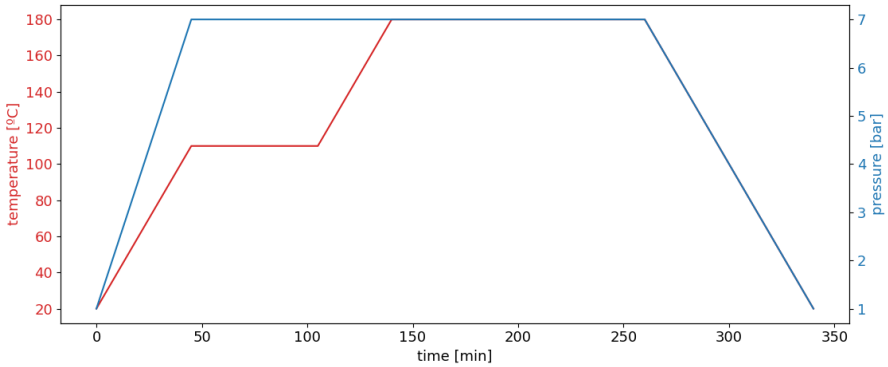

Figure 4.6: CFRP laminates autoclave curing cycle.

cycle's compatibility with the TBDC material and increase confidence in the curing of UD/TBDC hybrid laminates, thermal analyses were conducted on both the TBDC material and the AS4-8552 prepreg material.

A Thermogravimetric Analysis (TGA) was performed on the TBDC material to ensure it would not decompose at the temperatures associated with the cure cycle. Differential Scanning Calorimetry (DSC) analyses were carried out on both the TBDC and AS4-8552 prepreg materials to compare their curing time frames. Furthermore, to compare the recommended [48] and selected cure cycles for uncured TBDC material, DSC analyses were conducted using both temperature profiles.

4.2.1. Thermogravimetric analysis (TGA)

As previously mentioned, a Thermogravimetric Analysis (TGA) was conducted to determine the thermal decomposition temperature of the TBDC material. A *PerkinElmer* TGA 4000 machine was used.

Literature reports curing at a temperature of 150 ºC through press molding for TBDC material with MR70 fibers [48]. Given the elevated curing temperature of the chosen autoclave curing cycle with a maximum temperature of 180 ºC, it is crucial to assess whether thermal decomposition may occur at the intended curing conditions.

To achieve this, a TGA was conducted on uncured TBDC material, heating the sample from 30 ºC to 900 ºC at a rate of 10 ºC/min. The results are presented in Figure 4.7, where the unsubtracted sample mass refers to the combined mass of the TBDC sample and the crucible (sample holder). Since the crucible's material remains stable throughout the TGA temperature range, the observable mass loss corresponds solely to the TBDC sample, eliminating the need to subtract the crucible's mass for this analysis.

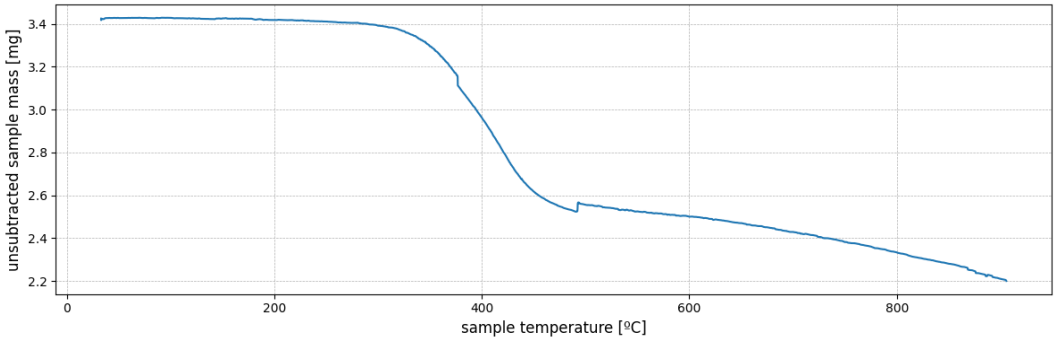

Figure 4.7: Thermogravimetric analysis of uncured TBDC material.

Figure 4.7 plots the sample's mass as a function of its temperature. A significant reduction in mass occurs at around 300 ºC, indicating significant thermal decomposition of the TBDC material. This

decomposition temperature is well above the highest temperature used in the cure cycle, set at 180 ºC, suggesting thermal stability of the TBDC material throughout the curing process. Therefore, no thermal decomposition is anticipated during the curing of TBDC when using the recommended AS4-8552 prepreg curing cycle [5] for the hybrid laminates.

4.2.2. Differential scanning calorimetry (DSC) analysis

The DSC, which measures heat flow in a sample over time and temperature, was used to evaluate the curing start and end times, enthalphy and glass transition temperature (T_g) of materials. Two analyses were performed on a *TA Instruments* mDSC250 machine:

1. Comparison of reaction enthalpy and T_g for TBDC using the recommended curing cycles for AS4-8552 prepreg [5] and TBDC material [48].
2. Comparison of TBDC and AS4-8552 curing time frames with the selected curing cycle, as recommended for AS4-8552 prepreg material [5].

For the first analysis, uncured TBDC samples were prepared for each DSC run. Both followed a ramp-up of 2 ºC/min from room temperature, with an isothermal phase of 120 minutes, cooling at 10 ºC/min, and a final heating at 10 ºC/min. The difference between them lay in the isothermal temperature: one at 150 ºC, as per the recommended TBDC material curing cycle [48], and the other at 180 ºC, as per the recommended AS4-8552 prepreg material curing cycle.

The initial ramp-up and isothermal phase were utilized to compare the curing enthalpies. Setting aside pressure effects, the literature suggests that the 150 ºC curing temperature should complete the reaction within less than two hours [48]. By comparing other temperature results, the extent of curing can be assessed. The final ramp-up was used to compare the glass transition temperatures after different curing temperatures. Based on the 150 ºC curing cycle being safe, any significant variations in T_g could indicate whether material degradation occurred during higher temperature curing.

The results from the first analysis can be seen in Figures 4.8 and 4.9.

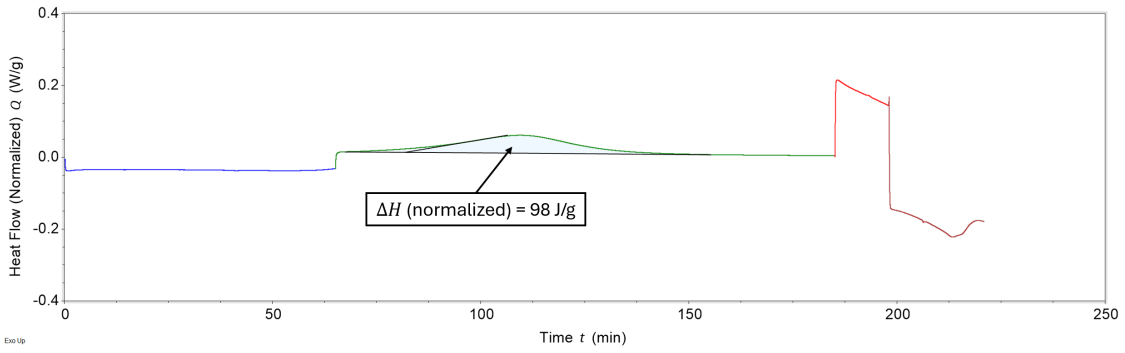

(a)

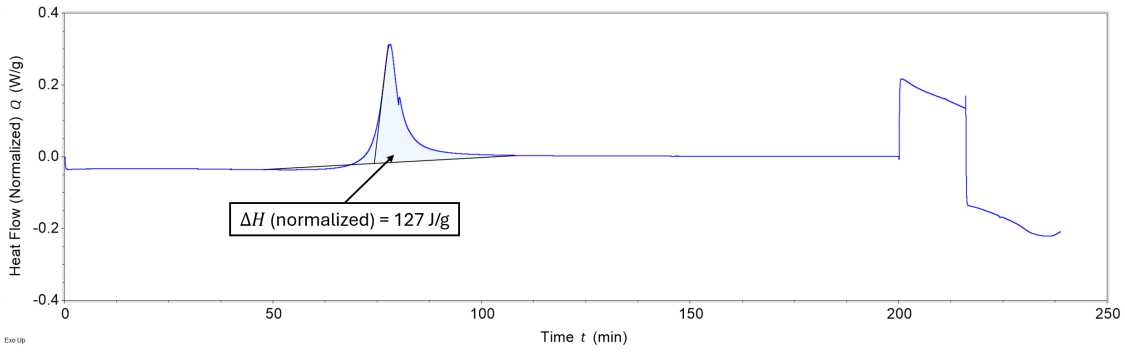

(b)

Figure 4.8: Isothermal 150 ºC (a) and 180 ºC (b) DSC run: TBDC material's curing enthalpy.

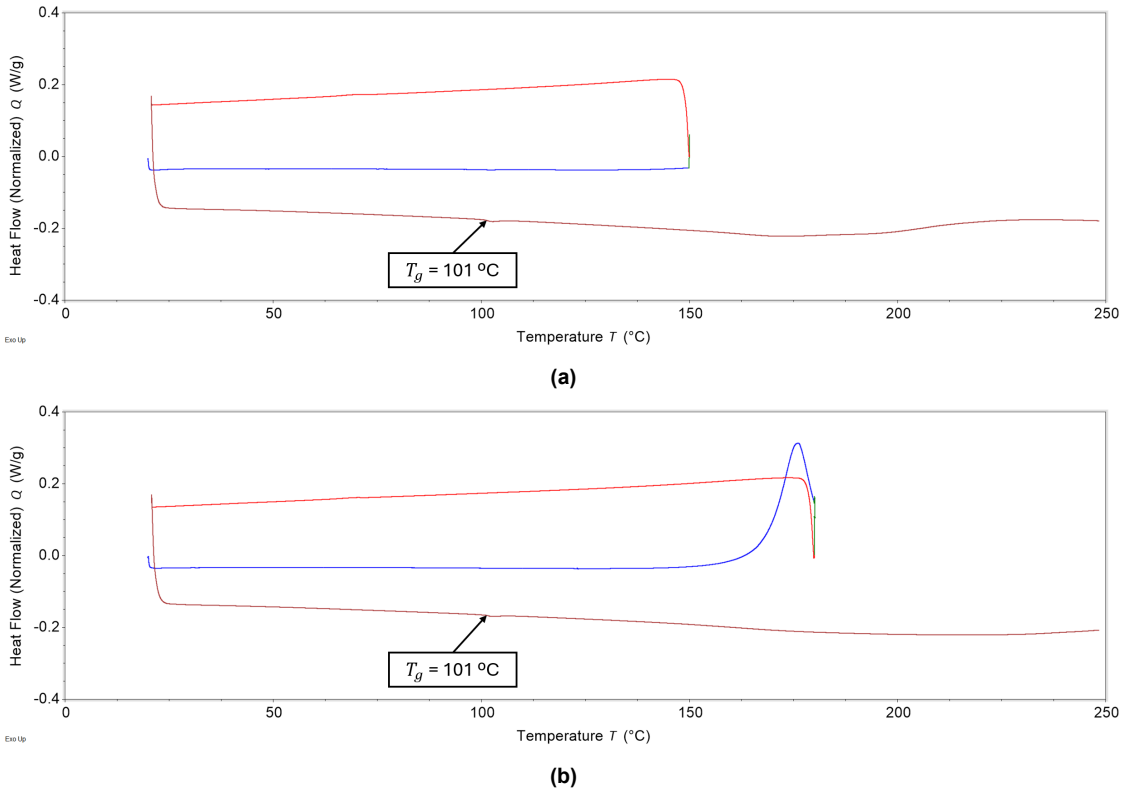

Figure 4.9: Isothermal 150 ºC (a) and 180 ºC (b) DSC run: TBDC material's T_g.

As shown in Figure 4.8, which plots heat flow over time, similar curing enthalpy values are observed for both temperature cycles, indicating that full curing occurred at the desired 180 ºC. Additionally, Figure 4.9, which plots heat flow over temperature, shows identical glass transition temperatures for both cycles. This, combined with the TGA results presented in subsection 4.2.1, suggests that the chosen curing cycle for the hybrid laminates in this thesis research provides a safe curing environment for the TBDC material.

For the second analysis, an uncured TBDC sample and an uncured AS4-8552 sample were prepared and run using the same temperature cycle planned for this thesis' manufacturing campaign, which follows the recommended autoclave curing cycle for the AS4-8552 prepreg material [5]. The results, which compare the curing time frames of both materials, are presented in Figure 4.10.

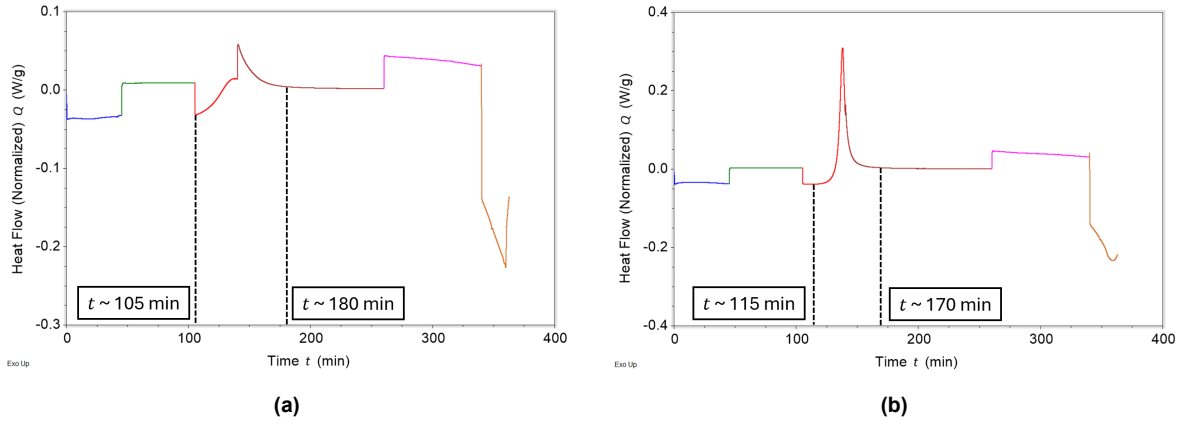

Figure 4.10: AS4-8552 (a) and TBDC (b) curing reaction start and end times at the chosen cure cycle.

By observing the curing behavior of both AS4-8552 and TBDC materials using the temperature cycle intended for this thesis' manufacturing campaign, it is apparent that the curing reactions of both materials begin and conclude at similar time points. This indicates that neither material completes its curing process significantly earlier than the other, which would otherwise negatively impact the hybrid UD/TBDC laminate's overall cure quality. The alignment of curing times supports the feasibility of producing cohesive, uniformly cured hybrid laminates for the project.

The thermal analysis results indicate that the recommended AS4-8552 prepreg curing cycle does not cause thermal degradation in the TBDC material. Therefore, this cycle will be used for curing the UD/TBDC ply hybrid CFRP laminates in this research project.

4.3. Specimen manufacturing

The manufacturing process for the DCB specimens will be covered in three main stages: (i) manufacturing of the laminates, (ii) cutting and secondary bonding of the substrates, and (iii) loading blocks attachment and lateral surface preparation for crack length measurement. It is important to note that for the DCB specimens designed to address the first research question the joining step will be omitted, since these specimens are not joints, and the starting crack is prepared during the initial manufacturing phase.

4.3.1. Laminate manufacturing

Epoxy-based CFRP prepregs consist of pre-impregnated carbon fibers within a thermoset matrix, with both matrix and hardener materials pre-mixed. To prevent curing or degradation, these materials are typically stored frozen at temperatures below -18 ºC [56]. Before use, the Hexply AS4-8552 prepreg was unfrozen overnight at room temperature. The TBDC material was shipped at room temperature and is usable for six months post-shipment, according to the manufacturer.

At room temperature, the UD AS4-8552 roll and TBDC preforms were cut into the required dimensions. The 300 by 300 mm TBDC preforms (see Figure 4.11), being isotropic, were cut in half to yield two 150 by 300 mm layers per preform. Five specimens were manufactured per configuration.

Figure 4.11: TBDC preform.

The UD/TBDC ply hybrid CFRP laminate specimens were produced in a single laminate manufacturing phase, while the joint specimens were secondary bonded at a later stage. Two composite plates were manufactured for each joint configuration with the dimensions specified in Figure 4.12, to later be secondary bonded. One of the plates was designed to accommodate three-point bending test specimens.

Due to the AS4-8552 prepreg roll's dimensions restriction, non-0-degrees plies cannot be cut as whole plies; therefore, the composite laminate's layers may consist of more than one cut ply, which were carefully sized and placed adjacent to one another. These connections can create weak spots in the laminates, either through overlapped or void areas. To minimize this risk, connections were strategically placed at the ends of the specimens, ensuring they were positioned away from critical areas such as

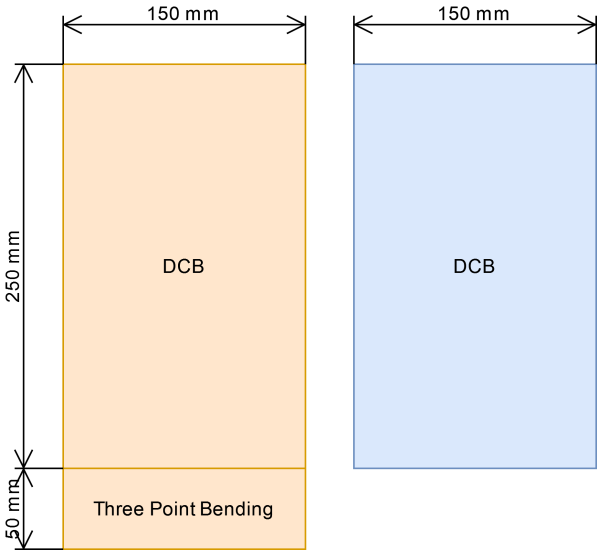

Figure 4.12: Composite plates dimensions.

the initial crack or critical crack propagation paths.

After cut, the CFRP prepreg and TBDC preforms were laid up to form the laminates for the specimens in the first research question and the substrate laminates for the second research question. During the prepreg layup process, debulking was employed to consolidate the layers, a technique that involves applying vacuum pressure to dry fibers or FRP prepregs to enhance fiber nesting and avoid voids [57]. This process was carried out using a debulking table, as shown in Figure 4.13. Given the volume of specimens and time constraints, debulking was performed for approximately fifteen minutes after every ten plies.

Figure 4.13: Debulking table.

To introduce a starting crack in the specimens designed to address the first research question, a 0.025 mm thick high-temperature PTFE film layer was placed in the mid-plane, covering the initial 50 mm of the specimen, as illustrated in Figure 4.14.

After a final debulking step, the laminates were prepared for autoclave curing. A base aluminum plate was cleaned with acetone, and release agent was subsequently applied. The laminates were positioned

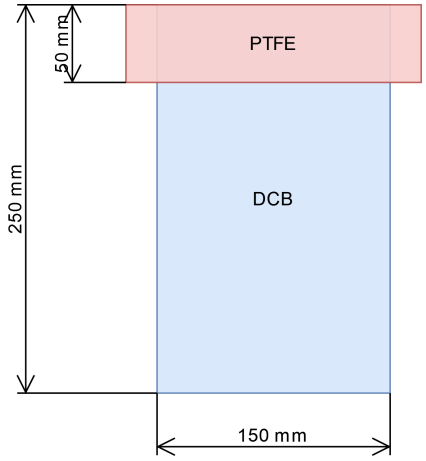

Figure 4.14: First research question DCB starting crack manufacturing schematic.

on top of a PTFE film layer to ensure smooth surface finishes on the composite plates. This was followed by the application of perforated film and peel ply to prevent bonding between the laminate and the vacuum bag's layers. Finally, breather cloth was added to ensure even vacuum distribution, and the vacuum bag was sealed to the base plate using tacky tape. The finalized setup can be seen in Figure 4.15.

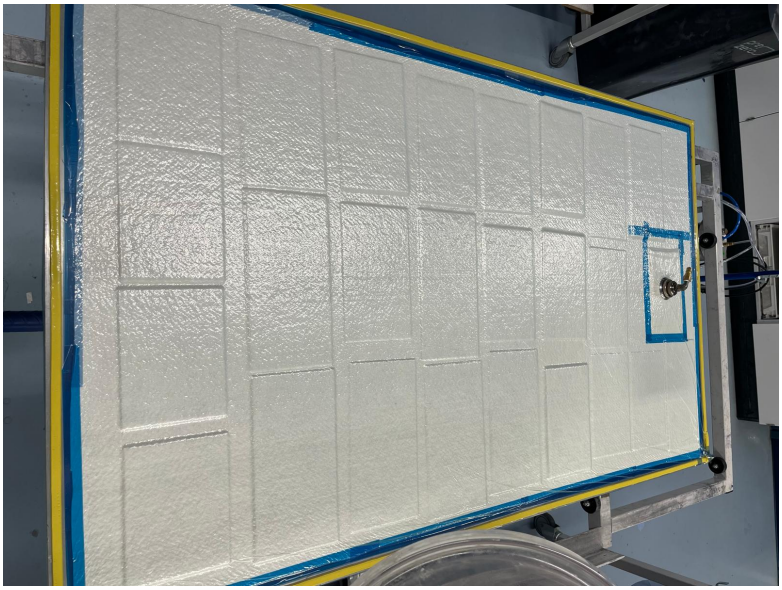

Figure 4.15: Laminate manufacturing's prepared vacuum bag.

The laminates were placed inside the autoclave running according to the cure cycle presented and discussed in section 4.2.

4.3.2. Laminate cutting and secondary bonding

Once the composite plates were fully manufactured, they were cut into sample-sized strips per the specified dimensions in Figures 4.4 and 4.5: 250 mm in length and 25 mm in width for DCB samples, and 50 mm in length and 13 mm in width for the three-point bending samples. This cutting process was performed using a Compcut composite plate saw, as shown in Figure 4.16.

On the larger manufactured composite plate for each laminate stacking sequence, a 50 mm section was trimmed from its largest dimension to create strips for the three-point bending samples. This 50 mm piece was further cut into 13 mm-wide strips, aligning with the plate's smallest dimension, ensuring

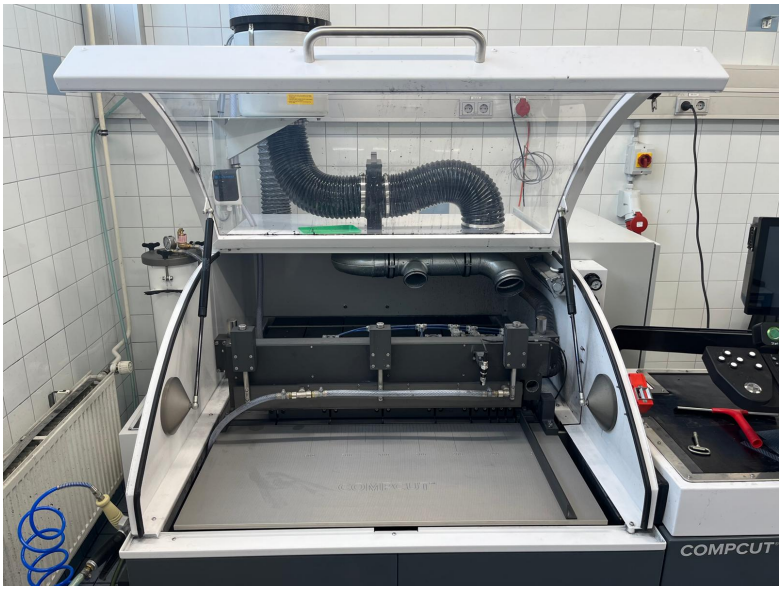

Figure 4.16: *Compcut* composite plate saw.

at least five three-point bending samples per plate. From the remaining 250 mm plates, margins were cut to ensure consistent thickness along the width of the DCB arms.

For the CFRP laminate samples, only cutting was necessary. However, for the joint samples, additional surface preparation was conducted prior to secondary bonding. Araldite 2015, a bi-component adhesive with a short working time, joints required preparation and bonding sample-by-sample. Conversely, the AF 163 film adhesive could be prepared on the plate directly, allowing for bonding in a single batch for all joint samples. This streamlined the process by enabling samples to be cut after bonding.

The smoother surfaces of the joint substrate laminates were selected for bonding and sanded with 400-grit sandpaper in a criss-cross pattern at a $\pm$45-degree angle. This process creates a roughened texture on the bonding surface, enhancing adhesion by promoting mechanical interlocking. This was followed by acetone cleaning. A 50 mm starting crack was established using a 25 mm wide, 0.1 mm thick PTFE tape layered on the bonding surfaces' initial region, as shown in Figure 4.17.

Figure 4.17: Secondary bonding prepared adherend surface.

Before secondary bonding, the bonding surfaces underwent UV/ozone surface treatment. This process enhances bond strength in two ways: topographically, by removing weakly bonded layers on the composite surface, and chemically, by breaking C–C bonds in the polymer surface. The chemical reaction initiates chain scission and crosslinking, promoting stronger adhesive bonds [58]. This treatment was

conducted using the UV apparatus shown in Figure 4.18, which exposed each bonding surface for a duration of seven minutes.

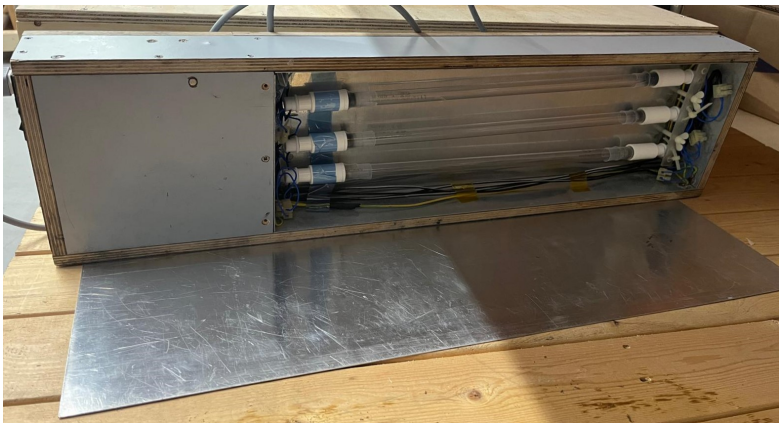

Figure 4.18: UV/Ozone apparatus.

The secondary bonding process for the Araldite joints was carried out using the mold shown in Figure 4.19. A 0.3 mm spacer was placed on the uncovered surface edge to ensure consistent adhesive thickness. The bi-component Araldite adhesive was dispensed along the bonding area, as demonstrated in Figure 4.19. The top adherend was aligned with the aid of the pins. A heavy plate was placed on top applying pressure to ensure even adhesive distribution and remove any excess. The mold was then placed in an 80 ºC oven for 60 minutes, from the point the samples reach the oven's temperature, allowing the adhesive to cure.

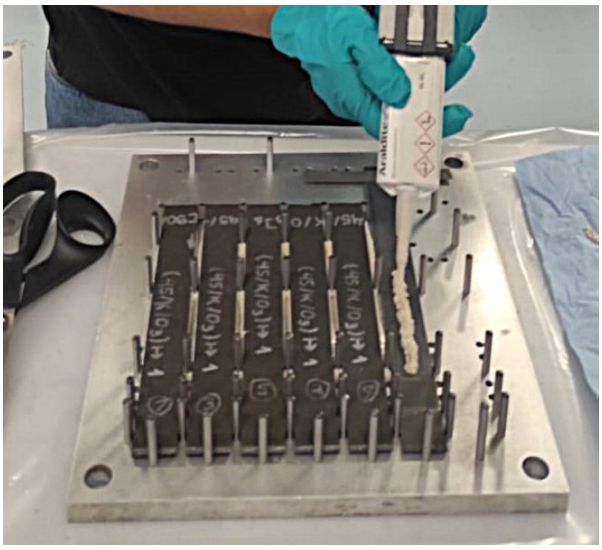

Figure 4.19: Araldite 2015-1 secondary bonding process.

The secondary bonding process for the AF 163-2U joints was performed without any aiding mold. Two layers of 0.14 mm thick adhesive material were cut and positioned beneath the PTFE tape on the bottom adherend. After placing the top adherend, the parts were placed in an autoclave-ready vacuum bag. The autoclave was run at 120 ºC and 3 bar for 90 minutes. After cooling, the final DCB samples underwent the same cutting process as those for the Araldite joints and hybrid CFRP laminate samples.

4.3.3. Loading blocks attachment and specimen painting and marking

The final step in preparing the DCB samples for testing involves attaching loading blocks and marking the sides of the samples for crack length measurement.

The outer surfaces of the test samples were sanded with 120-grit sandpaper and thoroughly cleaned using acetone. Additionally, the loading blocks underwent surface treatment through sandblasting to ensure good adhesion. The bi-component epoxy adhesive EA330 was applied to the loading blocks and, with the aid of the loading blocks attachment mold of Figure 4.20, applied to the prepared edge of the samples' outer surfaces. The samples were left overnight at room temperature to cure before removing them from the molds.

Figure 4.20: Loading blocks attachment mold.

After the loading blocks attachment process, one sample side was coated with a thin layer of white spray paint. The same process was carried out for the three-point bending samples. After the white paint dried, a black marker was used to draw marks 1 mm apart, starting from the samples' starting crack's tip.

A representative final DCB test sample is illustrated in Figure 4.21.

Figure 4.21: DCB test specimen.

4.4. Specimen post-curing condition

Defects were observed near the interface between the TBDC and UD prepreg materials in the UD/TBDC ply CFRP DCB samples, as seen in Figure 4.22.

In the case of the adhesively bonded UD/TBDC ply laminate specimens, where thinner TBDC layers were integrated into CFRP laminates, no visible defects were detected through microscopy inspection.

After performing the thermal analysis outlined in section 4.2, material degradation or curing time frame mismatches between AS4-8552 and TBDC materials seem unlikely contributors. However, matrix material incompatibility remains a possibility. Moreover, due to the highly anisotropic nature of the TBDC material and the directional-dependent mechanical properties of the unidirectional AS4-8552 prepreg, significant coefficient of thermal expansion (CTE) mismatches are expected. These mismatches likely led to the development of residual stresses near the UD/TBDC interface during curing, which may have caused the observed defects at those locations.

Five DCB samples were successfully retrieved for each joint configuration. However, for the CFRP laminate specimen configuration with the most TBDC interleaves, $[0_{12}/\text{TBDC}_4/0_{12}]$, only two samples were recovered.

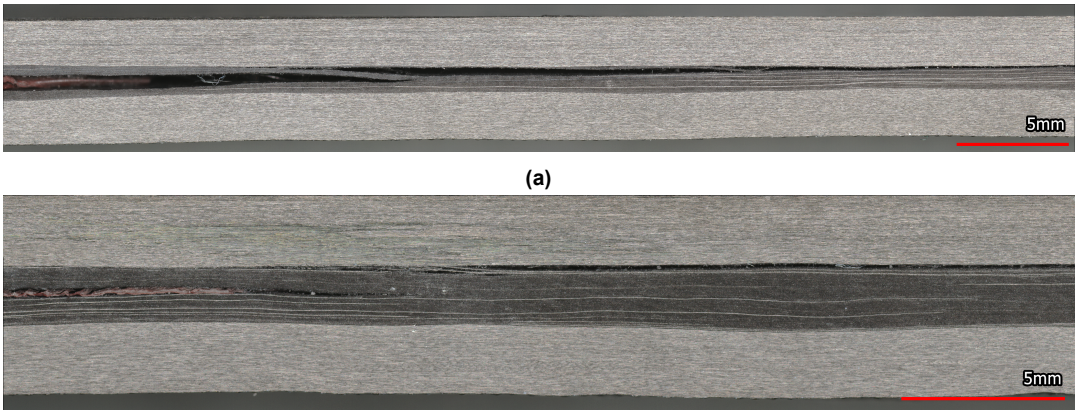

Figure 4.22: [0_{12}/TBDC$_2$/0_{12}] sample 2 (a) and [0_{12}/TBDC$_4$/0_{12}] sample 2 (b) defects.

4.5. Specimen measurements

It is important to measure all samples not only for data processing purposes but also to be able to justify any discrepancies that might exist from the expected results or between samples.

In Figure 4.23, the average, maximum, minimum, and standard deviation values for thickness measurements of two joint specimen configurations' substrates are shown: [90/45/-45/TBDC/0]$_s$, which includes TBDC material in its substrate laminates, and [0_8], which does not. Measurements were taken with calipers at three locations: the midpoint and 25 mm from each end of the sample, as specified in ASTM D5528 [37].

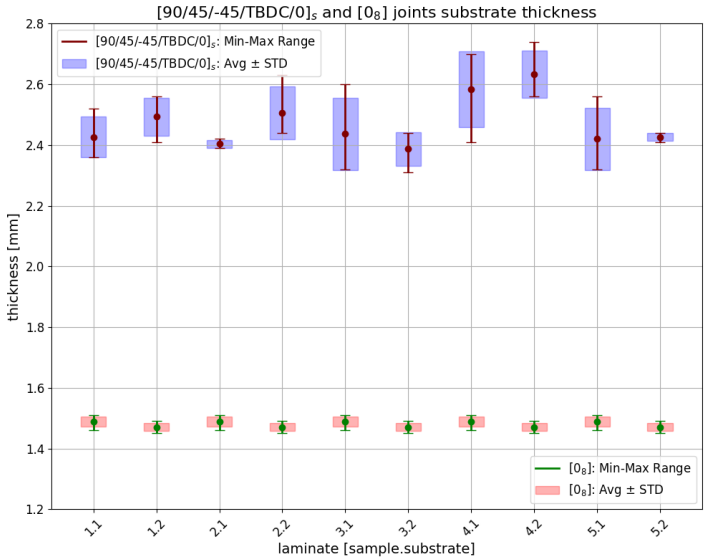

Figure 4.23: Average, maximum and minimum and standard deviation values for thickness measurements of [0_8] and [90/45/-45/TBDC/0]$_s$ laminates.

A clear difference between the two presented adhesive joint specimen configurations is evident: the UD/TBDC hybrid laminates display a much greater spread in thickness measurements compared to the UD laminates. It is important to note that this difference in the spread of thickness measurement values is characteristic of any other UD versus UD/TBDC ply hybrid configurations, such as [0_{24}] compared to [0_{12}/TBDC$_2$/0_{12}], for example.

As observed from the side view of the [0_{12}/TBDC$_2$/0_{12}] configuration's sample 2 (see Figure 4.24a), the TBDC layers exhibit a certain waviness that affects the overall shape of the DCB specimens in

both TBDC-toughened joint and UD/TBDC ply hybrid CFRP laminates, as seen in both sub-figures of Figure 4.24. This ”wavy” characteristic results in thickness gradients along the length of the specimens, evident in the results of Figure 4.23.

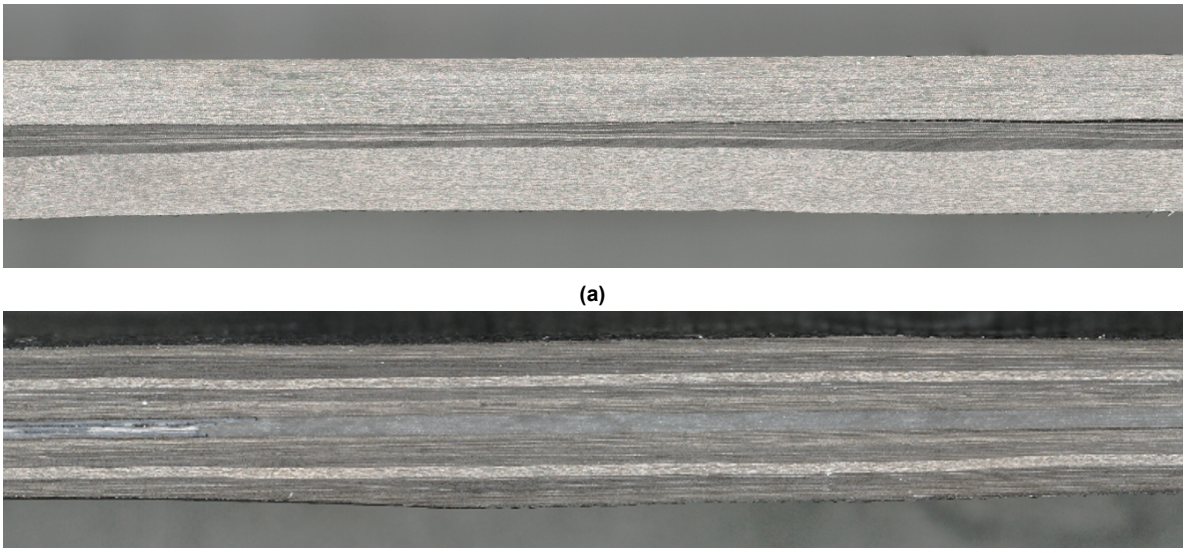

(a)

(b)

Figure 4.24: [0_{12}/TBDC$_2$/0_{12}] sample 2 (a) and [90/45/-45/TBDC/0]$_s$ sample 1 (b) side pictures.

Given the high standard deviation of the measured joint substrate thickness values, as seen in Figure 4.23 and discussed previously, there is likely a significant thickness gradient within the adhesive layer of TBDC-toughened adhesively bonded joints.

The average and standard deviation of the thickness and width measurements of each DCB sample and substrates are present, as well as the calculated adhesive layer thickness, in the case of joint samples, in section A.1 (Tables A.1 to A.14). The thickness and width measurements taken for the three-point bending test samples and used for flexural modulus calculations can be found in section A.2 (Tables A.15 to A.22).

5

Experimental Testing Methodology

In this chapter, the testing methodology for the manufactured specimens described in chapter 4 is presented. Additionally, the data processing methods used to analyze the experimental results and produce the findings shown and discussed in chapter 6 and chapter 7, respectively, are outlined.

5.1. Mode I fracture toughness test setup

This section will provide a detailed explanation of the equipment used for the tests and the testing procedure to acquire the necessary data to obtain the mode I fracture toughness values.

For clarity, this section will primarily reference the ASTM D5528 standard, as the test procedures and data processing methods are largely similar to the adhesively bonded joints mode I fracture toughness measurement standard ISO 25217 [36].

5.1.1. Test equipment

The mechanical tests were performed on a *Zwick* 10 kN tensile test machine, with a *Zwick* 1 kN load cell. The test samples' loading blocks were attached to the test machine's clamps through a pin, as can be seen in the highlights shown in Figure 5.1. During testing, the top clamp stays stationary, while the lower clamp is displaced at a constant rate, applying an opening load at the attachment points.

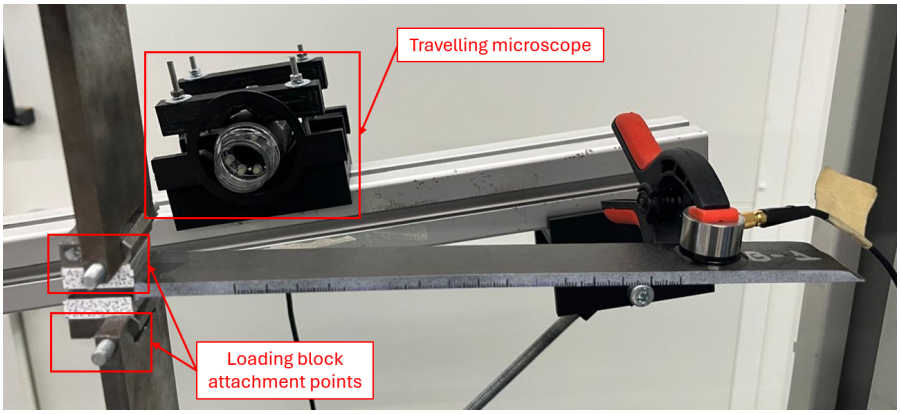

Figure 5.1: Mode I loading test setup (close-up view).

A 3D Digital Image Correlation (DIC) system, consisting of two 9-megapixel cameras, was employed to capture the propagation and path of cracks in the samples. However, within the scope of this thesis research, the camera pictures were used for visual measurement of the crack length at each required point; thus, no DIC data analysis was performed and the DIC system will be referred to as camera system. To ensure proper exposure of the test samples, two white LED lamps were positioned behind

the cameras.

Additionally, a travelling microscope was installed on the opposite side of the camera system, directed at the non-painted side of the test samples. This microscope, was utilized to closely monitor the crack propagation path and potentially capture detailed images of potential toughening mechanisms, such as fiber and tape bridging or crack deflection. The travelling microscope is also shown in Figure 5.1.

In Figure 5.2 the complete test setup can be seen, comprising of the test machine, camera system, LED lamps and travelling microscope.

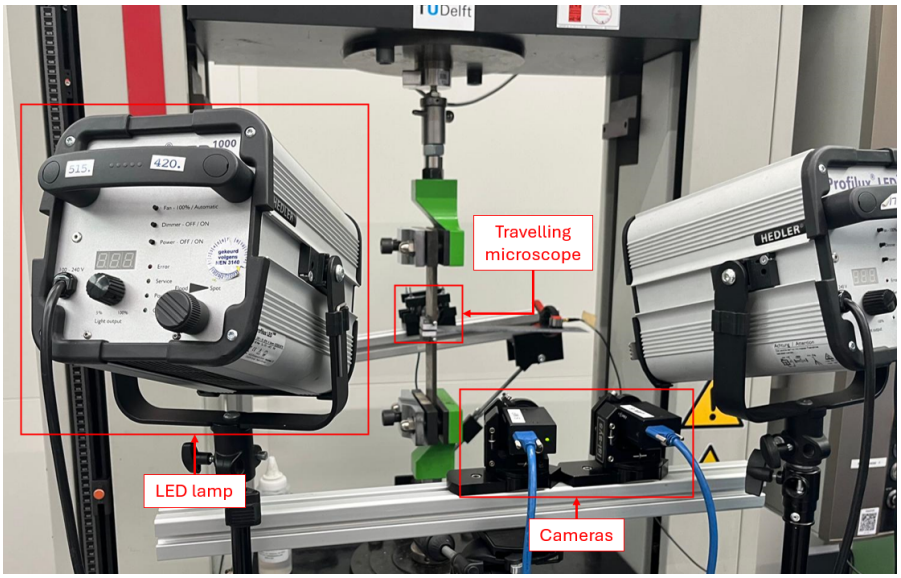

Figure 5.2: Test setup.

5.1.2. Test procedure

Before initiating the mechanical testing of the DCB specimens, it is crucial to establish the necessary parameters. Initially, limits must be set on the test machine's output signals directed to other data acquisition systems, such as the camera setup and travelling microscope. Since the output is transmitted in Volts, ranging from 0 to 10 V, the limits for both the applied load and displacement outputs must correspond to the signal's 10 V, knowing that 0 V signifies 0 N in applied load and 0 mm in displacement. The limits were established at 400 N for the applied load and 300 mm for displacement, ensuring the entire load-displacement curve is captured while minimizing signal noise.

The mode I loading mechanical test was conducted at a constant displacement rate, as per ASTM D5528 [37]. A displacement rate of 4 mm per minute was selected. Given the test machine's chosen displacement rate, a data recording rate of one picture every 4 seconds was chosen.

It is noteworthy that the travelling microscope was manually adjusted during the mechanical test to ensure a clear view of the crack front throughout the entire process.

5.2. Three-point bending test setup

This section will detail the equipment used for testing, and test procedure for the three-point bending tests of CFRP laminates.

5.2.1. Test equipment

Similar to the mode I fracture toughness tests, the same *Zwick* 10 kN tensile test machine and *Zwick* 1 kN load cell were used for the three-point bending tests. The test apparatus with 3 mm radius supports, as shown in the schematic of Figure 5.3, was attached to the machine and configured for a total span of 30 mm plus an additional 3 mm from the supports radius.

Since obtaining the test samples' flexural modulus requires only the their geometry, applied load and

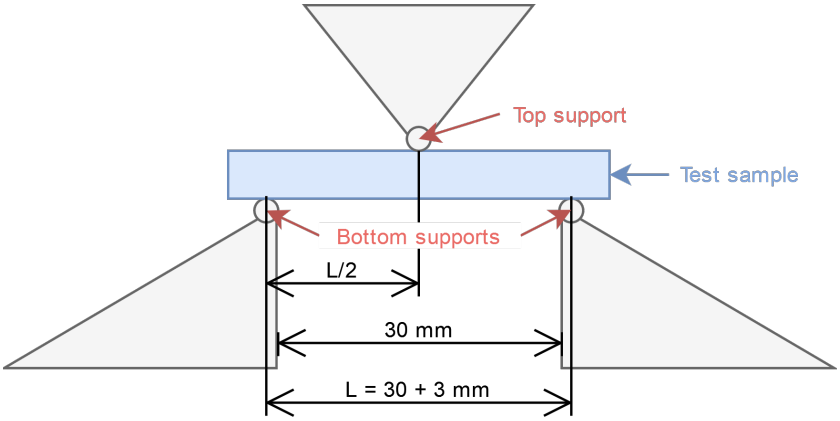

Figure 5.3: Three-point bending apparatus schematic.

displacement data, the acquisition relied solely on the outputs from the testing machine. Consequently, unlike the setup used for the mode I fracture toughness tests described in section 5.1, no external data acquisition systems were utilized.

5.2.2. Test procedure

The three-point bending tests were conducted at a constant displacement rate of 1 mm per minute, as recommended by ASTM D7264 [51]. The test machine's default output rate of 10 Hz exceeded the ASTM D7264 [51] recommended 50 data points for the entire force-deflection curve, allowing for effective data collection, and was thus used.

The tests were performed until an arbitrary point before failure, as the flexural strength of the laminates was not subject of measurement.

5.3. Data processing

In this section, the data processing methodologies for the mode I fracture toughness tests and the three-point bending tests will be explained in detail, with each method addressed in its own subsection.

5.3.1. Mode I fracture toughness calculation

As recommended by ASTM D5528 [37], the mode I fracture toughness was calculated using the Modified Beam Theory (MBT) as the chosen data reduction method. As discussed in subsection 2.2.1, the MBT method allows for the calculation of mode I fracture toughness, G_I, using the following equation:

$$G_I = \frac{3P\delta}{2ba} \tag{5.1}$$

Where P is the applied load, δ the load point displacement, b the specimen width and a the crack length. Since the equation assumes a perfectly built-in beam at the crack front which is not entirely realistic due to misalignments, an adjusted value of $a + |\Delta|$ is used to compensate. The correction factor, Δ, is determined experimentally via a least squares plot of the cube root of the compliance, as given by $C = \frac{\delta}{P}$, versus crack length. Δ corresponds to the crack length where $C^{1/3}$ = 0, as shown in Figure 5.4.

Furthermore, due to the relatively high load point opening displacement to crack length ratio of some test samples, the correction factor F, which accounts for the tilting of the loading block and the shortening of the moment arm was applied. Additionally, the correction factor N, which addresses the stiffening effects on the sample arms caused by the loading blocks, was used. This adjustment was necessary because the distance between the load line and the edge of the loading block (L') was less than 50 mm, as specified in ASTM D5528 [37]. Both correction factors can be calculated using the following expressions:

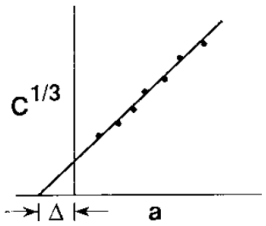

Figure 5.4: Modified Beam Theory Δ [37].

$$F = 1 - \frac{3}{10}(\frac{\delta}{a})^2 - \frac{3}{2}(\frac{\delta t}{a^2}) \tag{5.2}$$

$$N = 1 - (\frac{L'}{a})^3 - \frac{9}{8}[1 - (\frac{L'}{a})^2](\frac{\delta t}{a^2}) - \frac{9}{35}(\frac{\delta}{a})^2 \tag{5.3}$$

Where L' is the distance from the load line to the edge of the loading block and t the distance from the loading point to the middle of the arm substrate, as seen in Figure 5.5. Finally, the mode I fracture toughness can be calculated as follows:

$$G_I = \frac{3P\delta}{2b(a + |\Delta|)} \cdot \frac{F}{N} \tag{5.4}$$

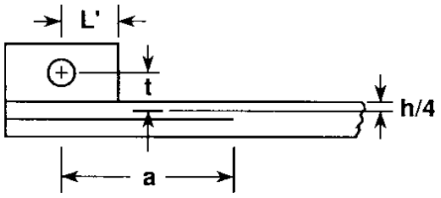

Figure 5.5: DCB samples L' and t [37].

The load (P), displacement (δ) and crack length (a) values necessary to calculate the corrected crack length ($a + |\Delta|$) and the effective fracture toughness were obtained from the data of the camera system (a) and the test machine (P and δ).

To measure the crack length, the ruler markings made during the sample manufacturing were utilized. The length of the ruler segment corresponding to the observed crack tip in the images was added to the initial crack length value a_0. In instances where two crack fronts coexist within the sample, the front-most one was considered. A visual representation of the crack length measurement method is provided in Figure 5.6.

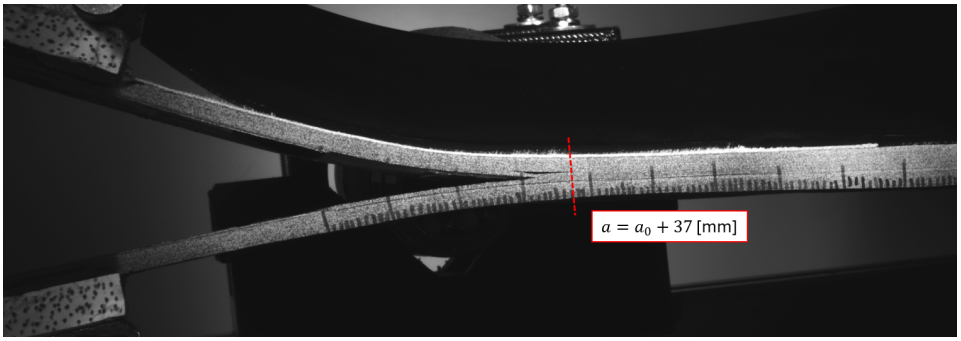

Figure 5.6: Crack length measurement example.

The first six data points from each test sample were discarded to avoid compliance miscalculations resulting from the test machine's inaccurate outputs at loads and displacements close to zero. Retaining these inaccurate values would impact the Δ value obtained from the cubic root of compliance versus crack length plot, consequently influencing the calculated fracture toughness values.

5.3.2. Flexural modulus calculation

The flexural modulus E_x^f can be determined using the equation:

$$E_x^f = \frac{\Delta\sigma_f}{\Delta\varepsilon_f} \tag{5.5}$$

This value is calculated within the strain range of 0.001 to 0.003, where $\Delta\varepsilon_f$ represents the difference between the two chosen flexural strain points (should be close to 0.002) and $\Delta\sigma_f$ is the difference between the flexural stresses at these strain points. The flexural stress and strain are obtained from:

$$\sigma_f = \frac{3PL}{2bh^2} \tag{5.6}$$

$$\varepsilon_f = \frac{6\delta h}{L^2} \tag{5.7}$$

Where P is the applied load, δ the displacement at the load point, L the span length, b the sample's width and h the sample's thickness.

Due to the intrinsic compliance of the test machine, it is essential to correct the measured displacements. The machine's displacement readings can be expressed as a sum of the displacements in the loading system and the displacements in the sample [59]:

$$\delta_R = \delta_S + \delta_M \tag{5.8}$$

Where δ_R is the recorded displacement, δ_S the sample displacement and δ_M the machine's displacement. To determine the machine's displacement δ_M, a steel sample with stable and known mechanical properties, high thickness and moment of inertia was tested in the same three-point bending setup. Knowing the theoretical sample displacement δ_S, δ_M can be calculated from the machine's readings using Equation 5.8. The theoretical steel sample displacement $\delta_{S_{\text{steel}}}$ can be calculated using:

$$\delta_{S_{\text{steel}}} = \frac{PL^3}{48E_{S_{\text{steel}}}I_{S_{\text{steel}}}} \tag{5.9}$$

Where $E_{S_{\text{steel}}}$ is the material's elastic modulus and $I_{S_{\text{steel}}}$ the sample's cross-section's moment of inertia which can be obtained as $I = \frac{bh^3}{12}$. Knowing δ_S for the steel sample ($\delta_{S_{\text{steel}}}$) allows for the determination of the loading system's displacement δ_M by subtracting $\delta_{S_{\text{steel}}}$ from the recorded displacements $\delta_{R_{\text{steel}}}$.

The recorded loads P and calculated machine displacements δ_M were fitted into a third-degree curve to derive the machine's displacements for any given load. The corrected displacements for the tested laminates can be determined using Equation 5.8 with the fitted curve's testing machine displacements. Subsequently, the flexural strains can be calculated, and Equation 5.5 can be utilized to derive the laminates' flexural modulus.

6

Results

6.1. Three-point bending results

The three-point bending tests were conducted to investigate the effect of the TBDC material on the flexural modulus of the joint substrate laminates and explore potential links between substrate flexural modulus and crack competition and deflection mechanisms between the bond line crack tip and the substrate.

The average flexural modulus and its standard deviation for each laminate are listed in Table 6.1.

Table 6.1: Flexural modulus for various laminate configurations.

Laminate	Flexural Modulus [GPa] (average $\pm$ standard deviation)
$[0_8]$	105.6 $\pm$ 3.4
$[90/45/-45/0]_s$ (2022)	18.9 $\pm$ 2.0
$[0/90_2/0]_s$ (2022)	66.2 $\pm$ 3.8
$[90/45/-45/TBDC/0]_s$	24.5 $\pm$ 2.6
$[90/60/90/-60/TBDC/0]_s$	13.7 $\pm$ 1.9
$[0/TBDC/90_2/0]_s$	63.1 $\pm$ 7.6

From examining the flexural modulus values presented, two main observations can be made:

1. TBDC toughening resulted in an increase of approximately 30% in the calculated flexural modulus of the multi-directional $[90/45/-45/0]_s$ laminate. However, in the stiffer cross-ply $[0/90_2/0]_s$ laminate, a decrease of around 5% is observed.
2. The TBDC-toughened laminates display a higher standard deviation from the average value.

Figure 6.1 shows the values present in Table 6.1 plotted for comparison. The minimum and maximum values for the samples in each configuration are displayed. These values are color-coded according to their Relative Standard Deviation (RSD), calculated using the following equation:

$$RSD = \frac{\text{standard deviation}}{\text{mean}} \cdot 100\% \tag{6.1}$$

From observing the RSD of the non-TBDC-toughened $[0_8]$ laminate compared to those of TBDC-toughened laminates, it is evident that the integration of TBDC material layers in the UD laminates leads to significant variance in their mechanical properties. The observed flexural modulus variance is likely attributable to the random nature of the TBDC material and thickness variations between samples. The variability in the mechanical properties of the UD/TBDC ply hybrid laminates should be kept in mind as it may explain some discrepancies observed in the DCB test results.

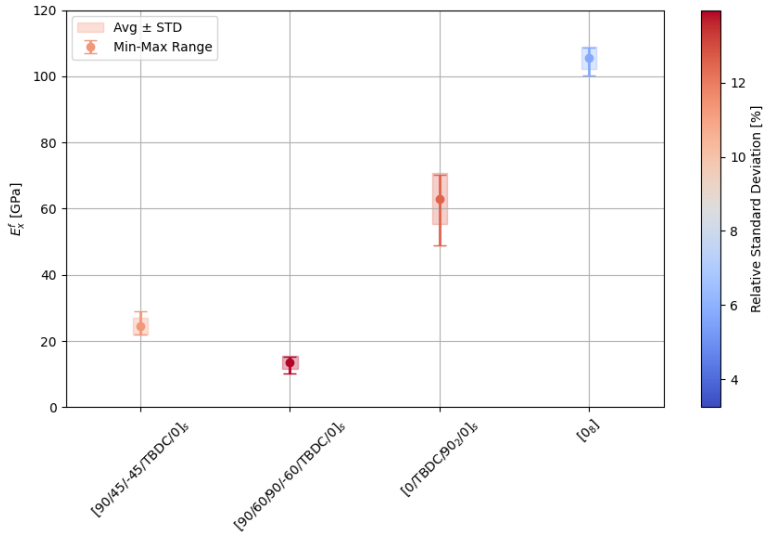

Figure 6.1: Average, maximum and minimum, standard deviation and RSD values for flexural modulus of tested joint substrates.

When comparing the observed behavior of the tested TBDC-toughened joint specimens with that of their non-TBDC-toughened counterparts, as reported in literature [5], it is important to note the flexural modulus results. The multi-directional TBDC-toughened [90/45/-45/TBDC/0]$_s$ laminate exhibits a significantly higher flexural modulus compared to that of the non-toughened [90/45/-45/0]$_s$ laminate. A similar trend can be expected for the TBDC-toughened [90/60/90/-90/TBDC/0]$_s$ laminate, due to its similar stacking sequence and TBDC layer positioning. In contrast, the cross-ply [0/TBDC/90$_2$/0]$_s$ laminate presents lower flexural modulus than its non-toughened counterpart, [0/90$_2$/0]$_s$. The impact of TBDC layers on the flexural modulus of composite laminates depends not only on the contrast between their flexural modulus and that of the TBDC material but also on the positioning of the TBDC interleaves: the flexural modulus influence of any given layer increases with its distance from the mid-plane.

The load-displacement curves obtained from the three-point bending tests can be consulted in Figures A.1 to A.5, in Appendix A.

6.2. Mode I fracture toughness results

In this section the outcomes of DCB tests are presented. First the results for each specimen configuration are presented, followed by a comparison between one representative sample from each relevant configuration, and the literature reported results [5] for the non-TBDC-toughened version of the test specimens, in the case of TBDC-toughened adhesively bonded joint specimens.

Representative samples were selected based on their alignment with the general fracture behavior observed in the load-displacement curves, R-curves, and calculated fracture toughness values. In cases where fracture behavior varied significantly between samples, the sample exhibiting the most desirable characteristics for exploring the toughening potential of TBDC material in CFRP laminates and adhesively bonded joints was chosen.

Due to the deviation of the crack from the mid-plane of the DCB samples, the loading conditions inevitably transition from pure mode I to a mixed-mode I+II. This crack path deviation will be covered in chapter 7. As a result, the calculated fracture toughness values will be referred to as effective fracture toughness (G_{eff}).

6.2.1. UD/TBDC ply CFRP laminates

Three UD/TBDC ply CFRP DCB configurations were tested.

Due to the defective conditions of the UD/TBDC ply hybrid CFRP laminates, as mentioned in section 4.4,

it became rather challenging to differentiate between an actively opening crack front and a specimen defect. Following MBT's assumption that the sample arms behave like clamped beams at the delamination front, there should be no deformation ahead of the crack front, which served as a visual aid for measuring crack lengths more accurately.

Moreover, assuming that the compliance should not alter significantly with growing crack length, despite inevitable deviations due to the crack tip's displacement from the midplane, the least squares plot of the cube root of the compliance $C^{1/3}$ versus crack length a was used to confirm the crack length measurements. Aligned data points that followed the least squares trend provided higher confidence in these measurements.

It is worth noting that, with an extended project timeframe, DIC could have been employed for more accurate crack length measurements. Another potential data reduction method, the Compliance-Based Beam Method (CBBM) [60], which uses an equivalent crack length concept rather than visual measurements, was considered. However, this method was deemed unsuitable for the tested samples, as the estimated crack lengths significantly deviated from the visually measured values.

[0_{24}]
The load-displacement and R-curve obtained for the non-toughened configuration [0_{24}], obtained from the MBT, can be seen in Figure 6.2. In Figure 6.3 a picture and a schematic, present for clarity of the surface fiber directions, of a [0_{24}] laminate representative sample is shown.

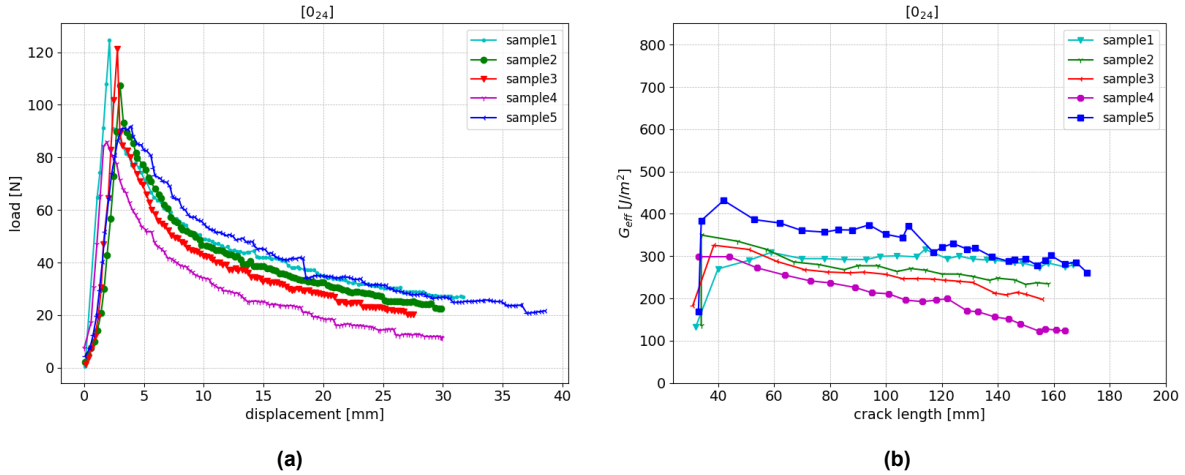

Figure 6.2: Load-displacement curves (a) and R-curves (b) of [0_{24}] samples.

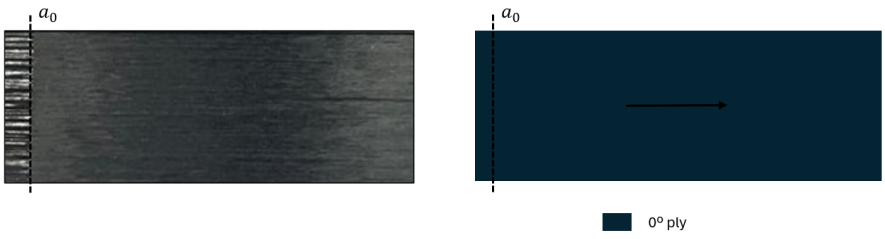

Figure 6.3: [0_{24}] sample 2 fracture surface (photo on the left and schematic on the right).

A maximum load value is observed between 85 N and 125 N, corresponding to an effective fracture toughness, G_{eff}, of around 300 J/m^2 which is in-line with values found in literature for the same AS4-8552 material [61]. Even though some variance can be seen between the different samples, no particularly different behavior was observed during testing or by analysing travelling microscope and DIC pictures or fracture surfaces.

$[0_{12}/TBDC_2/0_{12}]$
The load-displacement and R-curve obtained for the specimens configuration toughened with one TBDC layer directly above and below the initial crack plane $[0_{12}/TBDC_2/0_{12}]$ can be seen in Figure 6.4. In Figure 6.5, the fracture surface of a representative sample is shown.

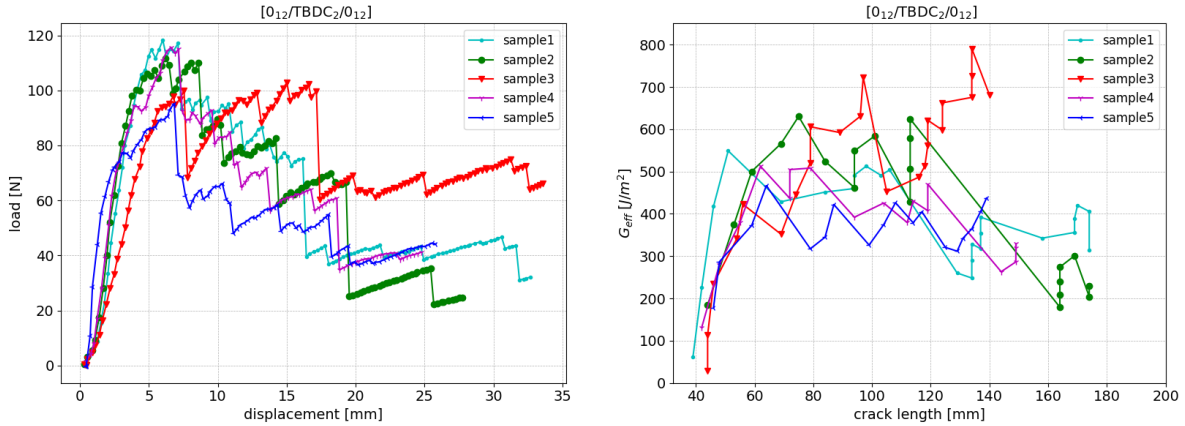

(a) (b)

Figure 6.4: Load-displacement curves (a) and R-curves (b) of $[0_{12}/TBDC_2/0_{12}]$ samples.

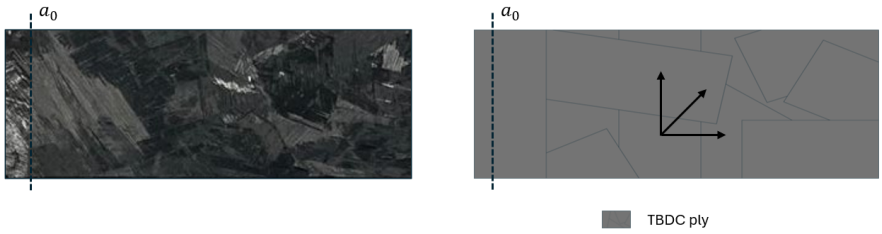

Figure 6.5: $[0_{12}/TBDC_2/0_{12}]$ sample 2 fracture surface (photo on the left and schematic on the right).

The maximum load values obtained are comparable to those of the non-toughened samples, ranging from 95 N to 120 N. Most R-curves exhibit a consistent trend, beginning with a lower crack initiation value that increases immediately, peaking at a crack length of approximately 60 mm to 80 mm. Subsequently, a reduction in effective fracture toughness is observed at crack lengths around 100 mm to 120 mm. However, some scatter in the effective fracture toughness is noted between samples at the same crack length.

$[0_{12}/TBDC_4/0_{12}]$
The results obtained for the specimens configuration toughened with four TBDC layers $[0_{12}/TBDC_4/0_{12}]$ can be seen in Figure 6.6, followed by the fracture surface of a representative sample in Figure 6.7.

Similar maximum load values between 95 N and 125 N to those of the samples toughened with two TBDC layers are seen. Furthermore, the same scattering in the R-curves between samples of the same configuration can be observed for this toughened configuration. Fracture toughness values observed are also very similar to those of the $[0_{12}/TBDC_2/0_{12}]$ laminate samples, as well as the same fracture behavior explained before, giving the R-curves a very similar general shape.

Representative samples
In Figure 6.8, the load-displacement and R-curve of one representative sample from each UD/TBDC ply hybrid CFRP laminate configuration are displayed.

Looking at Figure 6.8a, it can be observed that the maximum load value doesn't vary significantly between the three DCB configurations, with all three ranging roughly between 95 N and 110 N. Further-

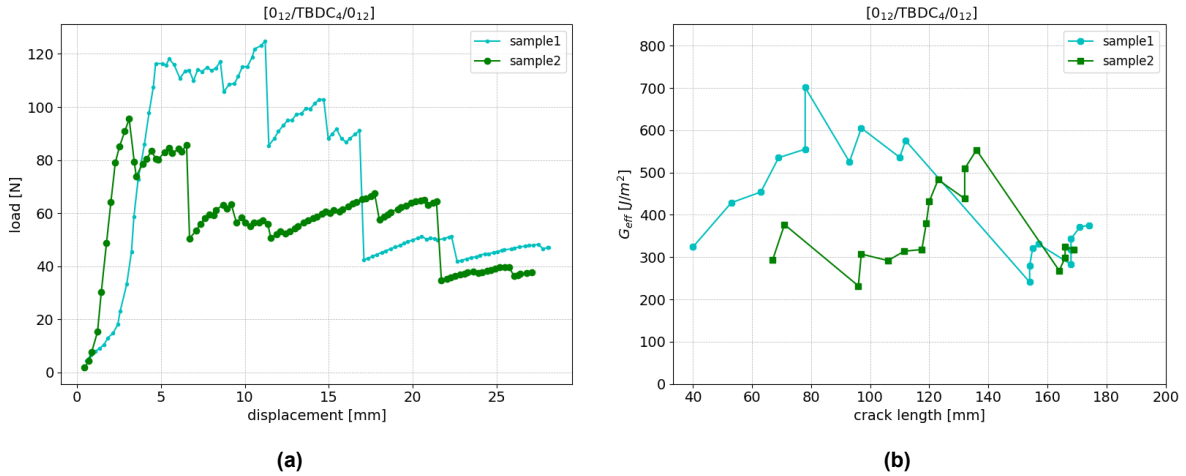

Figure 6.6: Load-displacement curves (a) and R-curves (b) of [0_{12}/TBDC$_4$/0_{12}] samples.

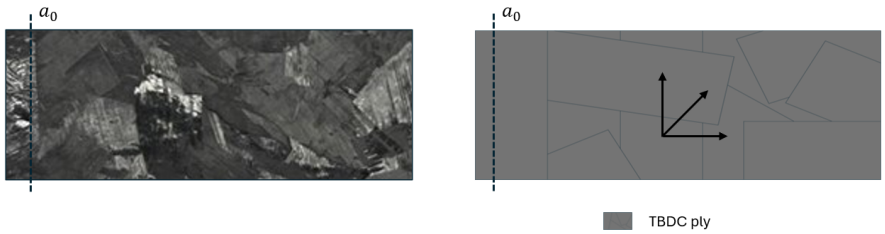

Figure 6.7: [0_{12}/TBDC$_4$/0_{12}] sample 2 fracture surface (photo on the left and schematic on the right).

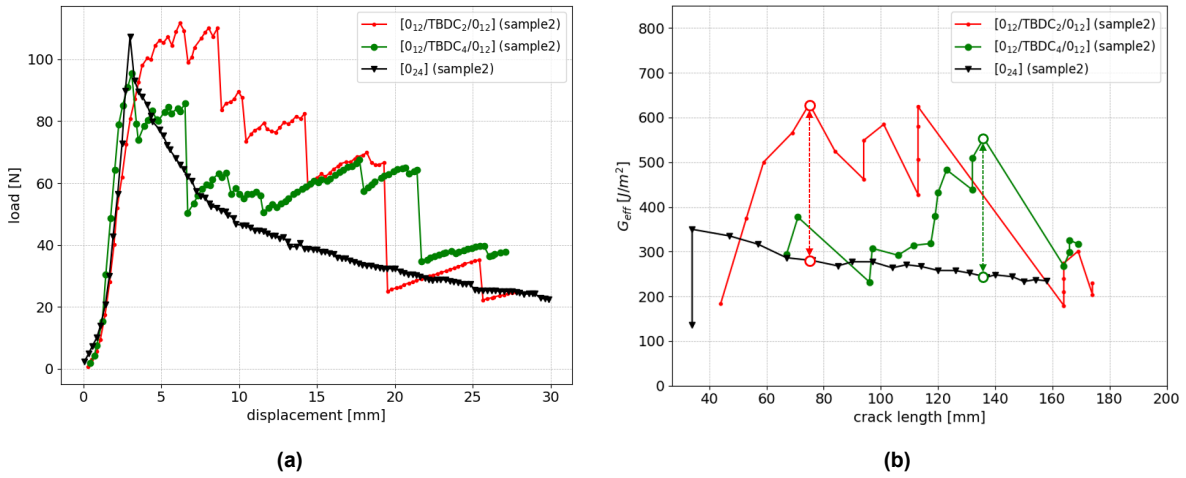

Figure 6.8: Load-displacement curves (a) and R-curves (b) of UD/TBDC ply CFRP laminates specimens.

more, it is noticeable that the initial slope in the load-displacement curves is very similar between the three representative specimens.

In contrast with the non-toughened configuration [0_{24}], both toughened configurations exhibit a less stable load drop after reaching the maximum. Unlike the consistent load decrease observed in [0_{24}], the [0_{12}/TBDC$_2$/0_{12}] and [0_{12}/TBDC$_4$/0_{12}] samples display cycles of slight load increases followed by sharp drops. This behavior leads to an overall more segmented load reduction as the displacement increases.

Looking at the R-curves presented in Figure 6.8b, a clear increase in fracture toughness can be observed from both toughened configurations, compared to $[0_{24}]$. An approximate 100% increase in G_{eff} is observed for the maximum fracture toughness values in the toughened configurations compared to the corresponding crack lengths in the $[0_{24}]$ sample, as highlighted in Figure 6.8b by circles marking the fracture toughness values, connected by an arrow illustrating the toughening effect. Near the end of the recorded crack propagation however, both fracture toughness curves reach values similar to those of the non-toughened configuration: around 300 J/m^2.

Given the very limited test results obtained of the $[0_{12}/\text{TBDC}_4/0_{12}]$ configuration, a significant difference can't be seen when comparing DCB samples toughened with two versus four TBDC layers. It is clear however, that a significant increase in the order of 100% in mode I fracture toughness can be obtained from adding around 18% to 30% volume fraction TBDC around mid plane initial cracks in CFRP laminates.

6.2.2. Araldite 2015 joint specimens

Two distinct TBDC-toughened Araldite 2015 bonded joint DCB configurations were tested, as detailed in Table 4.5. These Araldite 2015 joints constitute the low-toughness adhesive joint configurations examined in the current thesis research.

$[90/45/\text{-}45/\text{TBDC}/0]_s$

The load-displacement and R-curve obtained for the $[90/45/\text{-}45/\text{TBDC}/0]_s$ substrate joints can be seen in Figure 6.9. It should be noted that all samples failed cohesively, as illustrated in Figure 6.10's representative sample fracture surface.

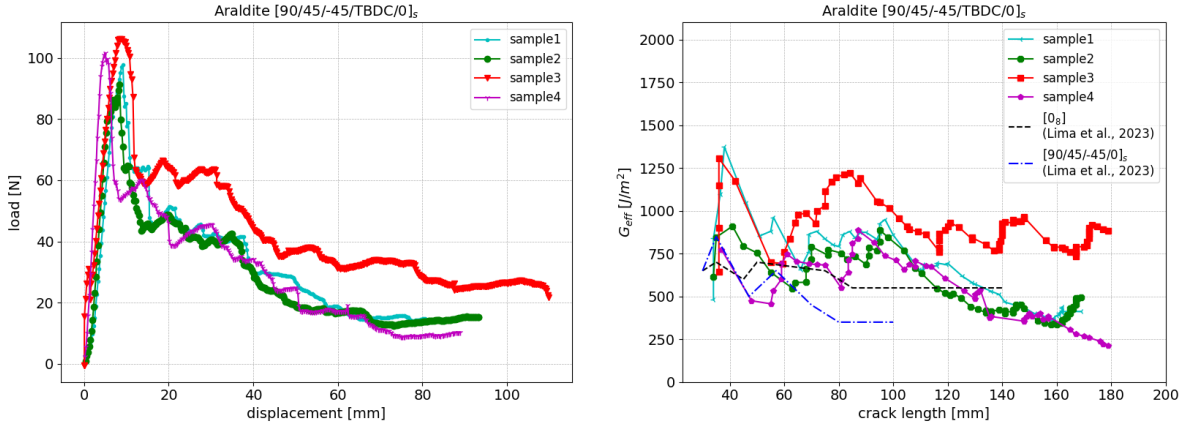

Figure 6.9: Load-displacement curves (a) and R-curves (b) of $[90/45/\text{-}45/\text{TBDC}/0]_s$ Araldite 2015 joint specimens.

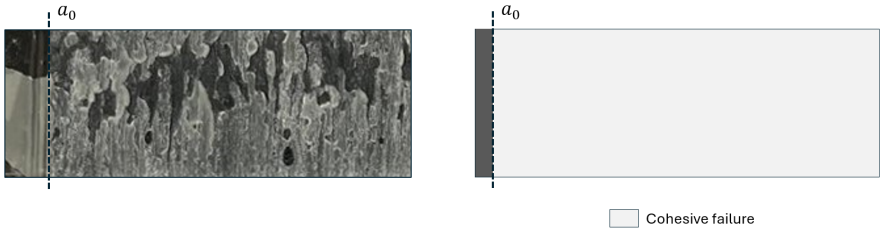

Figure 6.10: $[90/45/\text{-}45/\text{TBDC}/0]_s$ joint sample 2 fracture surface (photo on the left and schematic on the right).

In the load-displacement curves presented in Figure 6.9a, maximum loads ranging from 90 N to 105

N for the different test samples can be seen. Furthermore, a generally unstable decrease in load is observed after a maximum is reached.

In the R-curves of Figure 6.9b, the test samples calculated fracture toughness values are presented solid color plot lines. Literature reported fracture toughness results for the cohesive failure of $[0_8]$ substrate joints are also plotted in the black dashed plot line, along with the non-toughened version of the tested samples ($[90/45/-45/0]_s$), in the blue dash-dot plot line.

The fracture toughness values of the $[90/45/-45/TBDC/0]_s$ joint samples show various increase-decrease cycles throughout crack propagation, mirroring the unstable decrease in load seen in the load-displacement curves of Figure 6.9a. The cohesive failure curve for the $[0_8]$ substrate Araldite 2015 joint, on the other hand, shows stable fracture toughness values. Looking at the calculated fracture toughness values, however, even if unstable and scattered, they are in line with the values obtained by Fernandes et al. [55] for the same adhesive material and adhesive layer thickness range (600 to 1000 J/m^2).

A higher onset G_{eff} value is observed in all specimens, compared to most of the overall toughness values of the same samples, as well as the onset value obtained for the cohesive failure of the non-toughened $[0_8]$ substrate joint presented.

$[90/60/90/-60/TBDC/0]_s$

The load-displacement and R-curve obtained for the $[90/60/90/-60/TBDC/0]_s$ substrate joints can be seen in Figure 6.11. Two out of four tested samples experienced crack deflection from the bond line into the substrate, samples 2 and 4 in the green and purple plot lines respectively (as seen in the fracture surface of Figure 6.12a); while the other two experienced cohesive failure (as seen in the fracture surface of Figure 6.12b).

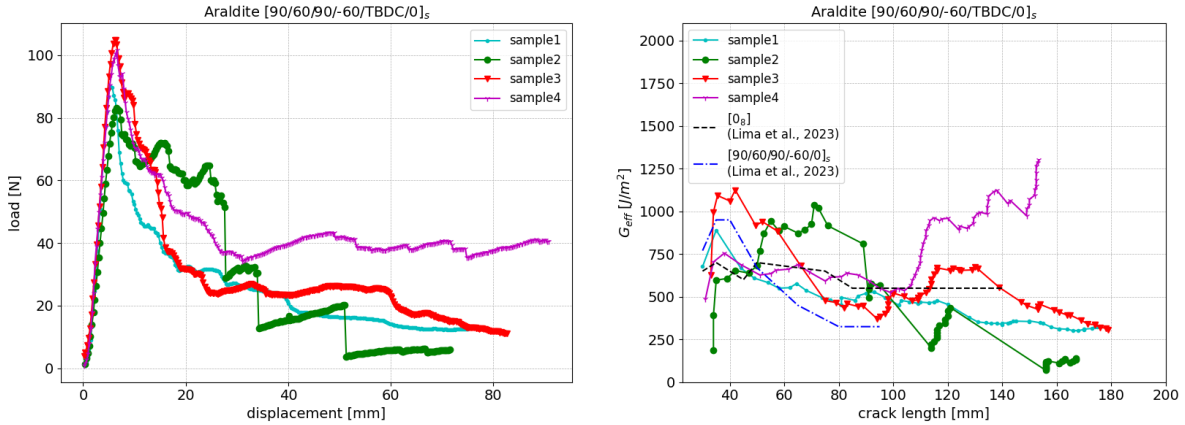

(a) **(b)**

Figure 6.11: Load-displacement curves (a) and R-curves (b) of $[90/60/90/-60/TBDC/0]_s$ Araldite 2015 joint specimens.

Maximum load values in the range of 80 N to 105 N can be observed for the $[90/60/90/-60/TBDC/0]_s$ joint test samples.

Looking at samples 1 and 3's R-curves in Figure 6.11b, an apparent onset toughening effect can be observed, resembling $[90/45/-45/TBDC/0]_s$ joint samples' results.

Samples 2 and 4, the ones that experienced crack deflection from the bond line into the composite substrate, present a slightly different load-displacement curve shape. Sample 2, for instance, shows a very similar curve shape to those of the UD/TBDC ply hybrid laminate specimens shown in Figure 6.8a from the point of maximum load, with cycles of slight increase in load followed by sharp drops.

Focusing on sample 2, G_{eff} values in-line with cohesive failure toughness values can be seen at the onset and beginning of crack propagation (see black dashed line of Figure 6.11b). At around 50 mm

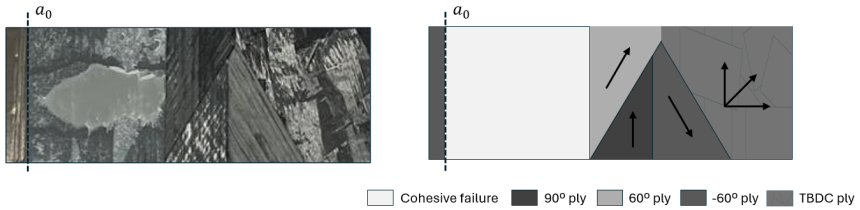

(a) [90/60/90/-60/TBDC/0]$_s$ joint - sample 2.

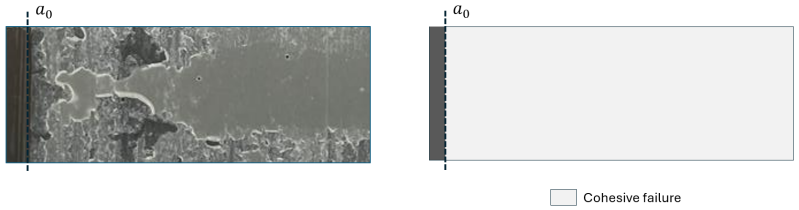

(b) [90/60/90/-60/TBDC/0]$_s$ joint - sample 3.

Figure 6.12: Fracture surface of representative samples for [90/60/90/-60/TBDC/0]$_s$ substrate Araldite 2015 joints (photo on the left and schematic on the right).

crack length, however, an increase in fracture toughness is observed until a maximum of 1040 J/m^2 is reached. Following the fracture toughness peak, a decrease takes place until a final fracture toughness value of 160 J/m^2 is reached.

Comparing sample 2's R-curve with the literature reported R-curve for the non-toughened [90/60/90/-60/0]$_s$ substrate joint, seen in the blue dash-dot line, a lower final fracture toughness value is reached. Contrarily to the non-toughened specimen's continuous and sharp drop, however, the decrease in fracture toughness recorded for the TBDC-toughened sample occurs more progressively. An overall less continuous drop is observed over 85 mm of crack propagation, resulting in a decrease in fracture toughness that is more than twice as long compared to the 40 mm recorded for the [90/60/90/-60/0]$_s$ joint specimen.

Sample 4's R-curve on the other hand exhibits cohesive failure level fracture toughness values up until a later crack length of 110 mm, followed by a toughness increase. From that point onward, a continuous increase in fracture toughness is observed in Figure 6.11b's R-curve and a consistent load value is maintained, as observed in Figure 6.11a, until the last recorded data point.

From the presented sample 2's fracture surface (see Figure 6.12a) it can be seen that, the crack path corresponds to what was expected and shown in Figure 4.2, with the final fracture happening at the TBDC layer. This was also the case for sample 4.

Representative samples

In Figure 6.13 the load-displacement and R-curve of one representative sample from each Araldite 2015 configuration are displayed.

The tested TBDC-toughened joint specimens results are plotted in solid color plot lines. Dash-dot and dotted lines of the same color, corresponding to the non-toughened version of the [90/45/-45/TBDC/0]$_s$ and [90/60/90/-60/TBDC/0]$_s$ joints, respectively, are also present.

Inspecting the [90/45/-45/TBDC/0]$_s$ specimen's R-curve, which failed cohesively, an apparent onset toughening effect of 30% is observed compared to the non-toughened [90/45/-45/0]$_s$ representative sample. This is noted in Figure 6.13b, with green circles connecting the onset toughness values of the TBDC-toughened and non-toughened laminate joints.

The R-curve of the [90/60/90/-60/TBDC/0]$_s$ specimen, represented by the solid red plot line, shows a notable increase in fracture toughness, with a maximum effective toughness gain of around 60% compared to cohesive failure, as noted in the red circles connecting the toughness values of the TBDC-

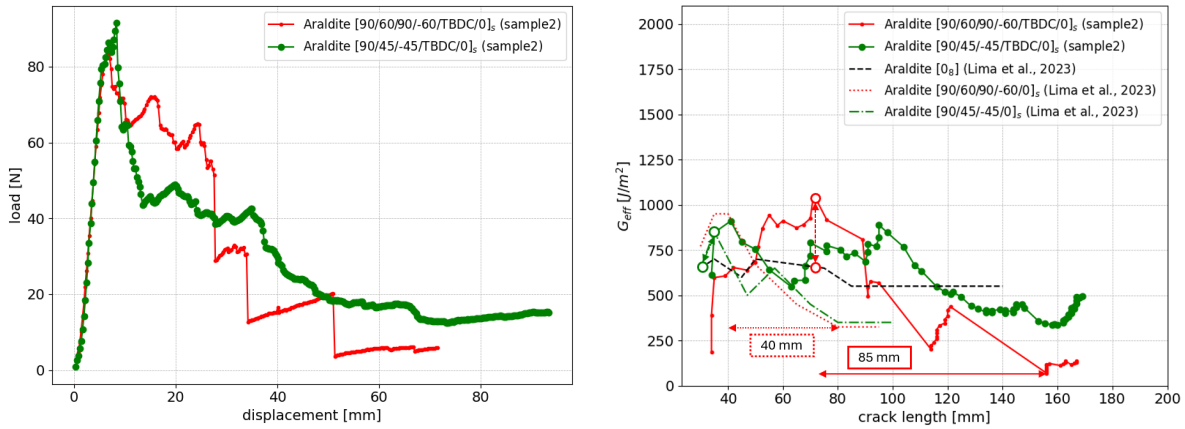

(a) (b)

Figure 6.13: Load-displacement curves (a) and R-curves (b) of Araldite 2015 joint specimens.

toughened and non-toughened joint configurations of Figure 6.13b. This peak value is approximately 10% higher than the maximum fracture toughness achieved by the non-toughened [90/60/90/-60/0]$_s$ joint specimen.

After reaching the peak, however, the TBDC-toughened and non-toughened configurations diverge further: while the drop from the maximum fracture toughness for the [90/60/90/-60/0]$_s$ specimen occurs over a crack propagation length of around 40 mm, a less continuous and more phased decrease is observed for the [90/60/90/-60/TBDC/0]$_s$ specimen. This decrease extends to over 85 mm, which is more than twice the length recorded for the non-toughened specimen, from the fracture toughness peak to the final toughness values. This toughness decrease lengthening can be seen, as noted, in Figure 6.13b.

6.2.3. AF 163-2U joint specimens

Two distinct AF 163-2U bonded joint DCB configurations were tested, one uni-directional and one TBDC-toughened cross-ply laminate, as detailed in Table 4.5. These AF 163-2U joints constitute the high-toughness adhesive joint configurations examined in the current thesis research.

[0$_8$]

The load-displacement and R-curve obtained for the UD, [0$_8$], substrate joints can be seen in Figure 6.14. Figure 6.15 shows the representative sample's fracture surface. All samples failed cohesively, enabling the calculation of the cohesive failure mode I fracture toughness values for the AF 163-2U adhesive material.

A maximum load of approximately 215 N was achieved for most samples, which exhibited very similar behavior from that point onward. As shown in Figure 6.14b, the calculated G_{eff} values are quite consistent among the samples, with an average value of around 2500 J/m^2 for crack propagation. Furthermore, comparable onset and maximum fracture toughness values can be observed between the tested AF 163-2U and the AF 163-2K results, as seen in the blue dash-dot line, reported in the literature [5].

[0/TBDC/90$_2$/0]$_s$

The load-displacement and R-curve obtained for the [0/TBDC/90$_2$/0]$_s$ substrate joint samples can be seen in Figure 6.16. The fracture surface of the representative sample (see Figure 6.17) shows that fractured happened inside the substrate laminate.

Examining the load-displacement curves presented in Figure 6.16a, varying maximum load values are observed, ranging from 280 N to 405 N. However, it is also evident that the overall load-displacement curve shape is similar among the samples. Each curve features an initial peak, followed by a sharp

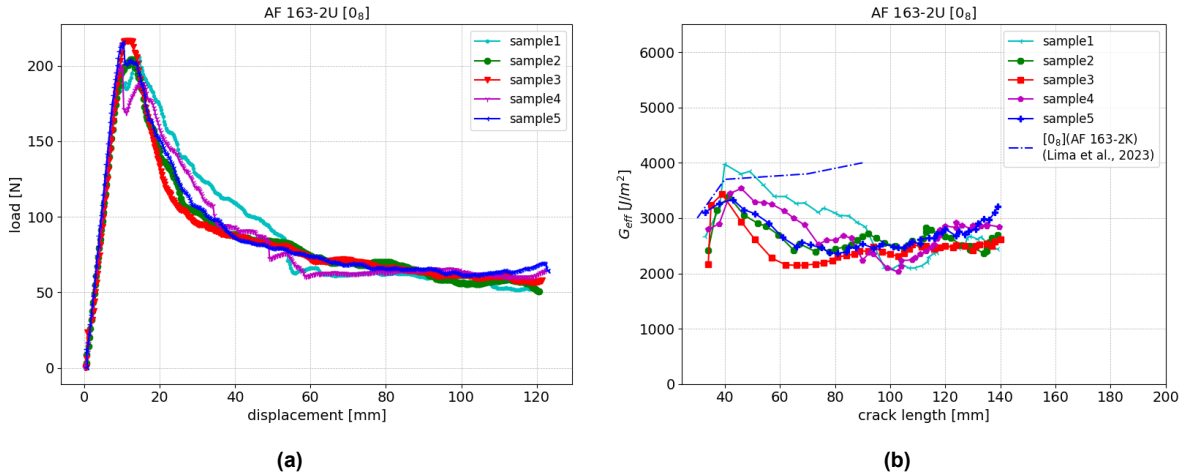

Figure 6.14: Load-displacement curves (a) and R-curves (b) of $[0_8]$ AF 163-2U joint specimens.

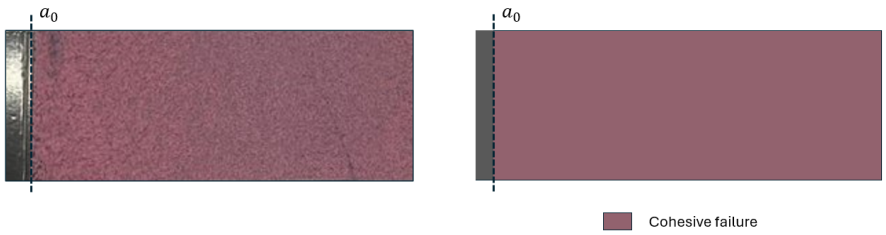

Figure 6.15: $[0_8]$ joint sample 2 fracture surface (photo on the left and schematic on the right).

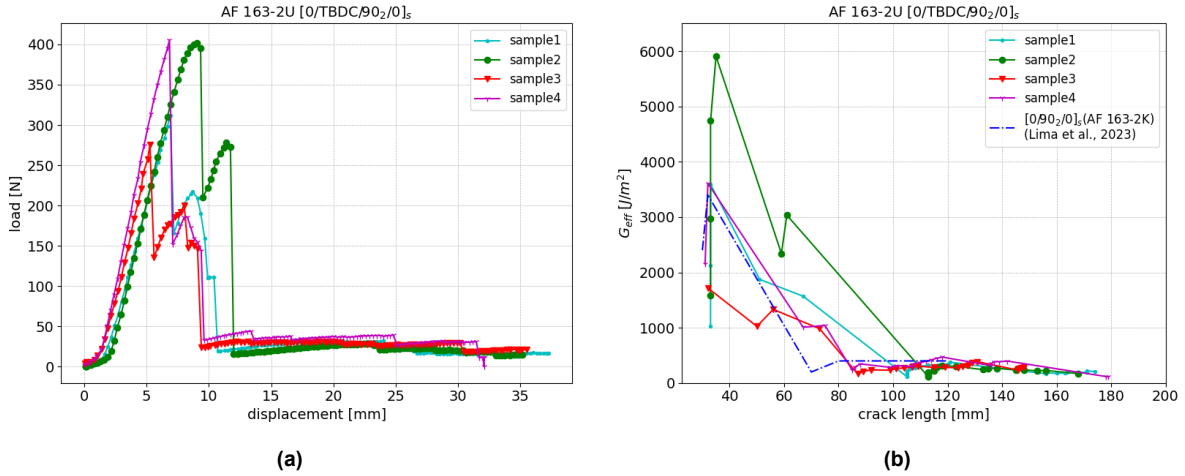

Figure 6.16: Load-displacement curves (a) and R-curves (b) of $[0/\text{TBDC}/90_2/0]_s$ AF 163-2U joint specimens.

drop in load, a subsequent second increase in load, and finally a second drop until a stable final load value is reached.

Figure 6.16b presents the fracture toughness values of the $[0/\text{TBDC}/90_2/0]_s$ substrate joint samples, in solid color plot lines, plotted against the cohesive failure fracture toughness value of a representative $[0_8]$ substrate joint, indicated by the black dashed line in Figure 6.16b. Additionally, it includes the R-curve of a representative sample of the non-TBDC-toughened $[0/90_2/0]_s$ substrate joint bonded with the AF 163-2K adhesive material, represented by the blue dash-dot line.

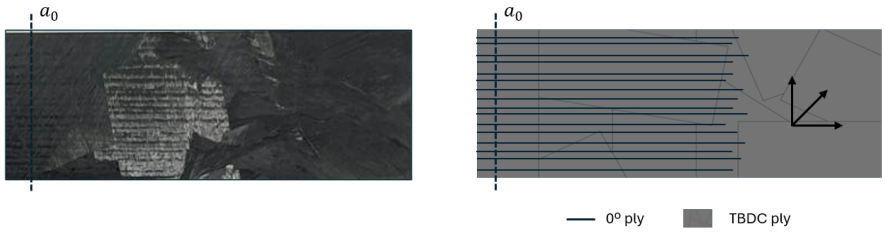

Figure 6.17: [0/TBDC/90_2/0]$_s$ joint sample 4 fracture surface (photo on the left and schematic on the right).

Upon closer inspection of the obtained G_{eff} results, a clear crack onset toughening effect is evident when compared to the cohesive failure's onset toughness in most samples, similar to the findings for the non-toughened [0/90_2/0]$_s$ substrate samples. It is important to note, however, that there is significant variance in the onset fracture toughness between samples. The similarities and differences observed in the R-curves reflect those found in the load-displacement curves.

Following the crack onset toughness peak, a decrease in fracture toughness is observed, highlighting the key differences between the TBDC-toughened and non-toughened specimens. The non-toughened [0/90_2/0]$_s$ substrate specimen experiences a sharp drop in toughness until a final fracture propagation toughness value is reached. In contrast, the toughened configuration, [0/TBDC/90_2/0]$_s$, exhibits this fracture toughness drop in two stages: after reaching a certain fracture toughness value, a small toughening cycle occurs, followed by another drop in toughness until it reaches a slightly lower final fracture toughness value compared to the non-toughened joint configuration.

It should be noted that the second fracture toughness drop happens at a crack length between 60 and 80 mm for all samples, which corresponds to the crack length at which the non-toughened substrate joint reaches its final fracture toughness: at this point the TBDC-toughened substrate joints present fracture toughness values 150% to 750% higher than the final fracture toughness values of non-toughened substrate joints. The TBDC-toughened joints' behavior enables a more segmented decrease in effective fracture toughness following a peak, similar to what was observed with the lower toughness adhesive material, Araldite 2015.

From the fracture surface of sample 4 (see Figure 6.17), the observed crack path aligns with expectations and matches the schematic in Figure 4.3, with final fracture occurring at the TBDC layer. Furthermore, 0-degree fibers are observed on the fracture surface at initial crack lengths. This behavior was consistent across all tested [0/TBDC/90_2/0]$_s$ joint samples.

Representative samples

In Figure 6.18, both the load-displacement and R-curves of one representative sample from each AF 163-2U configuration are displayed.

In Figure 6.18a, the load-displacement curves for the cohesive failure of the non-toughened [0_8] substrate joint specimen are displayed alongside the TBDC-toughened [0/TBDC/90_2/0]$_s$ specimen. Additionally, the R-curve of the [0/TBDC/90_2/0]$_s$ specimen is plotted against the AF 163-2U cohesive failure fracture toughness values obtained from the UD [0_8] joint specimens, both in solid color lines. The R-curve of the non-toughened [0/90_2/0]$_s$ specimen bonded with the AF 163-2K adhesive material is also presented in the purple dash-dot line.

Assessing the [0/TBDC/90_2/0]$_s$ specimen's R-curve, a similar onset fracture toughness to the non-toughened [0/90_2/0]$_s$ substrate joint is achieved. This corresponds to a 50% increase in onset fracture toughness compared to the cohesive failure onset toughness. After the fracture toughness peak, the differences between the TBDC-toughened and non-toughened versions of the [0/90_2/0]$_s$ substrate joints become clearer. As previously noted, the [0/TBDC/90_2/0]$_s$ specimen displays a secondary toughening phase after reaching its maximum toughness value, a behavior not observed in non-toughened substrates. In a final stage the TBDC-toughened specimen exhibits a slightly lower propagation toughness than the non-toughened specimen.

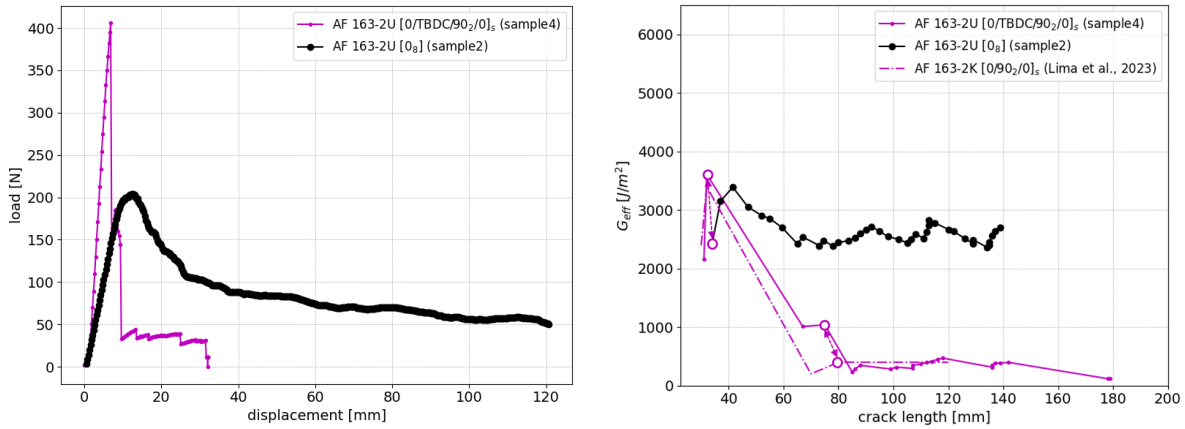

(a) **(b)**

Figure 6.18: Load-displacement curves (a) and R-curves (b) of AF 163-2U joint specimens.

It is worth noting that the onset toughening value may carry less significance due to the high variability among [0/TBDC/90$_2$/0]$_s$ joint sample results, as shown in Figure 6.16b.

Average effective fracture toughness and failure modes for all tested DCB configurations can be seen in Appendix A, Table A.23.

7

Discussion

In this chapter, the effective fracture toughness results of representative samples for each TBDC-toughened configuration will be presented in detail. These results will be accompanied by camera and microscope images, as well as topographical images of the samples' fracture surfaces. By correlating the different data collected, the fracture and toughening mechanisms responsible for the fracture toughness behavior observed in the R-curves, as presented in section 6.2, will be explored and discussed.

7.1. UD/TBDC ply CFRP laminates

Both UD/TBDC ply hybrid CFRP laminate configurations will be discussed in the present section.

$[0_{12}/\text{TBDC}_2/0_{12}]$

In Figure 7.1, the R-curve of a representative $[0_{12}/\text{TBDC}_2/0_{12}]$ sample is shown, with key aspects of the specimen's fracture path highlighted. These highlights are accompanied by corresponding test images and a topography image of the fracture surface, which shows the crack length at each highlighted point.

Looking at the fracture surface in Figure 7.1b, it is evident that fracture propagation occurred within the TBDC layers throughout the entirety of the propagation phase. However, as shown in the microscope images of Figure 7.1c, from point 7 onward, the final fracture occurs very close to the UD/TBDC interface.

Point 1 marks the initial crack propagation phase and occurs right after crack onset. It is important to note that, due to the defective condition of the test specimens, as discussed in section 4.4, determining the exact moment of crack onset is challenging.

As the crack progresses through the sample, the fracture toughness reaches its first peak at point 2. By examining the corresponding travelling microscope image in Figure 7.1c, the peak occurs simultaneously with crack deflection and branching through the laminate's TBDC layers. This peak is followed by a drop, corresponding to the crack propagating through one of the competing crack fronts from point 2. This can be observed in point 3's travelling microscope image, where only the main crack path and the sample's UD/TBDC interface region defect are visible.

From point 3 onward, up to point 6, additional toughening cycles can be identified as the crack continues to propagate through the TBDC layers, progressing downward toward the UD/TBDC interface. This crack deflection is visible by comparing the travelling microscope images at points 3 and 6: the crack front advances farther from the laminate's midplane as the crack progresses.

The fracture toughness observed between points 2 and 6 suffers a reduction and a minimum is reached at point 7. Microscope images in Figure 7.1c reveal that this G_{eff} minimum corresponds to the crack path approaching a UD/TBDC ply interface. At this stage, the fracture toughness is similar to that of the crack propagation toughness of the non-toughened $[0_{24}]$ laminate: around 200 J/m^2 as seen in Figure 7.1a.

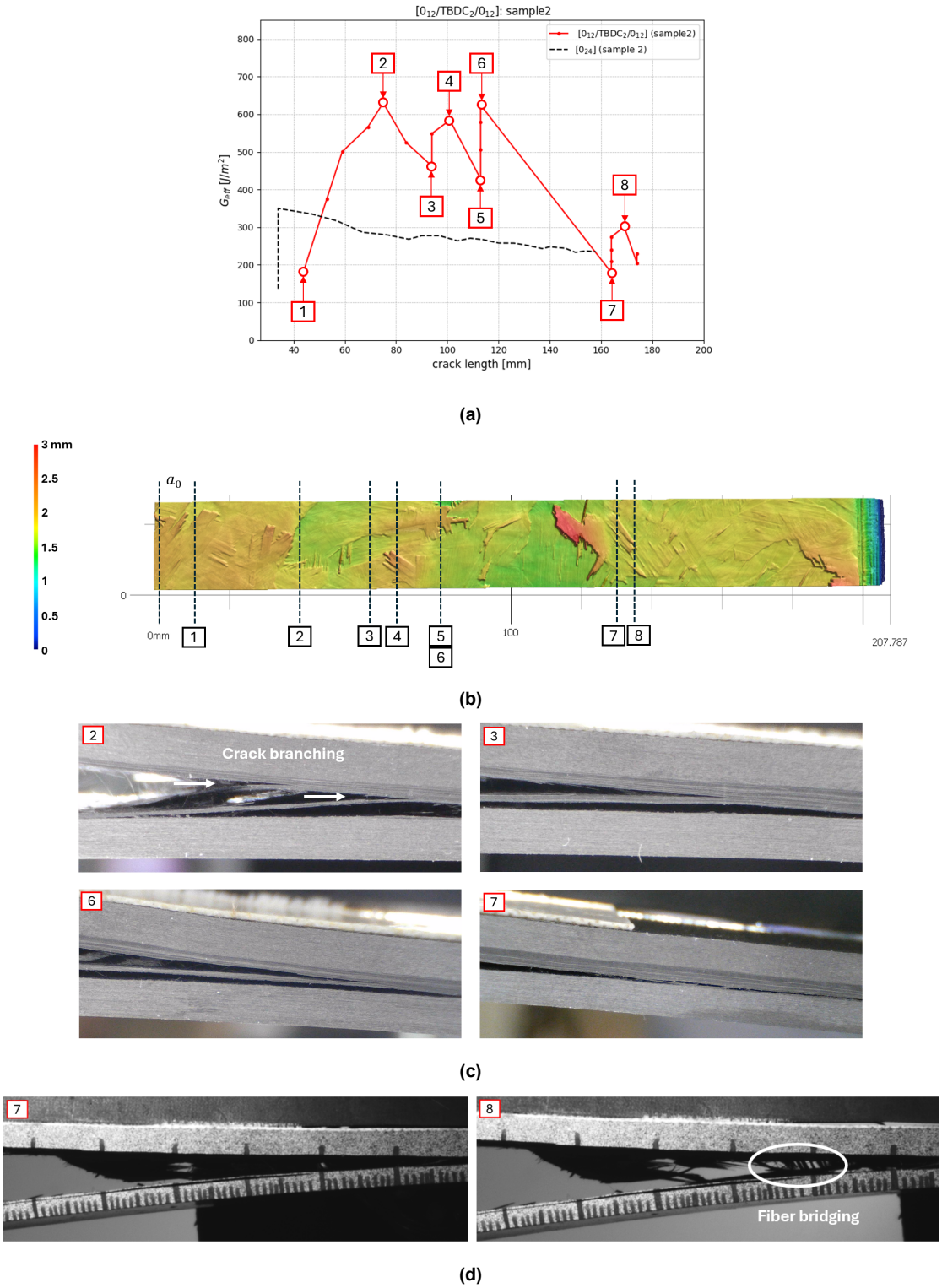

Figure 7.1: R-curve (a), fracture surface (b), travelling microscope (c) and camera pictures (d) of $[0_{12}/TBDC_2/0_{12}]$ sample 2.

During the crack's final path, a small final toughening cycle is visible in the R-curve of Figure 7.1. Examining the camera images corresponding to points 7 and 8, TBDC fiber bridging is visible.

$[0_{12}/TBDC_4/0_{12}]$

In Figure 7.2, the R-curve of a representative $[0_{12}/TBDC_4/0_{12}]$ sample is shown, with key aspects of the specimen's fracture path highlighted, accompanied by corresponding test images and a topography image of the fracture surface.

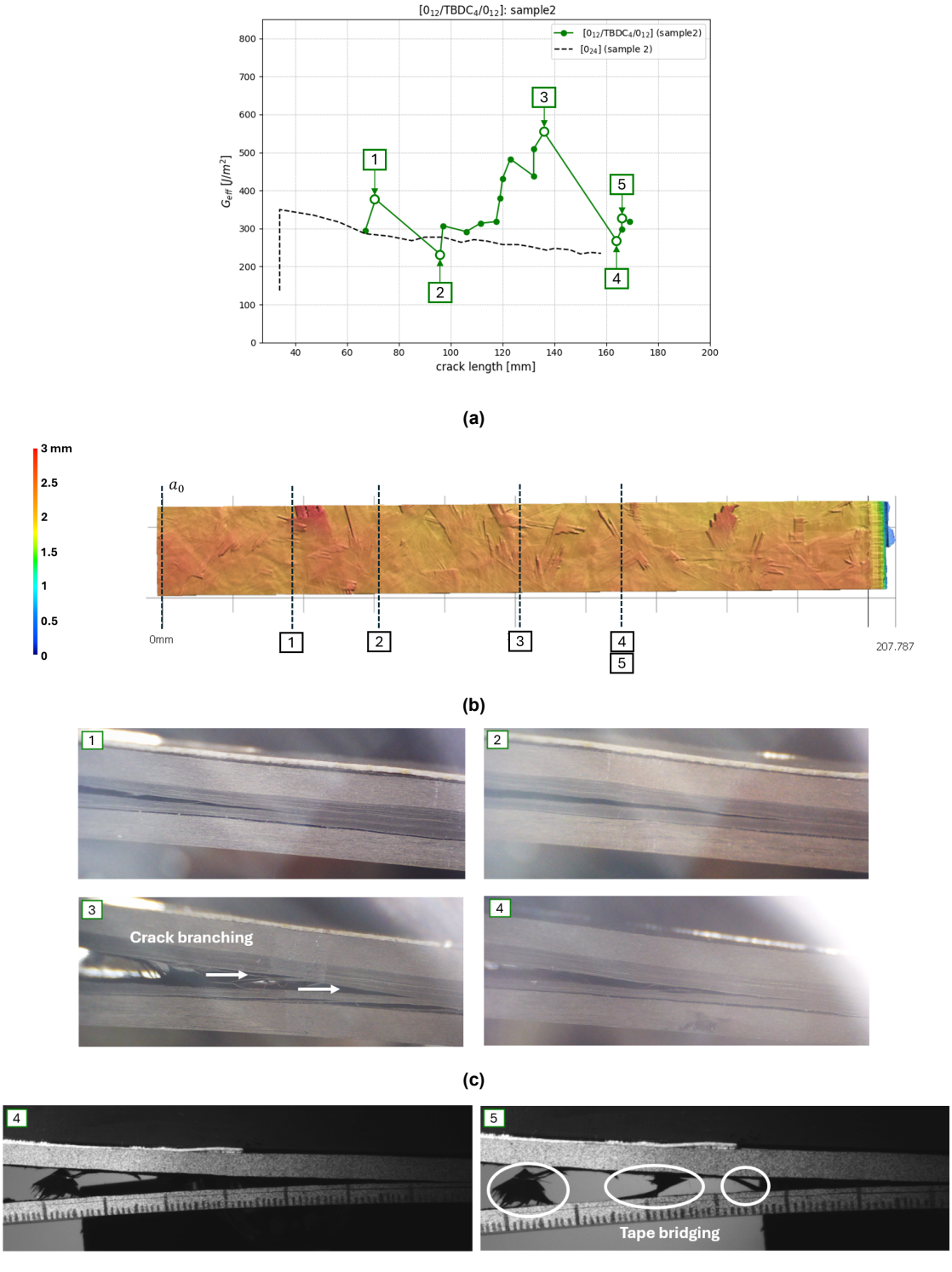

Figure 7.2: R-curve (a), fracture surface (b), travelling microscope (c) and camera pictures (d) of $[0_{12}/TBDC_4/0_{12}]$ sample 2.

From observing Figure 7.2b, it is clear that the crack propagation occurred entirely within the TBDC layers. However, in the case of the chosen representative sample, the crack front had not reached the UD/TBDC interface close vicinity by the time the last data point was recorded (see Figure 7.2c, point 4).

Points 1 and 2 reflect the initial crack propagation stage. As seen in the travelling microscope images from Figure 7.2c, no clear fracture mechanics responsible for increasing fracture toughness are apparent at this stage. The crack propagates steadily along the laminate's mid-plane and the black dashed line, of the non-toughened [0_{24}] laminate, and green solid line in Figure 7.2a can be seen very close between points 1 and 2, with similar fracture toughness values.

Beyond point 2, crack branching and deflection begin to develop ahead of the crack front. This behavior is evident from the travelling microscope image at point 3. Similarly, point 4 shows the crack tip has been deflected downward while remaining within the TBDC layers, corresponding to a decrease in fracture toughness.

Finally, from point 4 to point 5, a slight increase in fracture toughness is observed as the crack tip remains relatively still, while the arms of the sample continue to open. Visible fiber and TBDC tape bridging can be seen in the camera pictures of points 4 and 5 (see Figure 7.2d). The crack tip, however, is not seen to have reached near the UD/TBDC interface at the last recorded data point. As a result, a higher effective toughness is seen compared to the non-toughened [0_{24}] laminate, in the black dashed line, as the primary toughening mechanisms facilitated by crack propagation through the TBDC layers, such as crack deflection, are likely active at that stage.

General observations

From investigating both tested TBDC-toughened, non-joint DCB configurations, it is evident that the fracture mechanisms facilitated by the discontinuous and randomly oriented nature of the TBDC layers contribute significantly to increasing fracture toughness. In both tested configurations, crack branching and deflection are observed, which correspond to the highest peaks in the R-curves. Moreover, TBDC tape and fiber bridging are seen throughout the crack propagation in the TBDC material, further enhancing the toughening effects.

However, it is important to note that crack deflection within the TBDC material generally leads the crack tip toward a UD/TBDC interface, after which the crack finds its final propagation path. This last phase of fracture propagation, as shown in Figure 7.1, corresponds to effective fracture toughness values of around 200 J/m^2 to 300 J/m^2 - very similar to those of UD ply crack propagation in non-toughened laminates. Therefore, the substantial toughening effects, observed in UD/TBDC ply hybrid laminate DCB samples, hold until the crack front reaches near the UD/TBDC interface. At this stage, only slight TBDC tape and fiber bridging is seen, leading to an insignificant toughening effect as the fracture toughness values are compared to those of non-toughened samples.

Due to the post-curing defects of the test specimens and the limited number of samples tested for the [0_{12}/TBDC$_4$/0_{12}] configuration, it is difficult to draw definitive conclusions regarding the effect of the number of TBDC layers in the hybrid laminates.

Lastly, even though the general R-curve shape and crack propagation behavior of UD/TBDC ply hybrid CFRP laminates are similar, scatter was observed for TBDC material crack propagation (see Figures 6.2b and 6.4b). This has been reported in literature, by Katsivalis et al. [41], and is explained by the random stacking and orientation of the material's tapes, which create various small interfaces with random and different angle differences that contribute to the observed scatter.

7.2. TBDC-toughened adhesively bonded joints

The fracture toughness results of the three TBDC-toughened adhesively bonded joint configurations, utilizing two different toughness adhesive materials, will be discussed in this section.

7.2.1. Araldite 2015 joint specimens

The results of the two different TBDC-toughened joint configurations, using Araldite 2015, the low-toughness adhesive material in the present thesis research, will be discussed in detail.

$[90/45/\text{-}45/\text{TBDC}/0]_s$
In Figure 7.3, the R-curve of a representative Araldite 2015 joint sample is shown, with key aspects of the specimen's fracture path highlighted, accompanied by corresponding travelling microscope test images and a topography image of the fracture surface.

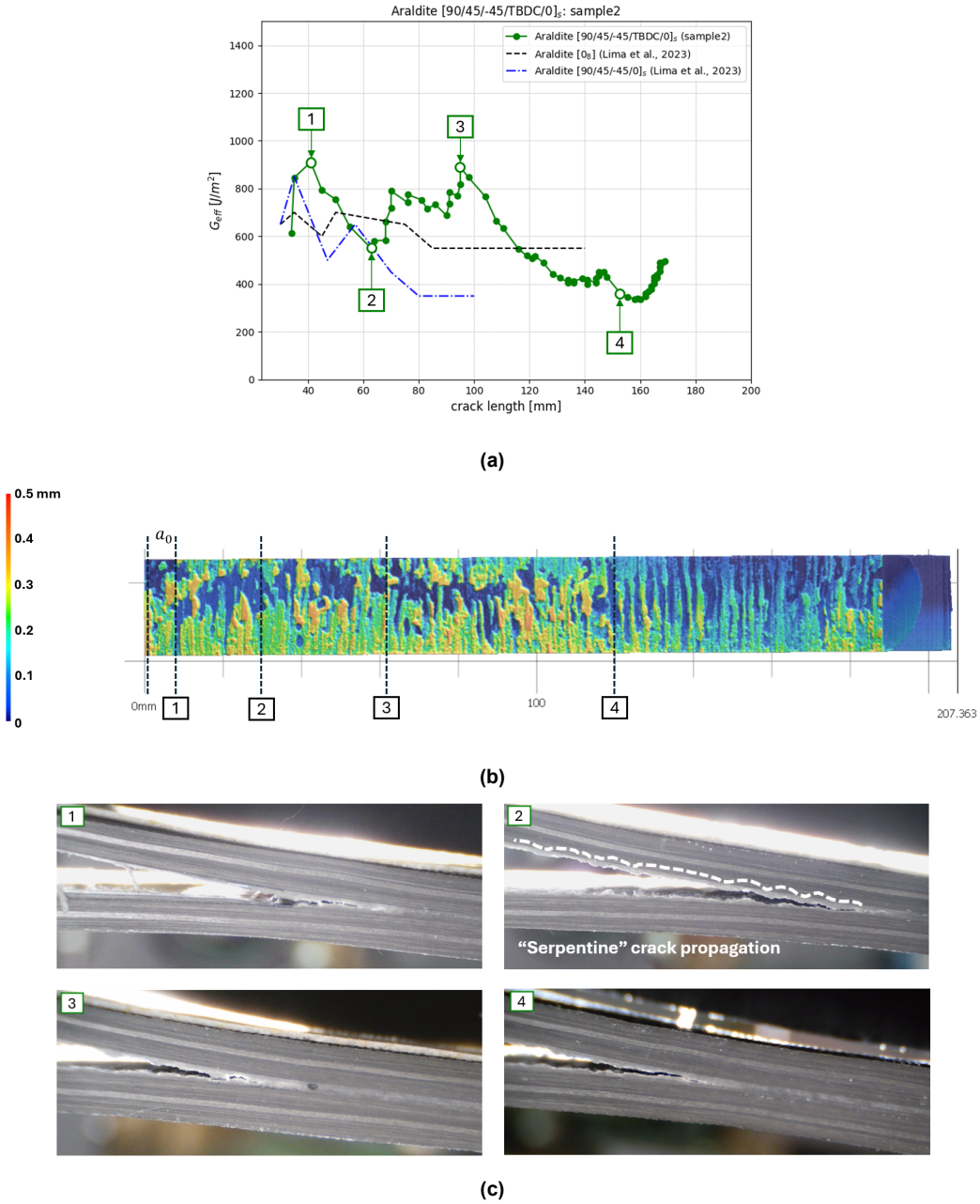

Figure 7.3: R-curve (a), fracture surface (b) and travelling microscope (c) of $[90/45/\text{-}45/\text{TBDC}/0]_s$ joint sample 2.

Observation of the fracture surface in Figure 7.3b reveals that fracture propagation occurred entirely within the adhesive layer, indicating cohesive failure.

The onset toughness value for the cohesive failure of the representative sample closely matches the maximum toughness reported in literature for non-toughened $[90/45/\text{-}45/0]_s$ specimens, as seen in the blue dash-dot line of Figure 7.3a. These experienced an onset toughening effect due to crack deflection to the substrate, which did not occur in the $[90/45/\text{-}45/\text{TBDC}/0]_s$ joint specimens. This higher

onset toughness is seen across most cohesive failure specimens, though no specific mechanism — whether in the bond line or substrate — could be identified to explain this observation. Furthermore, these values, although higher than those recorded at larger crack lengths, align with cohesive failure toughness values reported by Fernandes et al. [55].

After the crack onset, during crack propagation, the [90/45/-45/TBDC/0]$_s$ Araldite 2015 samples exhibit an unstable cohesive failure behavior, which is apparent in representative sample 2, as shown in Figure 7.3. In the fracture surface topography image of Figure 7.3b, a distinct ”patchy” pattern is observed. This correlates with the ”serpentine” crack propagation path visible in the travelling microscope images in Figure 7.3c. Across both the length and width of the test sample, the crack followed a non-linear, winding path.

Looking at the [90/45/-45/TBDC/0]$_s$ joint sample R-curve of Figure 7.3a, an unstable shape is seen, which alternates between fracture toughness values above and below those for cohesive failure of Araldite 2015 in joints with unidirectional substrate laminates (indicated by the black dashed line in Figure 7.3a). As the crack tip advances through the samples alternating thinner and thicker adhesive segments, the crack alters its path, leading to the observed instability in fracture toughness values. From these observations, the ”serpentine” crack propagation behavior seems to incur a fracture energy cost.

[90/60/90/-60/TBDC/0]$_s$

In Figure 7.4, the R-curve of a representative [90/60/90/-60/TBDC/0]$_s$ Araldite 2015 joint sample is shown, with key aspects of the specimen’s fracture path highlighted, accompanied by corresponding travelling microscope and camera test images and a topography image of the fracture surface.

The [90/60/90/-60/TBDC/0]$_s$ substrate joints were the only low-toughness adhesive material configuration that experienced crack deflection.

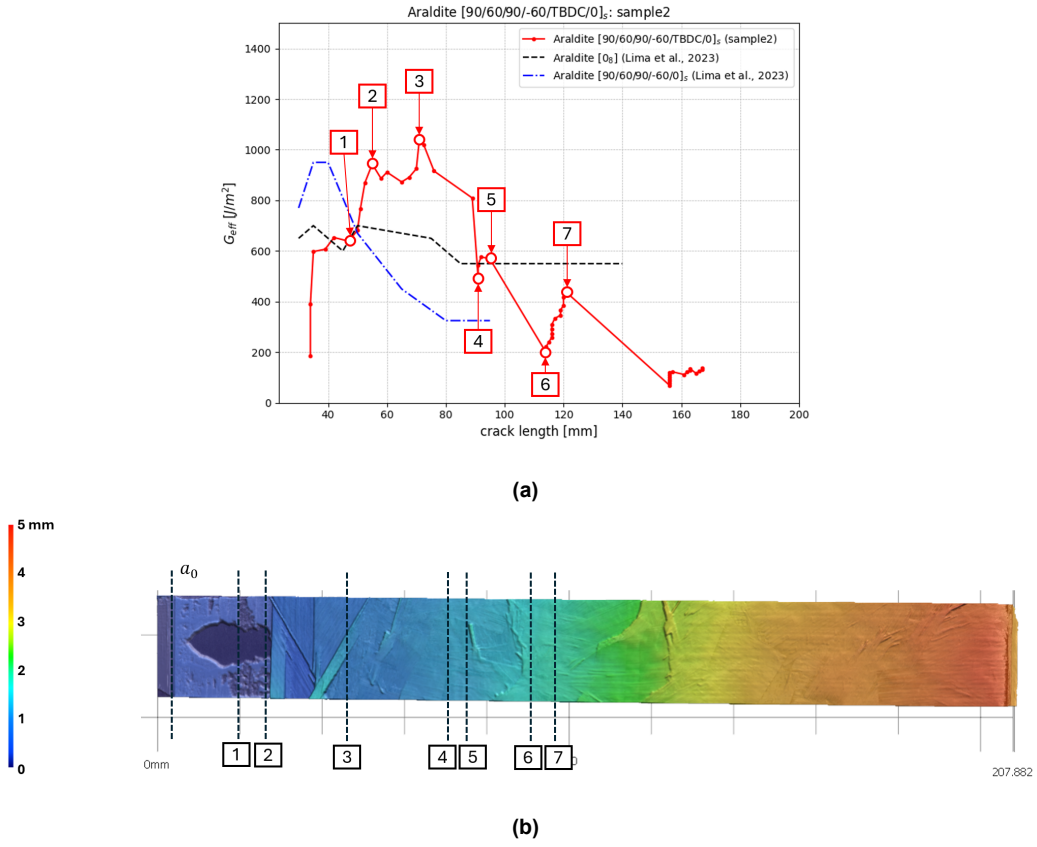

Figure 7.4: R-curve (a) and fracture surface (b) of [90/60/90/-60/TBDC/0]$_s$ joint sample 2.

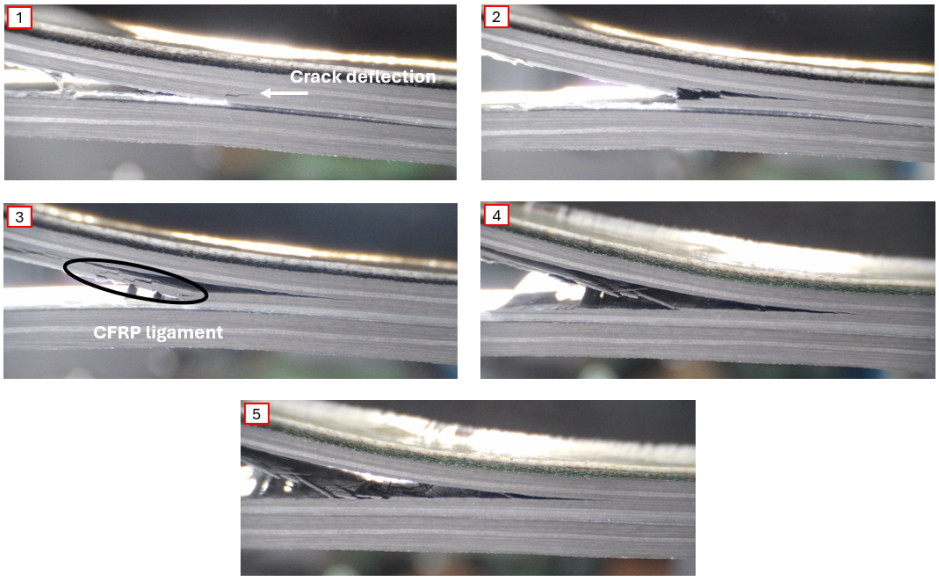

(c)

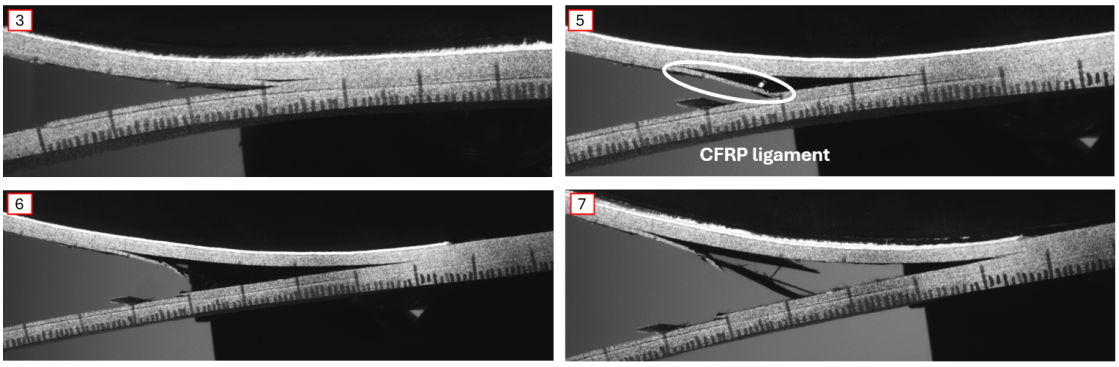

(d)

Figure 7.4: Travelling microscope (c) and camera pictures (d) of [90/60/90/-60/TBDC/0]$_s$ joint sample 2. (Continued from previous page.)

Looking at Figure 7.4a and its corresponding fracture surface in Figure 7.4b, as well as the travelling microscope images in Figure 7.4c, the changes in effective fracture toughness values can be linked to the crack path. From crack onset until point 1, the fracture toughness values are very similar to those reported in literature for the cohesive failure of Araldite 2015 (see black dashed line of Figure 7.4a). From point 1 to point 3, a significant increase in fracture toughness is observed. Examining the travelling microscope images, this coincides with the development of a new crack front in the substrate, followed by a subsequent crack deflection from the bond line to the substrate. Around a 60% increase in effective propagation fracture toughness at point 3 compared to cohesive failure at the same crack length is observed.

As the R-curve reaches its peak at point 3, a sharp drop in fracture toughness follows. The travelling microscope image at point 3 reveals a relatively thick CFRP ligament between the bond line and substrate crack fronts. Once the ligament breaks and the crack tip fully deflects from the bond line to the substrate, the fracture toughness drops significantly (see Figures 7.4a, 7.4b and 7.4c, point 4).

The observed drop in fracture toughness is consistent between both the tested TBDC-toughened sample and the non-toughened [90/60/90/-60/0]$_s$ joint sample, as illustrated by the blue dash-dot line in Figure 7.4a. However, there is a significant difference in the manner in which the effective fracture toughness decreases. In the case of the non-toughened [90/60/90/-60/0]$_s$ joint configuration, a contin-

uous, sharp decline in toughness occurs until a final fracture toughness value is reached. Conversely, the tested TBDC-toughened [90/60/90/-60/TBDC/0]$_s$ joint configuration exhibits a more segmented drop in fracture toughness before stabilizing at its final value.

Between points 4 and 5, and points 6 and 7, toughening cycles are evident until a subsequent drop in toughness occurs. An examination of the travelling microscope images at points 4 and 5 reveals that the CFRP ligament, visible at point 3, continues to oppose the advancement of the TBDC layer's crack front, albeit to a lesser extent than before the break. The wider camera images in Figure 7.4d further show that the CFRP ligament remains prominent at point 5, where a second rupture occurs, coinciding with another drop in fracture toughness. Finally, between points 6 and 7, the camera images reveal that although the CFRP ligament becomes slimmer and moves farther behind the crack tip, it continues to bridge the crack paths. This behavior aligns with one final toughening cycle before the ligament ultimately fails, enabling the crack to propagate at its final effective toughness value.

General observations

It's important to discuss why crack deflection from the bond line to the substrate happened in two [90/60/90/-60/TBDC/0]$_s$ joint samples and in none of the [90/45/-45/TBDC/0]$_s$ joints samples. Looking at the three-point bending results shown in section 6.1, two key observations can be made:

1. On average, the flexural modulus of the [90/45/-45/TBDC/0]$_s$ laminates is higher than that of the [90/60/90/-60/TBDC/0]$_s$ laminates.
2. There is significant variability in flexural response between samples with the same stacking sequence.

Similar crack deflection favorable angles, close to 90 degrees at the bonding surface, as reported by Lima et al. [5], are observed in both the [90/45/-45/TBDC/0]$_s$ and [90/60/90/-60/TBDC/0]$_s$ laminates. However, the laminates exhibit significantly different flexural moduli. This suggests a potential link between the flexural modulus and the likelihood of crack deflection from the bond line to the substrate in joints utilizing these laminates as substrates.

Additionally, the variability in flexural modulus within samples, combined with the likely adhesive layer thickness gradients (discussed in section 4.5 from the results shown in Figure 6.1), helps explain the differences in fracture behavior among the [90/60/90/-60/TBDC/0]$_s$ joint samples. While two samples experienced crack deflection or competition, the other two exhibited cohesive failure. This suggests that small differences in laminate properties due to the random nature of TBDC material and adhesive layer thickness can significantly influence the fracture mechanisms, leading to the variation observed across the different samples.

When crack deflection occurs from the bond line to a UD/TBDC ply hybrid laminate substrate a toughening effect is observed. This effect, with similar results, is also seen in non-toughened substrates however. Significant differences become apparent after the toughening phase, when a drop in fracture toughness occurs. The TBDC-toughened joints facilitate a more segmented and less continuous decline in fracture toughness compared to their non-toughened counterparts. This longer drop is attributed to CFRP ligaments bridging the initial and the more energetically favorable crack front in the substrate. As these ligaments break, they enable slight toughening cycles while allowing the substrate crack front to develop until a final propagation toughness value is reached. Notably, this segmented decrease in fracture toughness represents more than a 100% increase in the length recorded over the fracture toughness drop reported for the non-toughened specimen, from the peak fracture toughness to the final toughness values.

It is important to note, however, that contrary to initial expectations discussed in chapter 2, the final fracture toughness values — resulting from the crack propagating through the TBDC layer, as seen in the fracture surface of Figure 7.4b — are significantly lower than those observed for the non-toughened joints. The crack propagation through the TBDC layer presents effective toughness values as low as 140 J/m^2; around 60% lower compared to the 330 J/m^2 final fracture toughness value reported for non-toughened substrate joints (see the final fracture toughness values of blue dash-dot and solid red lines of Figure 7.4a).

7.2.2. AF 163-2U joint specimens

The results of the single TBDC-toughened joint configuration, $[0/TBDC/90_2/0]_s$, using AF 163-2U, the high toughness adhesive material in the present thesis research, will be discussed in detail.

$[0/TBDC/90_2/0]_s$

In Figure 7.5, the R-curve of a representative $[0/TBDC/90_2/0]_s$ AF 163-2U joint sample is shown, with key aspects of the specimen's fracture path highlighted, accompanied by corresponding travelling microscope and camera test images and a topography image of the fracture surface. It is important to note that the representative sample chosen for this section differs from the one selected in section 6.2. In section 6.2, an average fracture toughness sample was used as the representative sample. However, for the purposes of investigating and discussing the fracture and toughening mechanics involved, sample 2 - exhibiting the highest toughening effect - was chosen. Although all samples displayed the same fracture mechanisms, sample 2 provides the clearest images of these mechanisms, which is advantageous for the current discussion.

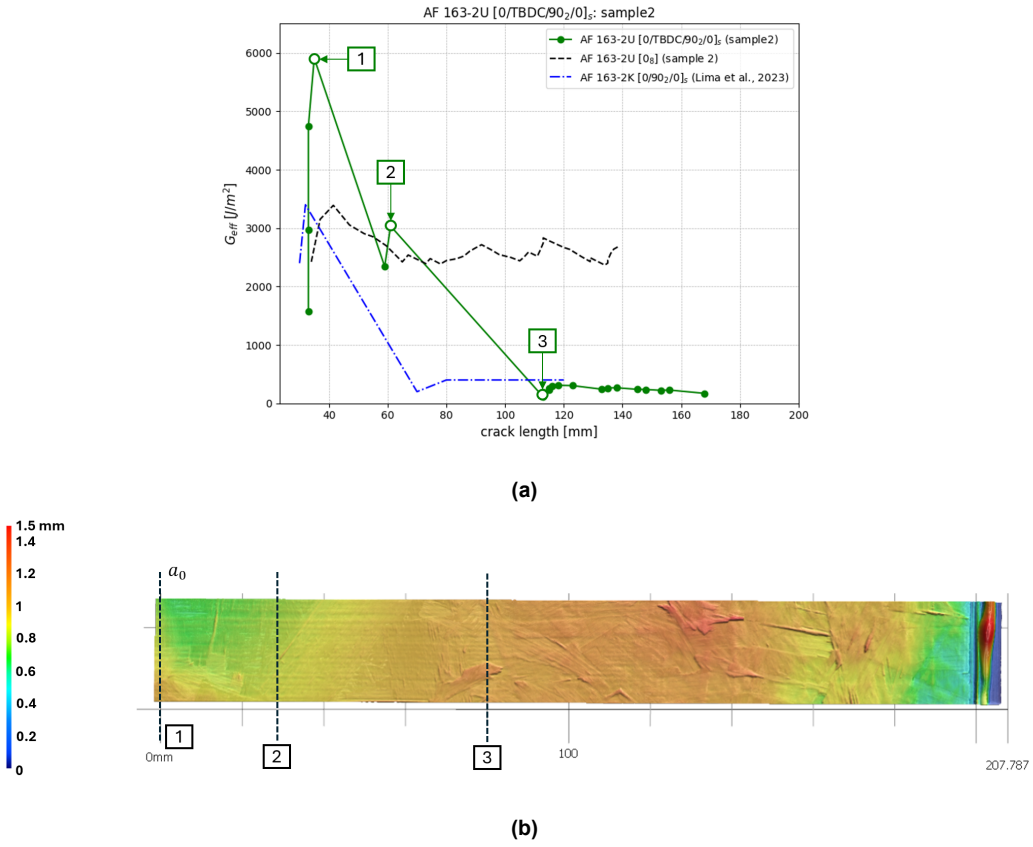

Figure 7.5: R-curve (a) and fracture surface (b) of $[0/TBDC/90_2/0]_s$ joint sample 2.

Examining the fracture surface in Figure 7.5b, it is evident that the final fracture surface is entirely within the TBDC layer of one of the joint's substrates. This suggests that the crack propagated fully within the adherend rather than deflecting from the bond line, where the initial crack is located.

A similar general R-curve shape to that of the non-toughened $[0/90_2/0]_s$ joint, as shown the blue dash-dot line of Figure 7.5a, is observed for the TBDC-toughened AF 163-2U joints. However, akin to the behavior seen with the low-toughness adhesive Araldite 2015, the effective fracture toughness drop that follows the maximum value is longer and more segmented compared to the sharp and continuous drop reported for the non-toughened joints.

A review of the travelling microscope and camera images at points 1 and 2, along with their corresponding fracture toughness values, reveals a competition between the initial bond line crack front and a new crack front developing within the substrate, specifically at the interface between the 0-degrees ply and

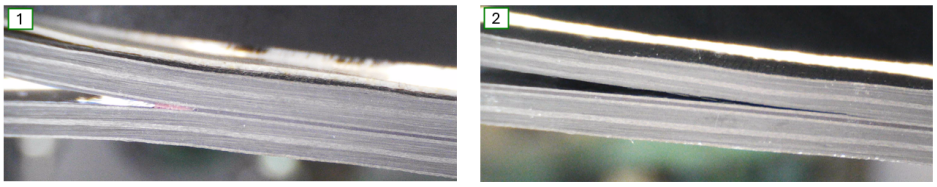

(c)

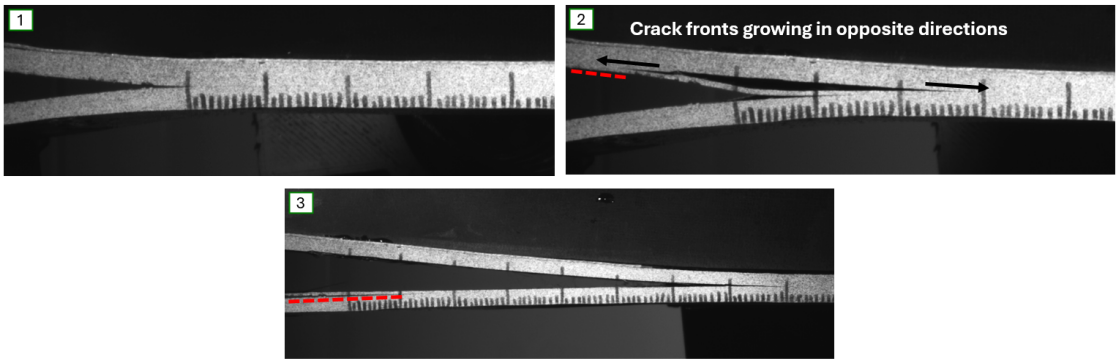

(d)

Figure 7.5: Travelling microscope (c) and camera pictures (d) of $[0/\text{TBDC}/90_2/0]_s$ joint sample 2. (Continued from previous page.)

the TBDC layer (see Figures 7.5c and 7.5d, points 1 and 2). Right before a new crack develops in the substrate, a peak in fracture toughness is seen (point 1). As the new crack front propagates through the substrate, a subsequent drop in fracture toughness occurs (point 2).

Focusing on the camera image at point 2, which corresponds to a second peak in the sample's R-curve (see Figure 7.5a), two crack fronts can be observed within the TBDC layer. By examining the subsequent image at point 3, it becomes clear that these crack fronts are advancing in opposite directions until the backward-growing front reaches the edge of the sample, separating the CFRP ligament that blocks the free advancement of the TBDC layer's crack front. Simultaneously, at point 3, when the CFRP ligament is released, a significant reduction in fracture toughness is evident. From point 3 onward, a final crack propagation fracture toughness of around 200 J/m^2 is observed, lower than that found for the non-toughened $[0/90_2/0]_s$ joint present in the blue dash-dot line of Figure 7.5a.

In the case of the TBDC-toughened $[0/\text{TBDC}/90_2/0]_s$ substrates the joints toughness decrease happens over a longer crack length range after reaching a maximum value, presenting a second toughening cycle at the crack length that the non-toughened $[0/90_2/0]_s$ substrate joints reach their final crack propagation value. The presence of the CFRP ligament in the toughened substrates plays a crucial role, as it is likely absent in the non-toughened joints or does not impede the fracture toughness drop to the same extent. This difference is evident in the blue dash-dot R-curve of Figure 7.5a and in the reported fracture surface shown in Figure 7.6, where remnants of cohesive failure are visible prior to the beginning of the 0-degrees ply.

From the examination of the fracture surface in Figure 7.5b and Figure 6.17, on the other hand, it is apparent that 0-degrees fiber tows are visible at the beginning of the crack's propagation path and gradually disappear along the sample's length in $[0/\text{TBDC}/90_2/0]_s$ joint samples. This indicates that the crack initiates at the interface of the 0-degrees and TBDC plies and, as it propagates, moves further into the TBDC layer, a behavior that is common between all $[0/\text{TBDC}/90_2/0]_s$ joint samples.

General observations

Considering the results and fracture mechanisms observed for all TBDC-toughened substrate joint specimens that experienced crack deflection from the bond line to the substrate — using both the low-toughness bi-component adhesive Araldite 2015 and the high-toughness film adhesive AF 163-2U

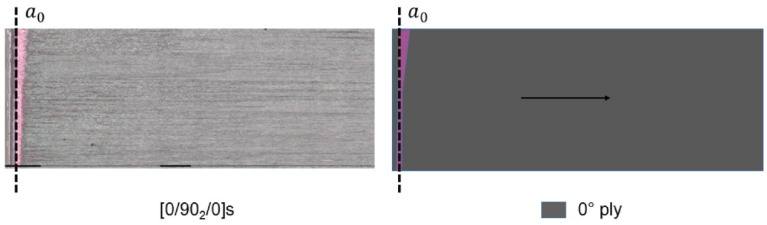

Figure 7.6: Fracture surface of $[0/90_2/0]_s$ AF 163-2K joint representative sample [5].

— it is clear that the same crack competition and deflection toughening mechanisms for non-TBDC-toughened substrate joints reported in literature [5] are present. However, the UD/TBDC ply hybrid laminate substrates only make a significant impact after the maximum effective fracture toughness is reached. These TBDC-toughened substrates promote the formation of CFRP ligaments connecting the initial bond line and substrate crack fronts, which induce small toughening cycles that delay the fracture toughness drop. This occurs as the CFRP ligament is progressively released through delamination or fiber failure, depending on the specific stacking sequence tested.

The final crack propagation toughness values for the joint samples where propagation occurred within the TBDC layer ranged approximately between 150 to 250 J/m^2. These values closely align with the toughness values observed in UD/TBDC ply hybrid laminate samples during the final phase, where the crack propagates in the close vicinity of the UD/TBDC interface (see Figure 7.1a). When the crack advances through TBDC layers with ample material above or below the crack plane, the primary TBDC toughening mechanisms are active. However, when the crack reaches a point where little to no TBDC material is present in one direction, the toughening effect becomes insignificant, and UD crack propagation fracture toughness values (in the order of 200 J/m^2 to 300 J/m^2) are observed. Since only one TBDC layer was stacked at a time in the TBDC-toughened joint substrates, it is possible that insufficient TBDC material was available on both sides of the crack plane, preventing the primary TBDC toughening effects observed in UD/TBDC ply hybrid CFRP laminate specimens from occurring during the joints' substrate crack propagation phase.

8

Conclusion & Recommendations

8.1. Conclusion

The present thesis research project focused on exploring the influence of Tow-Based Discontinuous Composite (TBDC) interleaves on the mode I fracture toughness of adhesively bonded Carbon Fiber Reinforced Polymer (CFRP) joints, aiming to enhance toughness.

The first objective was to understand how integrating TBDC interleaves into the midplane of unidirectional CFRP laminates with a mid-plane crack impacts mode I fracture behavior. Additionally, the study aimed to investigate the fracture mechanisms during TBDC crack propagation in hybrid UD/TBDC ply laminates and how the number of TBDC layers influences these mechanisms and the resulting fracture toughness.

Three different configurations of CFRP laminate Double-Cantilever Beam (DCB) samples were tested: [0_{24}], a non-toughened laminate used as the baseline for mode I fracture onset and propagation of the CFRP material; [0_{12}/TBDC$_2$/0_{12}], a laminate toughened with two TBDC layers (around 17% of the laminate's total volume) positioned above and below the initial crack plane; and [0_{12}/TBDC$_4$/0_{12}], a laminate toughened with four TBDC layers (about 29% volume), with two layers placed above and two below the initial crack plane.

A maximum of 130% higher effective fracture toughness was observed in representative samples of TBDC-toughened laminates compared to non-toughened ones, for the same crack length. These toughening effects resulted from mode I fracture mechanisms triggered by the crack's propagation through the TBDC layers, such as crack branching, crack deflection, and TBDC tape and fiber bridging.

However, once the crack deflected and approached the UD/TBDC interface, a reduction in fracture toughness was observed, with the values becoming similar to those found in unidirectional CFRP crack propagation.

In addition, a second study on adhesively bonded composite joints addressed the project's main goal: to explore how the toughening effects of TBDC materials in hybrid UD/TBDC ply laminates translate to secondary bonded joints when these laminates are used as substrates. The primary aim was to improve upon the previously literature reported crack competition and deflection, from the bond line into the substrate, toughening mechanisms by improving the drop in fracture toughness that typically occurs after the initial toughening phase, leveraging the fracture mechanisms provided by TBDC layers.

This joint study was conducted based on the effects of the substrates' stacking sequence and the toughness of the adhesive material used for their secondary bonding. As such, four different substrate configurations and two adhesive materials with varying toughness were utilized. The low-toughness Araldite 2015 adhesive was paired with the lower flexural modulus configurations, [90/45/-45/TBDC/0]$_s$ and [90/60/90/-60/TBDC/0]$_s$, while the high-toughness AF 163-2U adhesive was used with the higher flexural modulus substrate joint [0/TBDC/90$_2$/0]$_s$.

The addition of TBDC interleaves in the substrates caused a 30% flexural modulus increase in the

multi-directional, lower modulus, $[90/45/-45/0]_s$ joint configuration; and a 5% decrease in the cross-ply, higher modulus, $[0/90_2/0]_s$ configuration. This change in flexural modulus, coupled with the differing behaviors compared to literature-reported non-TBDC-toughened counterparts of the designed hybrid laminates, suggests a relationship between the crack competition and deflection mechanisms and the flexural modulus of the joints' substrates.

For specimens where the crack competition and deflection mechanisms occurred between the initial crack in the bond line and the substrate laminate, the same toughening effects reported in the literature for non-toughened joints were observed. Additionally, the use of TBDC-toughened substrates facilitated a less continuous reduction in effective fracture toughness after the toughening phase. The presence of CFRP ligaments between the initial bond line and the TBDC crack front played a significant role in this process. Regardless of the adhesive material used, an extended fracture toughness reduction period was observed compared to literature reported non-toughened joints with the same stacking sequence and adhesive material. In the case of the low-toughness adhesive material Araldite 2015, a more than 100% increase in the crack length from the fracture toughness peak to the final toughness value was recorded. Meanwhile, for the high-toughness adhesive AF 163-2U, fracture toughness values ranging from 150% to 750% higher were observed when a CFRP ligament was present compared to substrate crack propagation values for non-toughened joint configurations.

The primary toughening TBDC fracture mechanisms identified in the hybrid CFRP laminate specimens, however, were either insignificant or entirely absent in the joint specimens. The low final fracture toughness values, which were comparable to those observed during UD/TBDC interface vicinity propagation at the final propagation phase of the hybrid laminate specimens, may indicate that there was an insufficient amount of TBDC tapes surrounding the final crack plane for the primary toughening TBDC fracture propagation mechanisms seen in crack propagation for TBDC interleaved laminate DCB specimens to be activated.

The research questions outlined in section 3.2 will be addressed below.

- **How do TBDC interleaves affect the mode I fracture behavior of CFRP laminates?**
  1. *How do the fracture mechanisms manifest during TBDC crack propagation in TBDC interleaved CFRP laminates?*
     - During TBDC crack propagation in interleaved CFRP laminates, fracture mechanisms such as crack branching, deflection and TBDC tape and fiber bridging are observed. These mechanisms are not present or are less relevant in unidirectional CFRP crack propagation.
     - The TBDC-specific mechanisms remain effective while there is ample TBDC material on either side of the crack plane. However, as the deflected crack approaches a UD/TBDC interface, these mechanisms diminish significantly.
  2. *How do TBDC interleaves affect the mode I fracture toughness of CFRP laminates?*
     - TBDC crack propagation in interleaved CFRP laminates has demonstrated up to a 130% increase in effective fracture toughness compared to pure unidirectional laminates at the same crack length.
     - This toughening effect persists as long as the primary TBDC-specific fracture mechanisms remain active and significant.
  3. *How does the amount of TBDC interleaves affect the mode I fracture toughness of CFRP laminates?*
     - Due to the condition of the manufactured test samples and the limited data obtained, a definitive conclusion regarding the influence of the amount of TBDC interleaves on the mode I fracture toughness of CFRP laminates could not be reached.
- **How do TBDC interleaves in the CFRP substrates affect the mode I fracture behavior of adhesively bonded joints?**
  1. *How does the flexural modulus of TBDC interleaved CFRP substrate layups influence the mode I fracture mechanisms in adhesively bonded joints?*

- The TBDC interleaves in the substrate laminates exhibited a two-way effect on flexural modulus: they increased the modulus for multi-directional, lower modulus $[90/45/-45/0]_s$ and $[90/60/90/-60/0]_s$ laminates, while decreasing it for the cross-ply, higher modulus $[0/90_2/0]_s$ laminate.
- The specimens with increased modulus demonstrated a reduced likelihood of experiencing the crack deflection and competition mechanisms reported in the literature.
- A suggested link exists between DCB arm flexural modulus and the propensity for crack competition and deflection mechanisms to occur.

2. *How do TBDC interleaved CFRP substrate layups influence the mode I fracture toughness of adhesively bonded joints?*
   - The TBDC interleaved CFRP substrate layups appear to influence the observed toughening crack competition and deflection mechanisms.
   - Following an initial toughening phase due to crack competition and deflection mechanisms, the TBDC interleaved substrate joints exhibited a more segmented, less continuous reduction in effective fracture toughness, which can be quantified based on the toughness of the joint's adhesive material.
   - In specimens where crack deflection occurred from the bond line to the substrate, the anticipated final crack path through the TBDC layers was noted. However, the primary TBDC toughening fracture mechanisms observed in hybrid CFRP laminate specimens were not evident for substrate crack propagation, leading to final low toughness fracture.
3. *How does the adhesive toughness influence the mode I fracture toughness of adhesively bonded CFRP joints with TBDC interleaved substrates?*
   - The toughness of the adhesive material in TBDC interleaved CFRP joints exhibited similar influences on crack competition and deflection mechanisms as reported in the literature for non-TBDC-toughened joints.
   - In joints with the low toughness adhesive material Araldite 2015-1, where the crack deflected from the bond line to the substrate, a more than 100% increase in the crack length from the fracture toughness peak to the final toughness value was recorded, compared to non-TBDC-toughened joints.
   - In joints with the high toughness adhesive material AF 163-2U, where the crack deflected from the bond line to the substrate, fracture toughness values ranging from 150% to 750% higher were observed due to the formation of CFRP ligaments between the bond line and the substrate crack fronts, compared to substrate crack propagation values for non-toughened joint configurations.

To conclude, a concise reflection on the research objective presented in section 3.1 will be provided.

The research objective of this thesis research project is to increase the mode I fracture toughness of adhesively bonded joints using CFRP substrates toughened with Tow-Based Discontinuous Composite interleaves.

Overall, TBDC crack propagation in hybrid UD/TBDC ply laminates demonstrated an increase in effective fracture toughness compared to unidirectional CFRP laminates. In adhesively bonded joints, when crack deflection occurs from the bond line to TBDC-toughened substrates, a less abrupt and more gradual decrease in effective toughness is observed compared to non-toughened substrates. However, with the substrate laminates selected for this research project, no increase in final fracture toughness was found when the crack propagated solely through the TBDC material in the substrate. The primary TBDC-specific toughening fracture mechanisms, previously noted in UD/TBDC ply hybrid laminates, were not observed. Instead, the toughness values reverted to levels similar to those observed during crack propagation near the UD/TBDC interface in the hybrid laminates.

8.2. Recommendations for future work

Based on the scope and results of the present thesis work, new directions for further research can be identified, both in the context of Tow-Based Discontinuous Composites (TBDC) for toughening composite laminates and adhesively bonded composite joints, and in the broader study of mechanisms that might induce toughening effects in bonded composite joints.

8.2.1. Effect of the substrates' flexural modulus and local strains on the crack competition and deflection mechanisms

As reported by Lima et al. [5], higher opening displacements in mode I testing transition the loading conditions from pure cleavage to a mixed peel and cleavage load combination (please refer to Figure 8.1). This behavior is linked to lower flexural modulus laminates, which result in higher peel forces and greater local deformation at the crack tip.

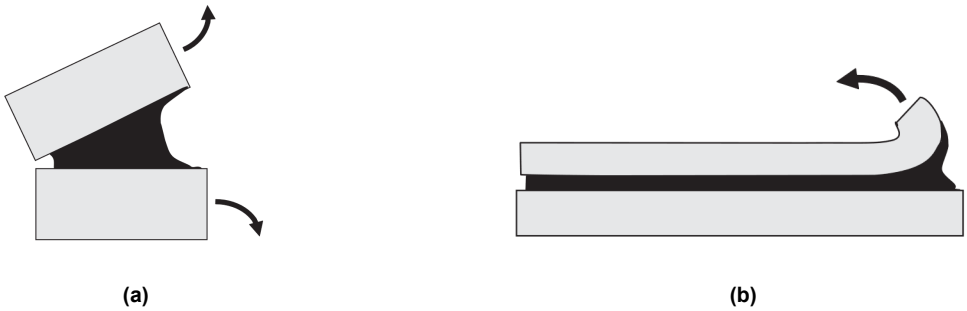

Figure 8.1: Cleavage (a) and peel (b) loading conditions [62].

Lower modulus specimens also displayed a greater propensity for crack deflection from the bond line to the substrate in the present thesis research. Therefore, it would be valuable to explore the connection between fracture mechanisms, local stresses and strains, peel and cleavage loading, and joint substrate flexural stiffness, both numerically and experimentally.

8.2.2. Effect of the number of TBDC interleaves on the mode I fracture toughness of CFRP laminates

Studying the effect of the number of TBDC interleaves on mode I fracture toughness was within the scope of this research project. However, due to defective samples and a limited number of test specimens, no definitive conclusions could be reached.

The limited data suggests an ambiguous effect from increasing the number of TBDC interleaves around the crack plane. Given the nature of the toughening fracture mechanisms, having more TBDC material for the crack to deflect through might extend the toughening period before the crack tip advances close to the UD/TBDC interface, where toughening mechanisms typically diminish.

8.2.3. Effect of number of TBDC interleaves on the CFRP substrate laminates on the mode I fracture toughness of composite bonded joints

During the present thesis work, crack propagation through TBDC interleaves in CFRP laminates revealed fracture mechanisms capable of increasing effective fracture toughness values. However, similar to the behavior observed at the UD/TBDC interface close vicinity, crack propagation through the single 0.45 mm thick TBDC layers in the substrates of adhesively bonded joints resulted in relatively low effective fracture toughness values, comparable to those seen in unidirectional CFRP crack propagation.

Drawing a link between the crack propagation near the UD/TBDC interface and that occurring in the single TBDC layer of the joint substrates suggests that in TBDC layers as thin as t= 0.45 mm, the primary TBDC-specific toughening fracture mechanisms — such as crack branching and deflection, and TBDC tape and fiber bridging — are not sufficiently prevalent to significantly alter fracture toughness during propagation.

Thus, it would be valuable to conduct a study investigating how increasing the thickness of TBDC interleaves in the substrate laminates of adhesively bonded composite joints impacts their mode I fracture behavior and subsequent toughness.

8.2.4. TBDC interleaves potential mode I onset toughening effects on cohesive failure of adhesively bonded composite joints

As observed and discussed in subsection 6.2.2 and subsection 7.2.1, most TBDC-toughened specimens that experienced cohesive failure exhibited higher onset mode I fracture toughness values than those reported in literature [5], approaching the maximum toughness values found for specimens where mode I toughening occurred due to crack deflection mechanisms.

If proven to exist, the potential onset toughening effect attributed to the TBDC interleaves in the substrate laminates could be significant. Achieving an increase in onset fracture toughness while maintaining cohesive failure toughness throughout crack propagation would represent a considerable advantage over the toughening behavior reported by Lima et al. [5] for non-toughened substrate joints.

A recommended approach for this further research would be to conduct numerical investigations of the stress distribution within the joint substrate and bond line during crack onset.

8.2.5. TBDC interleaves on mode II and mixed-mode fracture toughening of CFRP laminates

Tow-Based Discontinuous Composites (TBDC) interleaved in CFRP laminates have shown to promote toughening fracture mechanisms, increasing the mode I fracture toughness of the laminates.

It would therefore be beneficial to extend research to the fracture mechanisms facilitated by TBDC layers during pure mode II fracture onset and propagation, as well as mixed-mode I+II fractures. Understanding these mechanisms could provide insights into how they affect the fracture toughness of CFRP laminates under various loading conditions, including those more representative of the loading modes encountered in operational joints.

References

[1] A. Mahashabde et al. “Assessing the environmental impacts of aircraft noise and emissions”. In: *Progress in Aerospace Sciences* 47 (2011), pp. 15–52. ISSN: 03760421. DOI: 10.1016/j.paerosci.2010.04.003.

[2] J. Kupski and S. T. de Freitas. “Design of adhesively bonded lap joints with laminated CFRP adherends: Review, challenges and new opportunities for aerospace structures”. In: *Composite Structures* 268 (2021), p. 113923. ISSN: 02638223. DOI: 10.1016/j.compstruct.2021.113923.

[3] A. J. Timmis et al. “Environmental impact assessment of aviation emission reduction through the implementation of composite materials”. In: *International Journal of Life Cycle Assessment* 20 (2015), pp. 233–243. ISSN: 16147502. DOI: 10.1007/s11367-014-0824-0.

[4] M. D. Banea and L. F. M. D. Silva. “Adhesively bonded joints in composite materials: An overview”. In: *Proceedings of the Institution of Mechanical Engineers, Part L: Journal of Materials: Design and Applications* 223 (2009), pp. 1–18. ISSN: 14644207. DOI: 10.1243/14644207JMDA219.

[5] R. A. A. Lima et al. “Uncovering the toughening mechanisms of bonded joints through tailored CFRP layup”. In: *Composites Part B: Engineering* 263 (2023), p. 110853. ISSN: 13598368. DOI: 10.1016/j.compositesb.2023.110853.

[6] European Union Aviation Safety Agency. *Certification Specifications for Small Aeroplanes*. Tech. rep. CS-23 Amendment 3. 2012. URL: https://www.easa.europa.eu/en/document-library/certification-specifications/cs-23-amendment-3.

[7] I. Sioutis and K. Tserpes. “A Literature Review on Crack Arrest Features for Composite Materials and Composite Joints with a Focus on Aerospace Applications”. In: *Aerospace* 10 (2023). ISSN: 2226-4310. DOI: 10.3390/aerospace10020137.

[8] D. Quan, N. Murphy, and A. Ivankovic. “Fracture behaviour of epoxy adhesive joints modified with core-shell rubber nanoparticles”. In: *Engineering Fracture Mechanics* 182 (2017), pp. 566–576. ISSN: 00137944. DOI: 10.1016/j.engfracmech.2017.05.032.

[9] Q. Rao, Z. Ouyang, and X. Peng. “Enhancing mode I fracture toughness of adhesively bonded unidirectional composite joints using surfactant-stabilized multi-walled carbon nanotube and graphene nanoplate”. In: *Polymer Testing* 96 (2021), p. 107110. ISSN: 0142-9418. DOI: https://doi.org/10.1016/j.polymertesting.2021.107110.

[10] Q. Li et al. “Kirigami-inspired adhesion with high directional asymmetry”. In: *Journal of the Mechanics and Physics of Solids* 169 (2022), p. 105053. ISSN: 0022-5096. DOI: https://doi.org/10.1016/j.jmps.2022.105053.

[11] D. G. Hwang, K. Trent, and M. D. Bartlett. “Kirigami-Inspired Structures for Smart Adhesion”. In: *ACS Applied Materials and Interfaces* 10 (2018), pp. 6747–6754. ISSN: 19448252. DOI: 10.1021/acsami.7b18594.

[12] T. Löbel et al. “A hybrid bondline concept for bonded composite joints”. In: *International Journal of Adhesion and Adhesives* 68 (2016), pp. 229–238. ISSN: 01437496. DOI: 10.1016/j.ijadhadh.2016.03.025.

[13] L. F. da Silva and M. J. C. Lopes. “Joint strength optimization by the mixed-adhesive technique”. In: *International Journal of Adhesion and Adhesives* 29 (2009), pp. 509–514. ISSN: 01437496. DOI: 10.1016/j.ijadhadh.2008.09.009.

[14] A. Wagih, M. Hashem, and G. Lubineau. “Simultaneous strengthening and toughening of composite T-joints by microstructuring the adhesive bondline”. In: *Composites Part A: Applied Science and Manufacturing* 162 (2022), p. 107134. ISSN: 1359-835X. DOI: https://doi.org/10.1016/j.compositesa.2022.107134.

[15] F. Sarasini et al. “14 - Recent toughening strategies in carbon fiber reinforced composites”. In: *Fiber Reinforced Composites*. Woodhead Publishing Series in Composites Science and Engineering. Woodhead Publishing, 2021, pp. 405–437. ISBN: 978-0-12-821090-1. DOI: https://doi.org/10.1016/B978-0-12-821090-1.00002-8.

[16] D. Quan et al. “Interlaminar fracture toughness of CFRPs interleaved with stainless steel fibres”. In: *Composite Structures* 210 (2019), pp. 49–56. ISSN: 02638223. DOI: 10.1016/j.compstruct.2018.11.016.

[17] D. Quan et al. “On the mix-mode fracture of carbon fibre/epoxy composites interleaved with various thermoplastic veils”. In: *Composites Communications* 33 (2022), p. 101230. ISSN: 2452-2139. DOI: https://doi.org/10.1016/j.coco.2022.101230.

[18] S. Lee et al. “Effect of Interleaved Non-Woven Carbon Tissue on Interlaminar Fracture Toughness of Laminated Composites: Part II – Mode I”. In: *Journal of Composite Materials* 36.18 (2002), pp. 2169–2181. ISSN: 1530-793X. DOI: 10.1177/0021998302036018980.

[19] S. Lee et al. “Effect of Interleaved Non-Woven Carbon Tissue on Interlaminar Fracture Toughness of Laminated Composites: Part I – Mode II”. In: *Journal of Composite Materials* 36.18 (2002), pp. 2153–2168. ISSN: 1530-793X. DOI: 10.1177/0021998302036018981.

[20] J. Kupski, D. Zarouchas, and S. T. de Freitas. “Thin-plies in adhesively bonded carbon fiber reinforced polymers”. In: *Composites Part B: Engineering* 184 (2020), p. 107627. ISSN: 13598368. DOI: 10.1016/j.compositesb.2019.107627.

[21] R. W. M. Jr. *Joining of Advanced Materials*. Elsevier, 1993. ISBN: 9780750690089. DOI: 10.1016/C2009-0-26907-8.

[22] L. F. M. da Silva, A. Öchsner, and R. D. Adams. *Handbook of Adhesion*. Wiley, 2005. ISBN: 9780471808749. DOI: 10.1002/0470014229.

[23] S. Budhe et al. “An updated review of adhesively bonded joints in composite materials”. In: *International Journal of Adhesion and Adhesives* 72 (2017), pp. 30–42. ISSN: 01437496. DOI: 10.1016/j.ijadhadh.2016.10.010.

[24] T. A. S. Fuertes et al. “Bonding of CFRP primary aerospace structures – discussion of the certification boundary conditions and related technology fields addressing the needs for development”. In: *Composite Interfaces* 22 (2015), pp. 795–808. ISSN: 0927-6440. DOI: 10.1080/09276440.2015.1077048.

[25] N. G. C. Barbosa et al. “Comparison of different adhesively-bonded joint types for mechanical structures”. In: *Applied Adhesion Science* 6 (2018). ISSN: 21964351. DOI: 10.1186/s40563-018-0116-1.

[26] J. Ahn, S. Stapleton, and A. Waas. “14 - Advanced modeling of the behavior of bonded composite joints in aerospace applications”. In: *Composite Joints and Connections*. Woodhead Publishing Series in Composites Science and Engineering. Woodhead Publishing, 2011, pp. 423–434. ISBN: 978-1-84569-990-1. DOI: https://doi.org/10.1533/9780857094926.2.423.

[27] S. Shaikh et al. “Single Lap Adhesive Joint (SLAJ): A Study”. In: *International Journal of Engineering and Technology* (2017), pp. 64–70.

[28] R. B. Heslehurst and L. J. Hart-Smith. “The science and art of structural adhesive bonding”. In: *S.A.M.P.E. journal* 38 (2002), pp. 60–71.

[29] ASTM International. *Standard Practice for Classifying Failure Modes in Fiber-Reinforced-Plastic (FRP) Joints*. Tech. rep. D5573. 2019. URL: https://www.astm.org/d5573-99r19.html.

[30] O. Völkerink and C. Hühne. “Virtual testing for design and certification of (fusion) bonded longitudinal joints in a fibre composite fuselage: A proposal using FEM-based progressive damage analysis”. In: *Composites Part C: Open Access* 7 (2022), p. 100236. ISSN: 26666820. DOI: 10.1016/j.jcomc.2022.100236.

[31] S. Omairey, N. Jayasree, and M. Kazilas. “Defects and uncertainties of adhesively bonded composite joints”. In: *SN Applied Sciences* 3 (2021). ISSN: 25233971. DOI: 10.1007/s42452-021-04753-8.

[32] M. A. Meyers and K. K. Chawla. *Mechanical Behavior of Materials*. Cambridge University Press, 2008. ISBN: 9780521866750. DOI: 10.1017/CBO9780511810947.

[33] I. S. Floros, K. I. Tserpes, and T. Löbel. “Mode-I, mode-II and mixed-mode I+II fracture behavior of composite bonded joints: Experimental characterization and numerical simulation”. In: *Composites Part B: Engineering* 78 (2015), pp. 459–468. ISSN: 13598368. DOI: 10.1016/j.compositesb.2015.04.006.

[34] Y. Liu et al. “Understanding mixed mode ratio of adhesively bonded joints using genetic programming (GP)”. In: *Composite Structures* 258 (2021). ISSN: 02638223. DOI: 10.1016/j.compstruct.2020.113389.

[35] E. Preiß. “Fracture Toughness of Freestanding Metallic Thin Films Studied by Bulge Testing”. PhD thesis. University of Erlangen-Nürnberg, 2018. DOI: 10.25593/978-3-96147-118-8.

[36] ISO. *Adhesives — Determination of the mode 1 adhesive fracture energy of structural adhesive joints using double cantilever beam and tapered double cantilever beam specimens*. Tech. rep. 25217. 2009. URL: https://www.iso.org/standard/42797.html.

[37] ASTM International. *Standard Test Method for Determination of the Mode I Interlaminar Fracture Toughness of Unidirectional Fiber-Reinforced Polymer Matrix Composites*. Tech. rep. D5528. 2015. URL: https://www.astm.org/d5528_d5528m-21.html.

[38] ASTM International. *Standard Test Method for Determination of the Mode II Interlaminar Fracture Toughness of Unidirectional Fiber-Reinforced Polymer Matrix Composites*. Tech. rep. D7905. 2019. URL: https://www.astm.org/d7905_d7905m-19e01.html.

[39] P. Roy, A. Pathrikar, and D. Roy. “15 - Phase field–based peridynamics damage model: Applications to delamination of composite structures and inelastic response of ceramics”. In: *Peridynamic Modeling, Numerical Techniques, and Applications*. Elsevier Series in Mechanics of Advanced Materials. Elsevier, 2021, pp. 327–354. ISBN: 978-0-12-820069-8. DOI: https://doi.org/10.1016/B978-0-12-820069-8.00004-4.

[40] ASTM International. *Standard Test Method for Mixed Mode I-Mode II Interlaminar Fracture Toughness of Unidirectional Fiber Reinforced Polymer Matrix Composites*. Tech. rep. D6671. 2022. URL: https://www.astm.org/d6671_d6671m-22.html.

[41] I. Katsivalis et al. “Analysis of the damage mechanisms of adhesively bonded thin tow-based discontinuous composites”. Manuscript submitted for publication. 2024.

[42] M. Shokrieh, S. Ghoreishi, and M. Esmkhani. “11 - Toughening mechanisms of nanoparticle-reinforced polymers”. In: *Toughening Mechanisms in Composite Materials*. Woodhead Publishing Series in Composites Science and Engineering. Woodhead Publishing, 2015, pp. 295–320. ISBN: 978-1-78242-279-2. DOI: https://doi.org/10.1016/B978-1-78242-279-2.00011-1.

[43] R. Khan. “Fiber bridging in composite laminates: A literature review”. In: *Composite Structures* 229 (2019), p. 111418. ISSN: 02638223. DOI: 10.1016/j.compstruct.2019.111418.

[44] R. Khan. “Delamination Growth in Composites under Fatigue Loading”. PhD thesis. Delft University of Technology, 2013.

[45] P. P. Camanho et al. “Prediction of in situ strengths and matrix cracking in composites under transverse tension and in-plane shear”. In: *Composites Part A: Applied Science and Manufacturing* 37 (2006), pp. 165–176. ISSN: 1359835X. DOI: 10.1016/j.compositesa.2005.04.023.

[46] J. Kupski et al. “Composite layup effect on the failure mechanism of single lap bonded joints”. In: *Composite Structures* 217 (2019), pp. 14–26. ISSN: 02638223. DOI: 10.1016/j.compstruct.2019.02.093.

[47] Y. Li et al. “Experimental investigation of randomly-oriented tow-based discontinuous composites and their equivalent laminates”. In: *Composites Part A: Applied Science and Manufacturing* 102 (2017), pp. 64–75. ISSN: 1359835X. DOI: 10.1016/j.compositesa.2017.06.031.

[48] I. Katsivalis et al. “Strength analysis and failure prediction of thin tow-based discontinuous composites”. In: *Composites Science and Technology* 245 (2024), p. 110342. ISSN: 0266-3538. DOI: https://doi.org/10.1016/j.compscitech.2023.110342.

[49] S. Pimenta, A. Ahuja, and A. Y. Lau. “Damage tolerant Tow-Based Discontinuous Composites”. In: *20th International Conferences on Composite Materials (ICCM)*. 2015.

[50] A. Katunin et al. “Concept of a Conducting Composite Material for Lightning Strike Protection”. In: *Advances in Materials Science* 16 (2016), pp. 32–46. ISSN: 2083-4799. DOI: 10.1515/adms-2016-0007.

[51] ASTM International. *Standard Test Method for Flexural Properties of Polymer Matrix Composite Materials*. Tech. rep. D7264. 2015. URL: https://www.astm.org/d7264_d7264m-07.html.

[52] Grafil Inc. *Pyrofil HS40 Material Properties Data Sheet*. 2008. URL: https://www.rockwestcomposites.com/on/demandware.static/Sites-RWC-Site/Sites-rwc-master-catalog/-/downloads/HS40-12K_(07-2008).pdf.

[53] Mitsubishi Rayon Co., Ltd. *Pyrofil MR70 12P Material Properties Data Sheet*. 2014. URL: https://northerncomposites.com/wp-content/uploads/2020/07/MR-70-12P20140204.pdf.

[54] S. T. de Freitas and J. Sinke. “Failure analysis of adhesively-bonded metal-skin-to-composite-stiffener: Effect of temperature and cyclic loading”. In: *Composite Structures* 166 (2017), pp. 27–37. ISSN: 02638223. DOI: 10.1016/j.compstruct.2017.01.027.

[55] R. L. Fernandes et al. “From thin to extra-thick adhesive layer thicknesses: Fracture of bonded joints under mode I loading conditions”. In: *Engineering Fracture Mechanics* 218 (2019), p. 106607. ISSN: 00137944. DOI: 10.1016/j.engfracmech.2019.106607.

[56] C. Schmidt et al. “Influence of Prepreg Material Quality on Carbon Fiber Reinforced Plastic Laminates Processed by Automated Fiber Placement”. In: *Procedia CIRP* 67 (2018). 11th CIRP Conference on Intelligent Computation in Manufacturing Engineering, 19-21 July 2017, Gulf of Naples, Italy, pp. 422–427. ISSN: 2212-8271. DOI: https://doi.org/10.1016/j.procir.2017.12.236.

[57] M. Schey et al. “Effects of debulking on the fiber microstructure and void distribution in carbon fiber reinforced plastics”. In: *Composites Part A: Applied Science and Manufacturing* 165 (2023), p. 107364. ISSN: 1359835X. DOI: 10.1016/j.compositesa.2022.107364.

[58] M. Hamdi and J. A. Poulis. “Effect of UV/ozone treatment on the wettability and adhesion of polymeric systems”. In: *The Journal of Adhesion* 97 (2021), pp. 651–671. ISSN: 0021-8464. DOI: 10.1080/00218464.2019.1693372.

[59] S. R. Kalidindi, A. Abusafieh, and E. El-Danaf. “Accurate characterization of machine compliance for simple compression testing”. In: *Experimental Mechanics* 37 (1997), pp. 210–215. ISSN: 0014-4851. DOI: 10.1007/BF02317861.

[60] M. F. S. F. de Moura, J. J. L. Morais, and N. Dourado. “A new data reduction scheme for mode I wood fracture characterization using the double cantilever beam test”. In: *Engineering Fracture Mechanics* 75 (2008), pp. 3852–3865. ISSN: 00137944. DOI: 10.1016/j.engfracmech.2008.02.006.

[61] A. Argüelles et al. “Influence of the Matrix Type on the Mode I Fracture of Carbon-Epoxy Composites Under Dynamic Delamination”. In: *Experimental Mechanics* 51 (2011), pp. 293–301. ISSN: 0014-4851. DOI: 10.1007/s11340-010-9364-0.

[62] M. J. Troughton. “17 - Adhesive Bonding”. In: *Handbook of Plastics Joining (Second Edition)*. Second Edition. Boston: William Andrew Publishing, 2009, pp. 145–173. ISBN: 978-0-8155-1581-4. DOI: https://doi.org/10.1016/B978-0-8155-1581-4.50019-6.

A

Appendix

A.1. Mode I fracture toughness specimen measurements

Table A.1: $[0_{24}]$ thickness measurements.

$[0_{24}]$	Sample thickness [mm] (average $\pm$ standard deviation)
Sample 1	4.55 $\pm$ 0.0173
Sample 2	4.30 $\pm$ 0.0208
Sample 3	4.33 $\pm$ 0.0757
Sample 4	4.33 $\pm$ 0.0115
Sample 5	4.63 $\pm$ 0.0289

Table A.2: $[0_{24}]$ width measurements.

$[0_{24}]$	Sample width [mm] (average $\pm$ standard deviation)
Sample 1	25.12 $\pm$ 0.0306
Sample 2	25.07 $\pm$ 0.0100
Sample 3	25.03 $\pm$ 0.0100
Sample 4	25.06 $\pm$ 0.0200
Sample 5	25.16 $\pm$ 0.0451

Table A.3: $[0_{12}/\text{TBDC}_2/_{12}]$ thickness measurements.

$[0_{12}/\text{TBDC}_2/0_{12}]$	Sample thickness [mm] (average $\pm$ standard deviation)
Sample 1	5.63 $\pm$ 0.2100
Sample 2	5.40 $\pm$ 0.1102
Sample 3	5.57 $\pm$ 0.2858
Sample 4	5.66 $\pm$ 0.1858
Sample 5	5.60 $\pm$ 0.1002

Table A.4: $[0_{12}/\text{TBDC}_2/_{12}]$ width measurements.

$[0_{12}/\text{TBDC}_2/_{12}]$	Sample width [mm] (average $\pm$ standard deviation)
Sample 1	24.97 $\pm$ 0.0058
Sample 2	24.98 $\pm$ 0.0100
Sample 3	25.04 $\pm$ 0.0400
Sample 4	24.99 $\pm$ 0.0300
Sample 5	25.00 $\pm$ 0.0231

Table A.5: $[0_{12}/\text{TBDC}_4/_{12}]$ thickness measurements.

$[0_{12}/\text{TBDC}_4/0_{12}]$	Sample thickness [mm] (average $\pm$ standard deviation)
Sample 1	6.32 $\pm$ 0.0400
Sample 2	6.35 $\pm$ 0.1570

Table A.6: $[0_{12}/\text{TBDC}_4/_{12}]$ width measurements.

$[0_{12}/\text{TBDC}_4/_{12}]$	Sample width [mm] (average $\pm$ standard deviation)
Sample 1	24.90 $\pm$ 0.0321
Sample 2	25.01 $\pm$ 0.0361

Table A.7: $[90/45/\text{-}45/\text{TBDC}/0]_s$ DCB thickness measurements.

$[90/45/\text{-}45/\text{TBDC}/0]_s$	Substrate thickness [mm] (average $\pm$ standard deviation)	Sample thickness [mm] (average $\pm$ standard deviation)	Adhesive thickness [mm] (calculated from substrate)
Sample 1	2.43 $\pm$ 0.0833	5.37 $\pm$ 0.0794	0.45
Sample 2	2.40 $\pm$ 0.0153	5.41 $\pm$ 0.1626	0.50
Sample 3	2.44 $\pm$ 0.1457	5.36 $\pm$ 0.1060	0.53
Sample 4	2.58 $\pm$ 0.1531	5.47 $\pm$ 0.0929	0.26
Sample 5	2.43 $\pm$ 0.0153	5.27 $\pm$ 0.1650	0.42

Table A.8: $[90/45/\text{-}45/\text{TBDC}/0]_s$ DCB width measurements.

$[90/45/\text{-}45/\text{TBDC}/0]_s$	Sample width [mm] (average $\pm$ standard deviation)
Sample 1	24.87 $\pm$ 0.0404
Sample 2	24.87 $\pm$ 0.1102
Sample 3	24.66 $\pm$ 0.0624
Sample 4	25.04 $\pm$ 0.0569
Sample 5	24.93 $\pm$ 0.1350

Table A.9: $[90/60/90/-60/TBDC/0]_s$ DCB thickness measurements.

$[90/60/90/-60/TBDC/0]_s$	Substrate thickness [mm] (average $\pm$ standard deviation)	Sample thickness [mm] (average $\pm$ standard deviation)	Adhesive thickness [mm] (calculated from substrate)
Sample 1	2.86 $\pm$ 0.0800	5.88 $\pm$ 0.1474	0.23
Sample 2	2.80 $\pm$ 0.1589	5.83 $\pm$ 0.0351	0.42
Sample 3	2.83 $\pm$ 0.0929	5.95 $\pm$ 0.0802	0.34
Sample 4	2.68 $\pm$ 0.0781	6.06 $\pm$ 0.1179	0.58
Sample 5	2.69 $\pm$ 0.1464	5.87 $\pm$ 0.1114	0.50

Table A.10: $[90/60/90/-60/TBDC/0]_s$ DCB width measurements.

$[90/60/90/-60/TBDC/0]_s$	Sample width [mm] (average $\pm$ standard deviation)
Sample 1	24.85 $\pm$ 0.0917
Sample 2	24.86 $\pm$ 0.0361
Sample 3	24.81 $\pm$ 0.0777
Sample 4	24.94 $\pm$ 0.0208
Sample 5	24.81 $\pm$ 0.0551

Table A.11: $[0_8]$ DCB thickness measurements.

$[0_8]$	Substrate thickness [mm] (average $\pm$ standard deviation)	Sample thickness [mm] (average $\pm$ standard deviation)	Adhesive thickness [mm] (calculated from substrate)
Sample 1	1.48 $\pm$ 0.0172	3.11 $\pm$ 0.0569	0.16
Sample 2	1.48 $\pm$ 0.0172	3.09 $\pm$ 0.0404	0.14
Sample 3	1.48 $\pm$ 0.0172	3.25 $\pm$ 0.0954	0.30
Sample 4	1.48 $\pm$ 0.0172	3.09 $\pm$ 0.0231	0.14
Sample 5	1.48 $\pm$ 0.0172	3.16 $\pm$ 0.0961	0.21

Table A.12: $[0_8]$ DCB width measurements.

$[0_8]$	Sample width [mm] (average $\pm$ standard deviation)
Sample 1	25.13 $\pm$ 0.0153
Sample 2	24.99 $\pm$ 0.0231
Sample 3	25.09 $\pm$ 0.0351
Sample 4	25.00 $\pm$ 0.0115
Sample 5	25.06 $\pm$ 0.0306

Table A.13: $[90/TBDC/0_2/90]_s$ DCB thickness measurements.

$[90/TBDC/0_2/90]_s$	Substrate thickness [mm] (average $\pm$ standard deviation)	Sample thickness [mm] (average $\pm$ standard deviation)	Adhesive thickness [mm] (calculated from substrate)
Sample 1	2.25 $\pm$ 0.1637	4.90 $\pm$ 0.0902	0.31
Sample 2	2.25 $\pm$ 0.1637	4.88 $\pm$ 0.2346	0.29
Sample 3	2.25 $\pm$ 0.1637	4.76 $\pm$ 0.1365	0.16
Sample 4	2.25 $\pm$ 0.1637	4.96 $\pm$ 0.2042	0.36
Sample 5	2.25 $\pm$ 0.1637	5.02 $\pm$ 0.0513	0.43

Table A.14: $[90/TBDC/0_2/90]_s$ DCB width measurements.

$[90/TBDC/0_2/90]_s$	Sample width [mm] (average $\pm$ standard deviation)
Sample 1	25.15 $\pm$ 0.0600
Sample 2	25.22 $\pm$ 0.0945
Sample 3	25.01 $\pm$ 0.0058
Sample 4	24.99 $\pm$ 0.0265
Sample 5	24.98 $\pm$ 0.0231

A.2. Three point bending specimen measurements

Table A.15: $[90/45/-45/TBDC/0]_s$ three point bending samples' thickness measurements.

$[90/45/-45/TBDC/0]_s$	Sample thickness [mm] (average $\pm$ standard deviation)
Sample 1	2.50 $\pm$ 0.1735
Sample 2	2.69 $\pm$ 0.1229
Sample 3	2.80 $\pm$ 0.1513
Sample 4	2.61 $\pm$ 0.1587
Sample 5	2.61 $\pm$ 0.1873

Table A.16: $[90/45/-45/TBDC/0]_s$ three point bending samples' width measurements.

$[90/45/-45/TBDC/0]_s$	Sample width [mm] (average $\pm$ standard deviation)
Sample 1	13.12 $\pm$ 0.0520
Sample 2	13.10 $\pm$ 0.0100
Sample 3	13.12 $\pm$ 0.0058
Sample 4	13.17 $\pm$ 0.0611
Sample 5	13.14 $\pm$ 0.0000

Table A.17: $[90/60/90/-60/TBDC/0]_s$ three point bending samples' thickness measurements.

$[90/60/90/-60/TBDC/0]_s$	Sample thickness [mm] (average $\pm$ standard deviation)
Sample 1	3.13 $\pm$ 0.1834
Sample 2	3.03 $\pm$ 0.2464
Sample 3	3.03 $\pm$ 0.2464
Sample 4	2.62 $\pm$ 0.0503
Sample 5	2.56 $\pm$ 0.0961

Table A.18: $[90/60/90/-60/TBDC/0]_s$ three point bending samples' width measurements.

$[90/60/90/-60/TBDC/0]_s$	Sample width [mm] (average $\pm$ standard deviation)
Sample 1	13.14 $\pm$ 0.0153
Sample 2	13.14 $\pm$ 0.0493
Sample 3	13.10 $\pm$ 0.0058
Sample 4	13.10 $\pm$ 0.0058
Sample 5	13.11 $\pm$ 0.0252

Table A.19: $[0_8]$ three point bending samples' thickness measurements.

$[0_8]$	Sample thickness [mm] (average $\pm$ standard deviation)
Sample 1	1.61 $\pm$ 0.0404
Sample 2	1.59 $\pm$ 0.0306
Sample 3	1.58 $\pm$ 0.0173
Sample 4	1.61 $\pm$ 0.0321

Table A.20: $[0_8]$ three point bending samples' width measurements.

$[0_8]$	Sample width [mm] (average $\pm$ standard deviation)
Sample 1	13.02 $\pm$ 0.0058
Sample 2	13.01 $\pm$ 0.0000
Sample 3	13.03 $\pm$ 0.0000
Sample 4	13.04 $\pm$ 0.0100

Table A.21: $[90/TBDC/0_2/90]_s$ three point bending samples' thickness measurements.

$[90/TBDC/0_2/90]_s$	Sample thickness [mm] (average $\pm$ standard deviation)
Sample 1	2.39 $\pm$ 0.1537
Sample 2	2.37 $\pm$ 0.1286
Sample 3	2.42 $\pm$ 0.1644
Sample 4	2.41 $\pm$ 0.1050
Sample 5	2.53 $\pm$ 0.1044

Table A.22: $[90/TBDC/0_2/90]_s$ three point bending samples' width measurements.

$[90/TBDC/0_2/90]_s$	Sample width [mm] (average $\pm$ standard deviation)
Sample 1	13.10 $\pm$ 0.0000
Sample 2	13.12 $\pm$ 0.0000
Sample 3	13.10 $\pm$ 0.0058
Sample 4	13.10 $\pm$ 0.0058
Sample 5	13.10 $\pm$ 0.0000

A.3. Three point bending test results

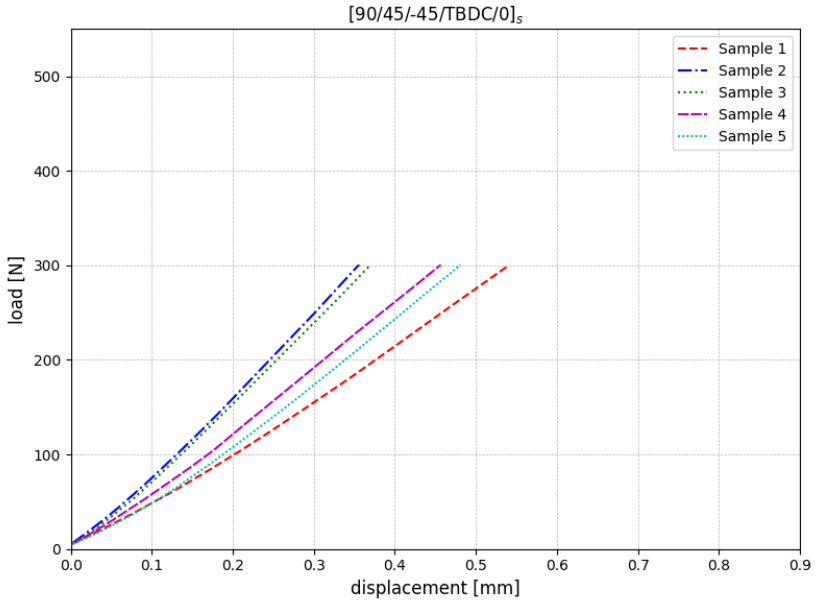

Figure A.1: Three point bending load-displacement curves of $[90/45/-45/TBDC/0]_s$ samples.

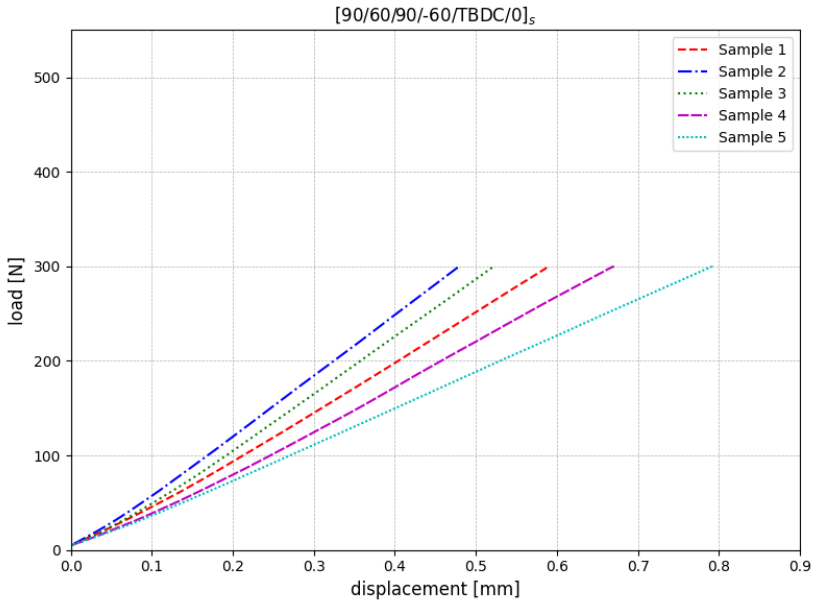

Figure A.2: Three point bending load-displacement curves of [90/60/90/-60/TBDC/0]$_s$ samples.

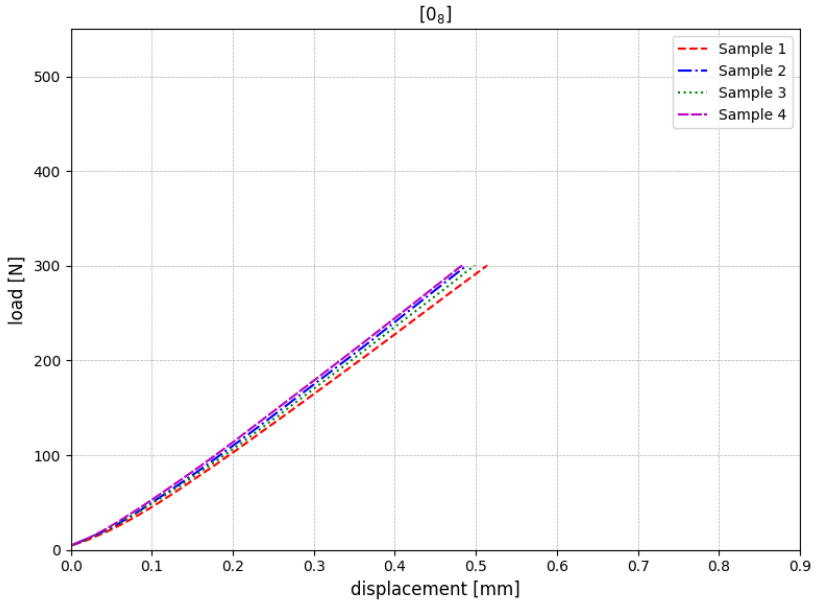

Figure A.3: Three point bending load-displacement curves of [0$_8$] samples.

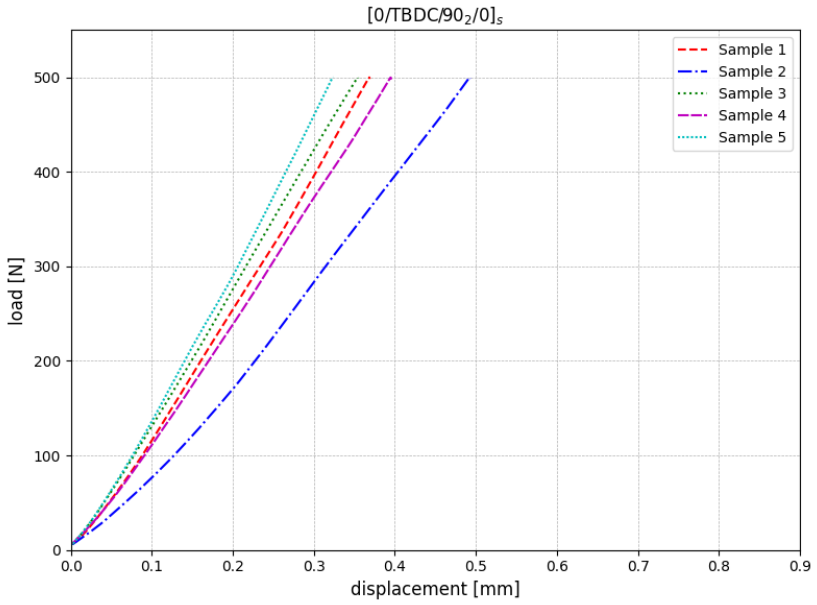

Figure A.4: Three point bending load-displacement curves of [0/TBDC/90$_2$/0]$_s$ samples.

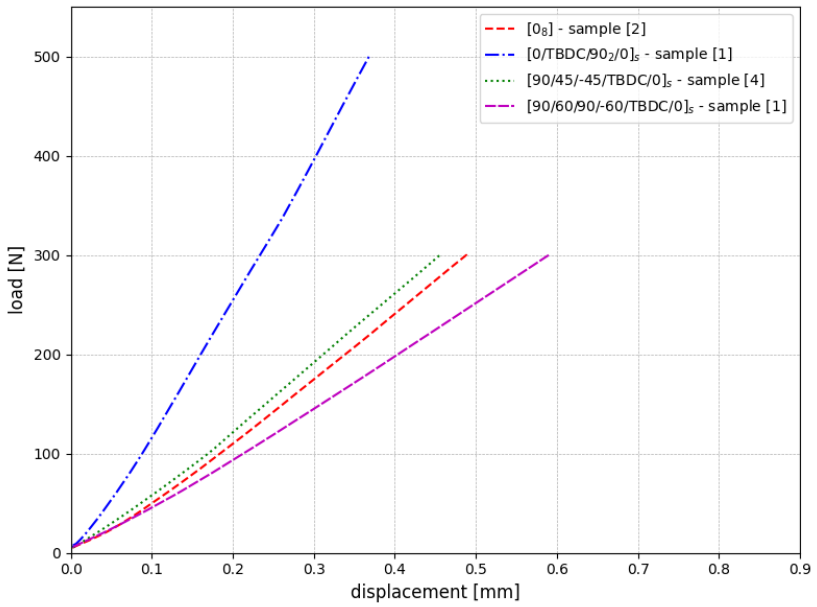

Figure A.5: Three point bending load-displacement curves of tests' representative samples.

A.4. Effective fracture toughness values

Table A.23: Average maximum and onset effective fracture toughness values and failure modes for tested specimens.

Adhesive type	Stacking sequence	Failure mode	Onset G_{eff} [J/m^2] (average $\pm$ standard deviation)	Max G_{eff} [J/m^2] (average $\pm$ standard deviation)
–	$[0_{24}]$	-	184 ± 68	345 ± 52
	$[0_{12}/\text{TBDC}_2/0_{12}]$	-	117 ± 69	590 ± 127
	$[0_{12}/\text{TBDC}_4/0_{12}]$	-	309 ± 21	627 ± 105
Araldite-2015	$[0_8]$ [5]	Cohesive	563 ± 49	563 ± 49
	$[90/45/\text{-}45/\text{TBDC}/0]_s$	Cohesive	941 ± 246	1120 ± 256
	$[90/60/90/\text{-}60/\text{TBDC}/0]_s$	Cohesive & Substrate	542 ± 82 838 ± 239	1170 ± 186 1007 ± 167
AF 163-2U	$[0_8]$	Cohesive	2848 ± 330	3534 ± 257
	$[0/\text{TBDC}/90_2/0]_s$	Substrate	3416 ± 1252	3708 ± 1714